University of Genoa
Department of Earth, Environmental and Life Sciences
PhD course on Sciences and Technologies for the Environment and the Territory
(Curriculum: Earth Sciences)

33rd PhD Cycle

GEOLOGIC, ENVIRONMENTAL AND NORMATIVE ISSUES IN THE NATURAL OCCURRENCES OF ASBESTOS (NOA) MANAGEMENT

PhD Supervisors:

Prof.ssa Laura Gaggero
Prof. Sebastiano La Maestra
Prof.ssa Rosalda Punturo

PhD Candidate:
Gaia Maria Militello

Year 2021

TABLE OF CONTENTS

ABSTRACT

The term “asbestos” refers to a group of silicate minerals with a fibrous habit, which belong to the serpentine and amphibole families. The fibrous minerals defined asbestos by the Legislative Decree of 15 August 1991 are six: chrysotile, amosite (fibrous variety of grunerite), crocidolite (fibrous variety of riebeckite), anthophyllite, tremolite and actinolite. The chemical-physical properties of asbestos have made them, in the past, one of the most important inorganic materials for industrial purposes and technological applications. However, the extraction, use and marketing of these minerals have been prohibited, due to the proven harmful effects, mainly affecting the respiratory system, that asbestos fibres can cause. Italy was among the first countries to ban the use of asbestos through Law 27/03/1992 n.257.

In addition to the known six minerals classified as asbestos, in nature exist also amphiboles and antigorite and lizardite (polymorphs of serpentine), which have the same composition of asbestos groups but not the same morphology. These minerals in fact are chemically and geometrically (length > 5 μm, width < 3 μm and length: diameter > 3:1) but not morphologically analogous to regulated asbestos. The debate about their potential hazardous properties is open and ongoing, therefore, their morphological characterization has a key role in establishing a reliable asbestos hazard scenario.

During these 3 years of PhD studies, multi-instrumental and multidisciplinary approaches have been implemented, starting from the study of the influence of textural constraints and the subsequent origin of asbestiform/non-asbestiform minerals in the massive rock.

Secondly, it was established whether asbestos fibres homogeneously distributed in the different fractions ground from asbestos-bearing lithotypes and was calculated the contribution of fibres from each fraction to the overall concentration in the sample. The Italian decree (M.D. 06/09/94), which regulates the counting criteria of asbestos fibres potentially present in excavated soil and rocks, suggests a method of sample preparation. This provides for the division of the sample into particle size classes before reaching the particle size fraction on which it will then be performed the fibre count. The powdered fractions were characterised using a Scanning Electron Microscope coupled with Energy Dispersive Spectroscopy (SEM-EDS). The still in use (in some cases), Italian normative M.D. 161/2012, specifies that analyses must be performed on the < 2 mm fraction and the concentration (mg/kg) correlated with the weight of the whole sample < 20 mm. However, the fibre counts yielded asbestos concentrations 50–60% lower compared with total asbestos analyses according to the new R.P.D. 120/2017. Consequently, there is a need to standardize the normative

worldwide regulations to manage asbestos-containing materials by re-evaluation of sample preparation and quantification of asbestos.

A subsequent part of the project focused on the SEM-EDS analysis of amphiboles with asbestiform and non-asbestiform habit, subject to mechanical stress by grinding for three different time intervals, in order to assess how different time lengths of comminution control geometry and morphology of the particles. The mode of comminution is fundamental for the following quantitative determination of fibres. It is a critical step because it can affect the morphology and geometric ratios of fibres, inducing positive or negative false. When mechanical stress is applied to rocks containing pristine prismatic or acicular amphiboles, these mineral phases can break, originating particles with dimensions and geometrical ratios that would label them as asbestos. Therefore, a normative and scientific gap arise in the classification criteria of a particle as a real asbestiform mineral or as a "cleavage fragment".

In the third and final part of the thesis work, the same samples previously used were prepared to perform biological assays. The capacity of several asbestiform and non-asbestiform powders to cause both cytotoxic effects and carcinogenic potential in BALB/c 3T3 cells was then monitored and evaluated.

1. INTRODUCTION

Asbestos, a substance included among group I carcinogens, is considered one of the most dangerous types of dust for human health (IARC, 1987; 2012).

The term asbestos is a commercial term used to identify six minerals represented by hydrous silicates belonging to the serpentine group (chrysotile) and amphiboles (amosite, crocidolite, anthophyllite, tremolite and actinolite), which are easily separable in thin, flexible fibres, resistant to traction and heat and almost chemically inert.

During the twentieth century, asbestos was widely used in buildings and industrial installations, but the evidence of the health risks that it can cause due to the inhalation of fibres has pushed health authorities to issue stringent norms to avoid industrial and domestic applications. Later, Asbestos Containing Materials (ACM) have been declared harmful to health and banned in Italy by law No. 257 of 27/03/1992 and subsequently in the entire European Commission by directive 1999/77/CE as identified as a mutagenic agent, the cause of pleural mesothelioma and other asbestos-related pathologies. More than 52 countries, including the 28 member States of the European Union, have banned or restricted the use of asbestos in accordance with the campaign carried out by the World Health Organization (WHO) to stop the use of all types of asbestos (Bloise et al., 2020). However, countries such as China, India, Russia, Kazakhstan, Zimbabwe, Brazil, and Canada and Colombia are still producers and consumers of asbestos (Figure 1).

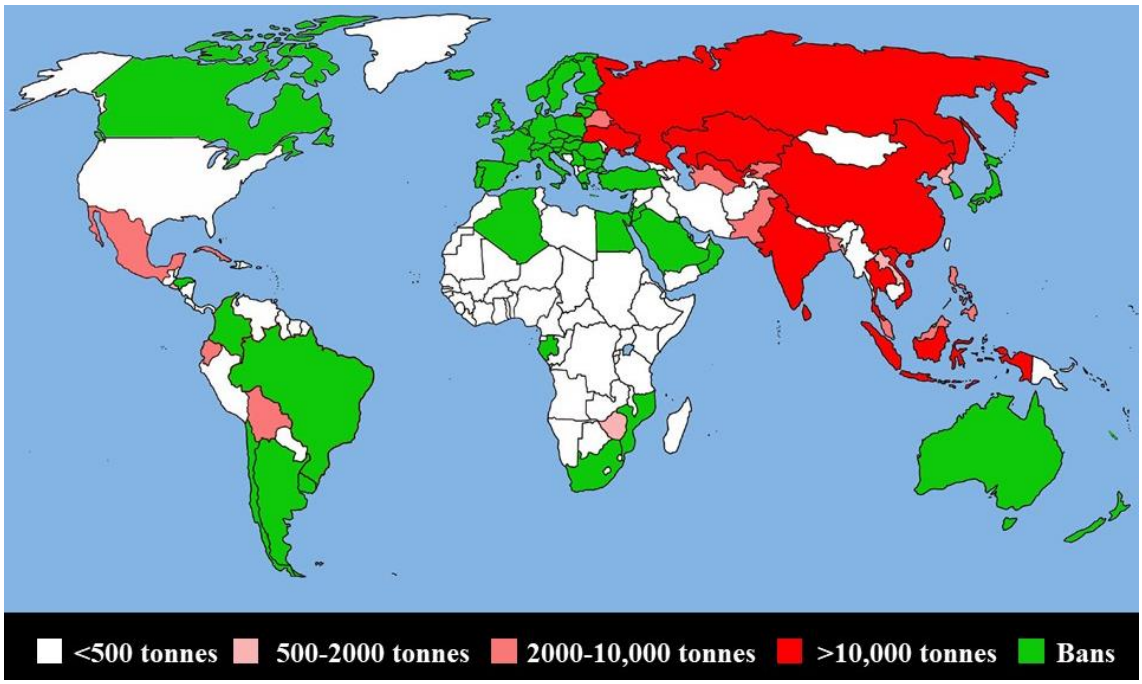

Figure 1. *Asbestos consumption and national bans (updated to 2019). In green, countries with full or partial bans. In white, pink, dark pink and red the asbestos consumption (http://www.ibasecretariat.org/alpha_ban_list.php.*

In Italy, the anthropogenic sources of asbestos exposure mainly belong to the now-abandoned mining areas and processing plants. The mere occurrence of asbestos does not necessarily represent a risk but becomes dangerous if it disperses fibres in the surrounding environment, for example, due to mechanical or thermal stress. Actually, large works recently built through ophiolitic matrices or under construction in the country (among these the Genoa-Milan high-speed railway line, called "Terzo Valico"), have highlighted that natural asbestos outcrops must be managed as for the health of workers, the destination of excavated products and the use of asbestos-free construction materials. The excavation of asbestos rocks, in fact, induces the release of fibres in heterogeneous and unpredictable concentrations in space.

However, the asbestos management is ruled by quite obsolete legislation and does not consider many parameters for correct phase classification. Therefore, controversies over the health impact, identification criteria and regulatory limits are still ongoing (Finkelstein, 2013; Bernstein et al., 2013; Jargin, 2015; Baur et al., 2016). Furthermore, the drop in the use of asbestos in developed countries is at odds with emerging countries that continue to produce materials containing asbestos (Baur et al., 2015; Marsili et al., 2016), and most of the countries must face the management of the removal of existing asbestos and of the naturally occurring asbestos (EU Parliament, 2012; Hashim and Boffetta, 2014).

The acronym NOA, Natural Occurrences of Asbestos, refers to asbestos fibres dispersed in the environment when asbestos has not been extracted and refined for marketing purposes but has been exposed as a consequence of the excavation activity and construction of infrastructure works (Gaggero et al., 2017; Wagner, 2015d; Harper, 2008; Lee, 2008).

Therefore, the management of excavation activities in rocks containing asbestos is critical for either professional exposure and or environmental management (Gaggero et al., 2017). Epidemiological studies have shown that an asbestos exposure threshold below which health risks are to be excluded cannot be defined (IARC, 2012, WHO, 2014), however, it is necessary to adopt reference values to ensure health surveillance and to put in place protective measures.

To date, it seems to be clear that anthropogenic and natural processes contribute to the continuous production of Elongated Mineral Particles (EMP) of amphibole and serpentine, in the air and in the water, in urban, rural and construction site environments (Wylie & Candela, 2015). These EMPs include cleavage fragments of minerals belonging by composition, but not necessarily by morphology, to the group of asbestos and other asbestiform minerals (that often are even more common) whose potential hazard is not fully investigated.

In fact, the definition of fibre to date is not univocal: according to Wylie & Candela (2015) more than seven definitions are possible, with results that are not comparable. Research and debates are in progress about the composition and morphology of the various types of asbestos and the related fibrous minerals not classified as asbestos, such as erionite, fibrous lizardite and antigorite (Ballirano et al., 2018; Cardile et al., 2007). For instance, antigorite is regulated as asbestos only in the New Caledonia legislations (Petriglieri et al., 2017).

The reason for these inconsistencies is mainly related to different and dated legislations worldwide. Consequently, quantitative determinations can yield highly variable results even for similar environments, preventing a risk assessment based on univocal data.

In fact, in the case of construction projects involving the production and handling of excavated soils and rocks containing asbestos, establishing requirements for environmental quality and appropriate destination for excavated products impose proper characterization of asbestos concentration. Official survey techniques prescribed by the normative for assessing the presence of asbestos in bulk samples, by qualitative and quantitative analysis, do not guarantee a unique and reproducible quantification of asbestos content (Militello et al., 2019a). Notable variables, depending on the material under examination, reside on the context from which the sample is issued, and a vision on evaluating the investigation objective (Cavariani et al., 2010). In addition, several sources of error can affect the calculation of asbestos concentration in a sample.

Interpretation and classification problems have emerged regarding restrictive regulations and protocols, which require analytical techniques with highly sensitive detection thresholds. The limits sometimes conflict both with the analytical sensitivities of the currently available techniques, but above all, with the lack of ministerial protocols that uniquely prescribe the methods of preparation and analysis of the samples, causing variability in the results.

The evaluation of the asbestos hazard (Gaggero et al., 2017) is based on counting criteria used to determine the number of regulated fibres (Belardi et al., 2018). In this perspective, different procedures were proposed for refining the classification of particles as asbestos or fibres originated by preferential cleavage of particles (Wyle et al.,1985; AHERA, 1987; OSHA 1994a, 1994b; Harper et al., 2008, 2012; Van Orden et al., 2008, 2009; NIOSH, 2011).

In fact, the worldwide normative and scientific gap concerns the classification criteria of asbestos. If the asbestiform amphiboles have been clearly identified and banned, acicular/prismatic amphiboles are not univocally regulated as asbestos. Asbestiform amphibole can have a neat fibrous and asbestiform habit. In contrast, its non-asbestiform analogue can derive from size reduction of a pristine prismatic/acicular mineral with dimensions and geometrical ratio that often fit with the definition of fibre (length > 5 μm, diameter < 3 μm, and length to width ratio > 3:1). The non-

asbestiform amphibole can develop a prismatic or fibrous habit, characterised by a parallel growth of elongated crystals, having nanometric width and micrometric length (Harper et al., 2012). Also, among serpentine polymorphs, the fibrous antigorite and lizardite sometimes occur very similar in morphology to the polymorph chrysotile and therefore are not easily distinguishable, especially if associated. This issue involves considerable uncertainty because, under similar chemical composition, the morphological characterization of the phases cannot be disregarded if the aim is to quantify fibres and define their carcinogenicity. Moreover, non-asbestiform particles are a potentially major source of exposure worldwide, so adverse health effects may derive (Hwang et al., 2014).

In sample preparation, comminution is a fundamental step for the subsequent quantitative determination of fibres, as it can affect the variability of the geometric and morphological relationships of particles. However, the preparation methods described in the Italian Ministerial Decree (M.D. 06/09/1994) and other ministerial protocols from other countries, lack precise coding, thus not guaranteeing comparable and reproducible intra- and inter-laboratory results. For Ham et al. (2019 and references therein), quantitative analysis and the accuracy of the results also depend on the experience of the analyst. Consequently, quantitative calculations can produce high variance results, inhibiting a risk estimate based on univocal data (Militello et al., 2019b). As already demonstrated, when mechanical stress (such as grinding) is applied to rocks containing non-asbestiform amphiboles, the latter can break, originating particles with different lengths but still with dimensions and geometric ratios that make them included in the asbestos classification. The recast of concentration takes thus to false positives or false negatives, generating a critical issue.

The aim of this PhD project was to carry out an accurate review of the technical and legislative critical issues useful for updating the methods in force, regarding the analysis for quantification of asbestos. A significant contribution was also made on cytotoxic and genotoxic tests based on the development of more precise and univocal analysis protocols in the classification criteria for asbestos minerals.

1) The first goal was to compare, at different investigation scales, by a multi-instrumental approach the morphological features and the influence of textural constraints in massive samples, which determine the origin of fibrous and asbestiform or fibrous but not asbestiform products, or rather the EMP of amphibole and serpentine groups. Moreover, a new application of the synchrotron radiation X-ray microtomography, not yet used before for asbestos detection, was adopted. This semi-destructive technique was chosen because it

can help to better observe the arrangement of the fibres in the three dimensions and facilitate the comparative description of cleavage fragments.

2) The second goal was to quantify whether asbestos fibres homogeneously occur in the different fractions when ground from different lithotypes. Using SEM-EDS, the contribution of fibres was counted from each fraction to the overall concentration in the sample and then calculated.

3) The third goal was to observe samples containing tremolite-actinolite amphiboles with asbestiform and non-asbestiform habit by SEM-EDS over a statistically significant population. The samples were subject to mechanical stress for three different time intervals to observe how the geometry and the morphology of the particles varied according to the length of comminution.

4) Lastly, bioassays were carried out to better understand the different carcinogenic potential of serpentine and amphibole minerals as a function of the crystalline habit, i.e., the aspect ratio and the morphology of the fibres.

It is necessary to debate what aspect ratio is to be considered as lower and upper limits of a range. The risk of developing chronic diseases by inhalation of fibres is linked to different factors as particle morphology, size, physical-chemical properties and bio-persistence correlated to the crystalline habits and can produce relevant consequences to the human respiratory system. Having more constraints on this issue plays an essential role in establishing health risk because, as part of the analysis for environmental monitoring, acicular fibres could influence the final calculation of the asbestos concentration.

2. STATE OF THE ART

The generic term "asbestos" is referred to a group of six natural (Figure 2) minerals represented by easily separable silicates in thin, flexible fibres, resistant to traction or heat and chemically inert. The common characteristic of these minerals is the crystalline habit that include the asbestiform varieties of the serpentine and of some amphibole type.

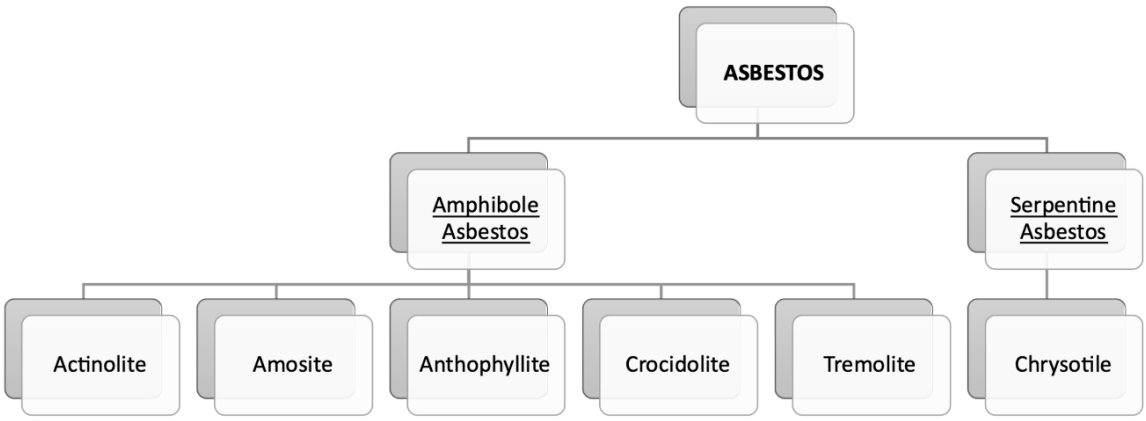

Figure 2. *Sketch of regulated asbestos minerals.*

Amphibole Asbestos

- Actinolite $Ca_2(Mg, Fe^{2+})_5Si_8O_{22}(OH)_2$
- Anthophyllite $Mg_7Si_8O_{22}(OH)_2$
- Amosite (brown asbestos – commercial name of the cummingtonite/grunerite serie) $(Mg, Fe^{2+})_7Si_8O_{22}(OH)_2$
- Crocidolite (blu asbestos – commercial name of riebeckite) $Na_2(Mg, Fe^{2+})_3Fe_2^{3+}Si_8O_{22}(OH)_2$
- Tremolite $Ca_2Mg_5Si_8O_{22}(OH)_2$

Asbestos of Serpentine

- Chrysotile (white asbestos) $Mg_3Si_2O_5(OH)_4$

Compared to other varieties of silicates, asbestos fibres have diameters in the micron up to nanometre range, thanks to the particular property of separating in a longitudinal direction which generate very fine and potentially inhalable fibres (Pisu, et al., 2008).

2.1 Minerals of the serpentine group

The minerals of the serpentine group are T:O phyllosilicates, whose structure is formed by the alternation (in a ratio of 1:1) of tetrahedral layers and octahedral layers, such as brucite, united to form a package. Subsequent packages are held together by hydrogen bonds. The three phases belonging to the serpentine group (ideal formula $Mg_3Si_2O_5(OH)_4$.) are chrysotile and lizardite and antigorite. The connection between the octahedral and tetrahedral layers occurs easily as their lateral dimensions are quite similar (lateral dimension of the tetrahedral layer is 9.15 Å, against the 9.43 Å of the octahedral layer). However, each of the three phases (lizardite, antigorite, chrysotile) responds differently to compensate the misfit in order to ensure the stability of the structure.

2.1.1 Chrysotile

Chrysotile is composed of Si-centred tetrahedral (T) sheets in a pseudo-hexagonal network joined to Mg-centred octahedral (O) sheets in units with a 1:1 (T-O) ratio (Figure 3). Because the T-O unit is polar and a misfit exists between the smaller parameters of the T sheet and the larger ones of the O sheet, a differential stress occurs between the two sides of the layers. The stress is relieved by rolling the T-O layers around the fibre axis. Therefore, the curving and rolling of the tetrahedral and octahedron layers, usually around the crystallographic a axis is responsible for the fibrous habit (Gualtieri, 2017 and references therein).

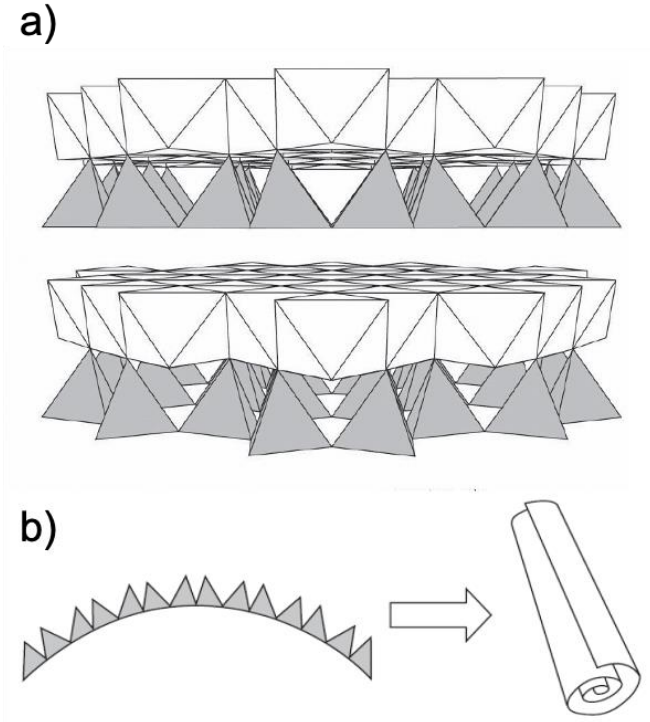

Figure 3. *(a) Sketch of the structure unit of chrysotile asbestos with a Si-centred tetrahedral sheet joined to a Mg-centred octahedral sheet (b–c crystallographic plane); (b) Bending of the layers in chrysotile at a molecular scale (Pollastri et al., 2016).*

2.1.2 Lizardite

In lizardite the misfit between T-O layers is compensated by a rotation of the SiO_4 tetrahedra in the plane through deformations of the tetrahedral layer. Therefore, the lizardite package has a planar morphology (Figure 4), which is reflected in the usual lamellar morphology of this mineral.

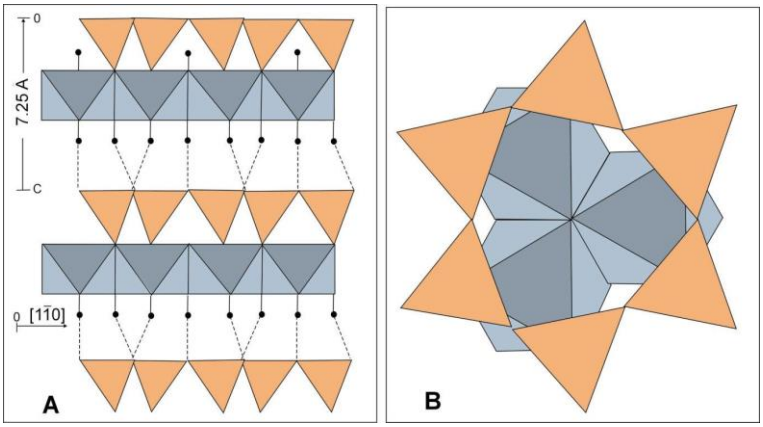

Figure 4. *Crystal structure of lizardite, viewed along [110] (a) and [001] (b). Dashed lines represent hydrogen bonds (Groppo PhD thesis, 2005).*

2.1.3 Antigorite

The antigorite structure, on the other hand, shows a wavy appearance due to the periodic inversion of the polarity of the polyhedral coordination that compensates the misfit between the

tetrahedral and octahedral layer (Figure 5). Like lizardite, antigorite also has generally lamellar habit, although fibrous antigorite is also described in the literature.

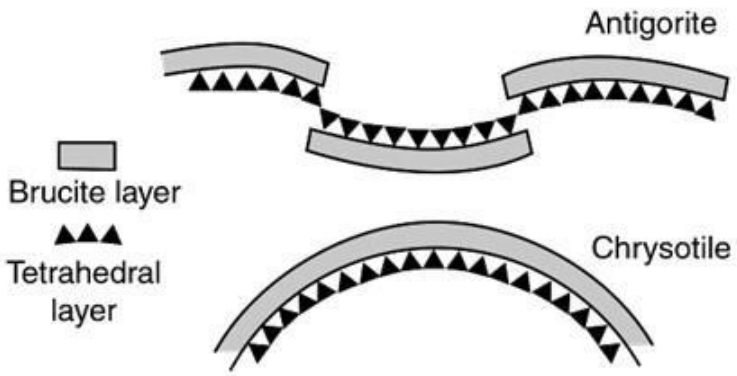

Figure 5. *Comparison between the structure of antigorite and that of chrysotile.*

2.2 Amphiboles

Amphiboles are inosilicates whose structure is organised in double chains of long and parallel silica oxide tetrahedra (SiO_4) that share three of the four oxygen presents (Figure 6), with a consequent Si:O ratio equal to 4:11 (or 8:22). The oxygen atoms of the chains coordinate not only Si (Al) but also other cation sites, corresponding to the following simplified formula: $A_{0-1}B_2C_5T_8O_{22}(OH,F)_2$ with the following possible combinations:

· A = Na^+, K^+;
· B = Ca^{2+}, Na^+, Mn^{2+}, Fe^{2+}, Mg^{2+}, Li^+;
· C = Mn^{2+}, Fe^{2+}, Fe^{3+}, Mg^{2+}, Al^{3+}, Ti^{4+};
· T = Si^{4+}, Al^{3+}.

The structure of these minerals, has double Si_4O_{11} chains, parallel to axis c. There are also other cationic sites, called A, M4, M3, M2 and M1. The A has variable coordination from X to XII. The M4 site has VI-VIII coordination and hosts the B cations. Finally, the M3, M2 and M1 octahedra form strips by sharing edges and contain the C cations; the belts are parallel to the silicate chains and develop along the c axis.

Therefore, because of the strong bond, amphiboles are normally elongated along the c crystallographic axis. Hence, the fibrous crystal habit is due to the tetrahedral chains linked laterally to octahedral rows (Gualtieri, A.F., 2017).

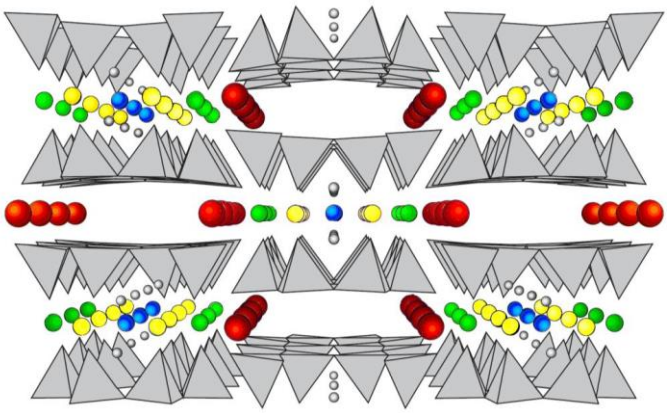

Figure 6. *An idealised model of the amphibole asbestos structure showing the chain of tetrahedra, the strip of octahedra. Yellow=M(1), green=M(2), blue =M(3), red=M(4) and the A site (Pollastri et al., 2016).*

Minerogenetic conditions are responsible for the variation in crystal habit of a species; the fibrous and asbestiform habit is the least common form for amphiboles. Conversely, the common crystal habit of amphiboles varies from prismatic to acicular; the c axis is the direction of elongation and two other dimensions that are approximately equal (Campbell et al., 1977). These particles are comprehensively named as cleavage fragments, that is the preferential breaking of crystals along planes of structural weakness. All monoclinic amphiboles have perfect (110) cleavage and orthorhombic amphiboles have perfect (210) cleavage (Shelley, 1975). These cleavage fragments are formed by breaking, so they do not depend on the crystallization, unlike fibrous and asbestiform amphibole particles. Therefore, the fibrous amphibole can have an identical chemical and atomic structure but a diversity of crystalline form or growth habit (Van Orden et al., 2008).

2.3. Definitions of asbestos

The term asbestos has both a mineralogical and a commercial use, that in time caused misunderstandings. Key words and debated items within the scientific community are the following:

1) *Fibrous*, term linked to the geometry of the particles. For the definition of "breathable fibre", the parameters indicated by the World Health Organization (WHO, 1997) are:

   - Length > 5 µm
   - Width < 3 µm
   - Aspect Ratio (length of the particles divided by the width, A/R) > 3:1

2) *Asbestiform*, refers to a specific type of mineral fibrosity where the fibrils possess high tensile strength or flexibility.

The morphological distinction among the two habits was defined by the National Research Council (1984), which defines asbestiform the structure characterised by crystals that appear singularly similar to organic fibres such as cotton or hair or made up of bundles composed of many parallel fibres (fibrils). The non-asbestiform habit is characterised by prismatic crystals, even with an irregular shape, or by crystals with acicular growth.

Therefore, in nature there are minerals such as those belonging to the group of serpentine and amphiboles, which can have a fibrous and asbestiform aspect or fibrous but not-asbestiform aspect.

These morphological differences derive from changes in the crystalline structure which nevertheless entail significant variations in its physical properties (Langer et al., 1991). This structure will be of fundamental importance to be analysed as there is a strong impact on the dimensional distribution of dust following comminution or on the potential carcinogenicity upon inhalation.

2.3.1 Other definitions

Recently, additional terms were added to clarify any classification misunderstandings. Among these it is common to speak of:

- Cleavage fragments: proposed by Occupational Safety and Health Administration (OSHA) in 1992. It is a term that refers to amphibole (crocidolite, amosite, anthophyllite, tremolite, actinolite) or serpentine (antigorite and lizardite) that, from a morphological point of view, cleave into fragments rather than separate longitudinally into fibrils like asbestos varieties. Therefore, they have the same chemical composition of asbestos species but in geometrical ratios they fall within the definition of fibre, although they are not asbestiform. Considering the indexing of crystal faces, monoclinic amphiboles have perfect cleavage along the 110 face, and orthorhombic amphiboles have perfect cleavage along the 210 face (Shelley, 1975).

- Elongate Mineral Particles (EMP): proposed by National Institute for Occupational Safety and Health (NIOSH, 2010) to describe all of these particles if specific attributes are applicable to a broad class of particle types. In particular, this term refers to mineral particles with a length ≥ 5 μm and a minimum aspect ratio of 3:1 that correspond to breathable size (Williams et al., 2013), avoiding the use of the term “fibre” which leads to characterization misunderstandings.

Due to the difficulty of distinguishing between asbestiform and non-asbestiform EMP, the relationship between the size of non-asbestiform EMP and carcinogenic lung disease is still open to interpretations. Indications are confusing are and, moreover, that the definition lacks standardised operating definitions for fibres (Keane et al., 1999).

3. NATURAL OCCURRENCE OF ASBESTOS

The asbestos mineralization is mainly related with ophiolites, which are slices of oceanic crust and of the underlying mantle (i.e., oceanic lithosphere) unroofed and exposed during orogenic events and subsequent erosion. Generally found in veins or in pseudomorphic structure, serpentine (formed during oceanic metamorphism) and amphibole (formed during high to medium grade ocean floor and orogenic metamorphism) asbestos are minerals of ultramafic and mafic rocks in ophiolitic complexes and occur mainly in ductile-brittle structures, such as shear zones, fault planes and fractures (Gaggero et al., 2006). High concentrations are also found at the reaction zones between ultramafic and mafic rocks (actinolite–tremolite-rich schist). Therefore, several lithotypes can potentially contain asbestos, depending on: i) the metamorphic conditions (e.g., Giacomini et al., 2010), ii) the composition of the host rock, iii) the structural framework, i.e., the presence of fractures where the fluids circulating in the rock trigger the growth processes of fibrous minerals (Gaggero et al., 2013, 2017). High concentrations are also found in metamorphic or metasomatic reaction edges between ultramafic and mafic rocks (actinolite-tremolite schists). Finally, asbestos minerals can spread within the rock matrix due to hydraulic fracturing effect (Ross, 1981, Ross & Nolan, 2003, Schreirer, 1989, Wruke, 1986).

Among ophiolites, serpentinites can potentially contain the highest concentrations of asbestos minerals; other lithotypes potentially containing asbestos minerals are represented in metabasites by chlorite-schists, and ophicalcite (Labagnara et al., 2013). Lower concentrations are also found in sedimentary rocks deriving from the dismantling of lithotypes containing asbestos.

3.1 Asbestos in the Italian territory

Asbestos occurs all over the world, but the most important examples of natural asbestos are in Libby (Montana, USA), El Dorado Country (California, USA), Fairfax Country (Virginia, USA), Cappadocia (Turkey), South Africa, China, Cyprus, France, Greece, Spain and Russia (Paglietti, et al., 2011).

The main Italian asbestos-bearing ophiolitic complexes are the Lanzo Massif (area of important disused asbestos mines in Piedmont region), the area of calc-schists with ophiolites in the western Alps. Here is situated the largest asbestos quarry in Europe, at Balangero (Piedmont, Italy), which was closed in 1990 to begin the reclamation work and which was never reopened in application of the Italian law n.257/1992. Other asbestos mines are in Valmalenco (Lombardy) and Emarese (Aosta Valley). In Italy, about 10% of the territory (Figure 7) is made up of ophiolite tectonic units (cropping

out in Lombardy, Aosta Valley, Piedmont, Liguria, Calabria and Basilicata) or flysch containing ophiolitic allochthones (Emilia Romagna and Tuscany).

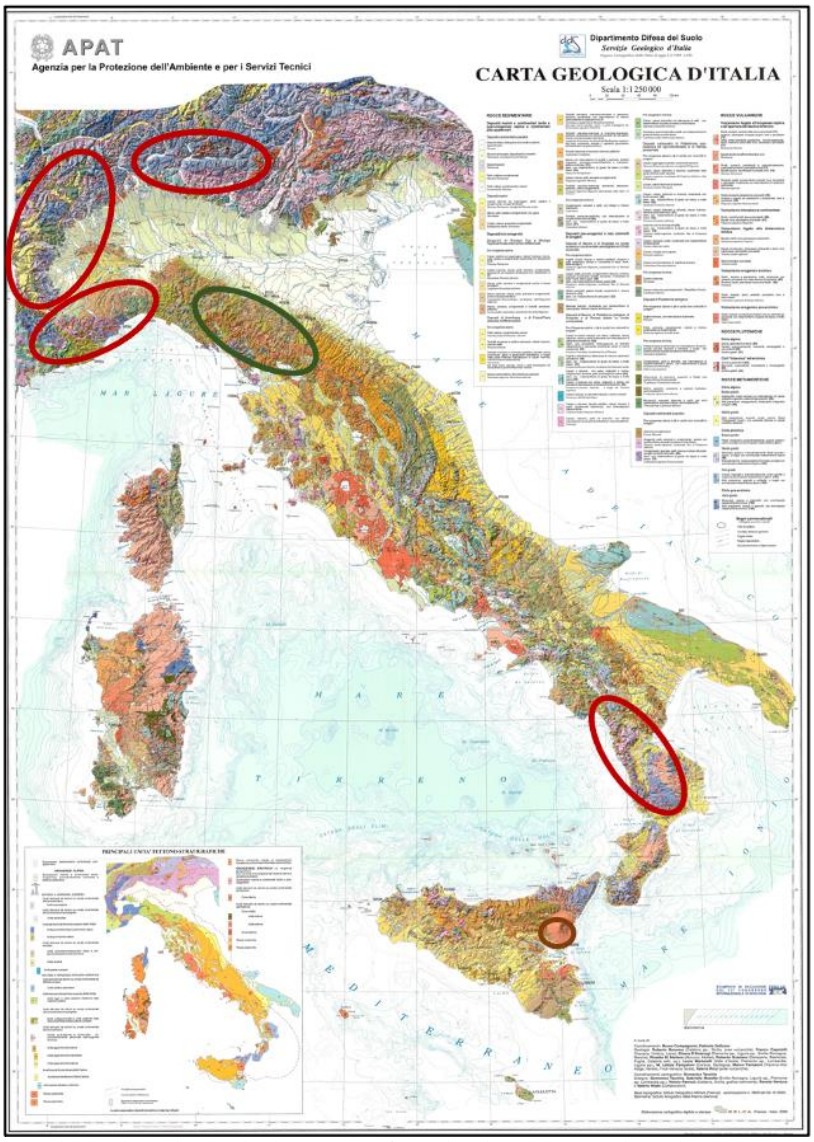

Figure 7. *NOA in Italy. Red circles: ophiolitic units of Lombardy, Trentino Alto Adige, Aosta Valley, Piedmont, Liguria, Basilicata and Calabria. Green circles: flysch units containing sedimentary rocks derived from the dismantling of asbestos-bearing lithologies of Emilia Romagna and Tuscany. Brown circle: benmoreite volcanic rocks of Sicily. www.isprambiente.gov.it.*

The main varieties of asbestos found in the Italian territory are chrysotile, tremolite and actinolite. According to Compagnoni and Groppo (2006), chrysotile is almost always associated with serpentinised ultramafic rocks, a fibrous phase from low-grade ocean floor metamorphism. Conversely, tremolite and actinolite can form in calc-schists, actinolite schists, chlorite-schists, greenschist facies metabasites and ophicarbonate rocks of low-grade orogenic metamorphism processes.

In general, the ophiolitic sequences of the western Mediterranean (Alps, Apennines and Alpine Corsica) are considered fragments of the oceanic lithosphere of the Tethyan basin, the ancient

Ligurian-Piedmont ocean that developed in the Middle Jurassic between the passive continental margins of the diverging plates Europe and Adria in connection with the opening and the expansion of the Central Atlantic Ocean (Bortolotti & Principi, 2005).

In addition to the classical ophiolitic model, along the Alpine chain some tectonic units show associations between ophiolites and rocks of continental origin (e.g., External Ligurian Units, Northern Apennines). Associations of this type are currently interpreted as representing original transitional domains between the oceanic crust of the Ligurian-Piedmont Jurassic basin and the continental crust of the Adria plate (Marroni & Pandolfi, 2007).

The ophiolites, or the fragments of the ocean basin, are preserved within the Ligurian Units, which have been divided into Internal and External based on their lithostratigraphic and structural characteristics (Elter & Pertusati, 1973; Elter, 1975a; Elter, 1975b). While the succession of the external Ligurian Units derives from a sector adjacent to the continental margin of the Adria plate (Abbate et al., 1980), the internal Ligurian Units show a typically oceanic character (Decandia & Elter, 1972). The subsequent subduction of the European paleo-margin and the Ligurian-Piedmont basin below the African paleo-margin, followed by the subsequent continental collision.

In central-western Liguria outcrop the Alpine ophiolites that belong to the Voltri Unit and the Sestri–Voltaggio Zone). Also, Palaeozoic amphibolites are regarded as rocks with potential asbestos content. Meanwhile, in eastern Liguria outcrop the Apennine ophiolites in the Bracco–Graveglia Unit (Internal Liguride Units) (Figure 8).

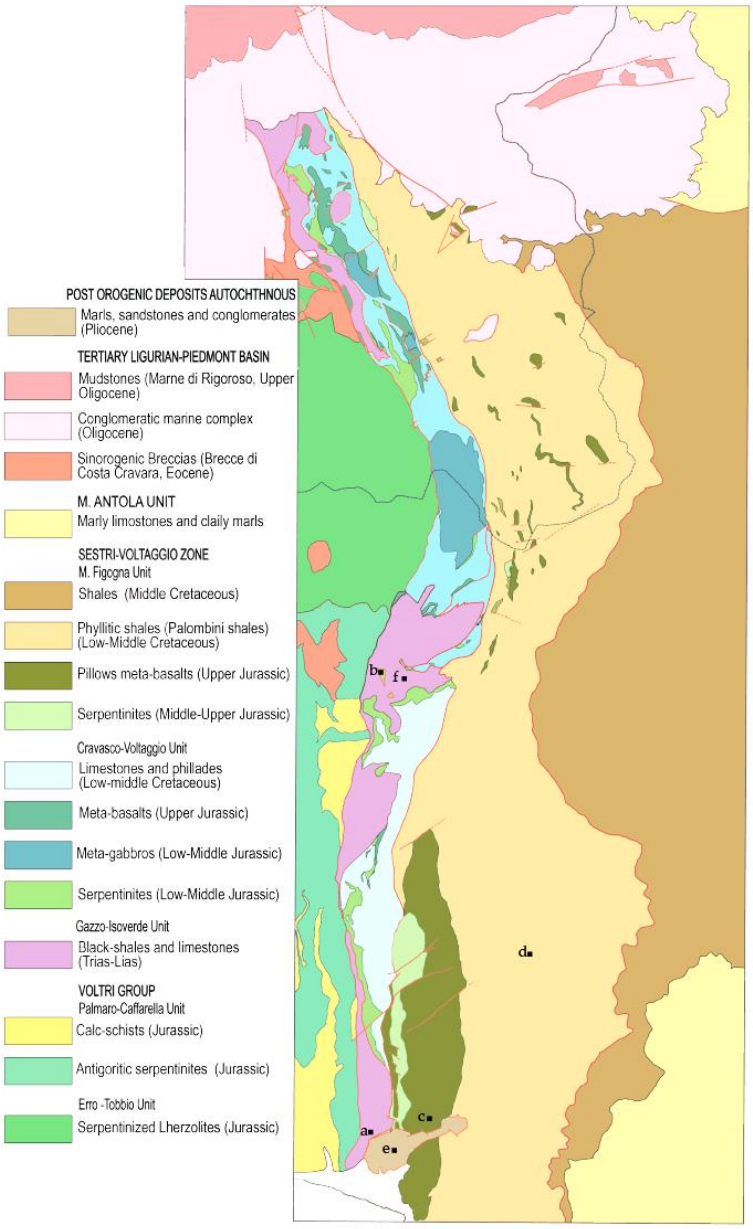

***Figure 8**. Geological sketch map of the Sestri–Voltaggio Zone and sampling area, respectively: (a) meta-argillites, (b) serpentinite, (c) metabasalts, (d) calc-schists, (e) debris, and (f) soil (Gaggero et al., 2017, modified after Cortesogno and Haccard, 1984).*

The units belonging to the External Ligurides also crop out in Emilia-Romagna and Tuscany and are commonly included in marls and sandstones.

An ophiolitic detrital component was found in tertiary clastic sedimentary rocks (sandstone, conglomerates and breccias, etc.) and in the quaternary deposits (fluvial, fluvial and glacial) derived from the erosion of Jurassic ophiolites and of marly-arenaceous sedimentary formations belonging to the Piedmont Tertiary Basin (BTP).

Asbestos minerals are also found in the southern segment of the Apennines in the ophiolitic sequence along the Calabrian–Lucania border and in northern Calabria: the Sila Piccola area.

In the Sila Piccola area (Figure 9), the ophiolitic sequence belongs to the Gimigliano-Mount Reventino Unit. This Unit consists of metabasites (i.e., metabasalts, gabbros and dolerites) and serpentinites with a metasedimentary cover made up of marble alternating with calc-schists and quartzites (Punturo et al., 2015 and references therein; Bloise et al., 2016). Asbestiform tremolite is the main constituent of metabasites followed by minor actinolite. Some rare chrysotile fibres occur within metabasite that crop out in the surroundings of Mt. Reventino. Asbestiform tremolite occur within the serpentinites together with chrysotile.

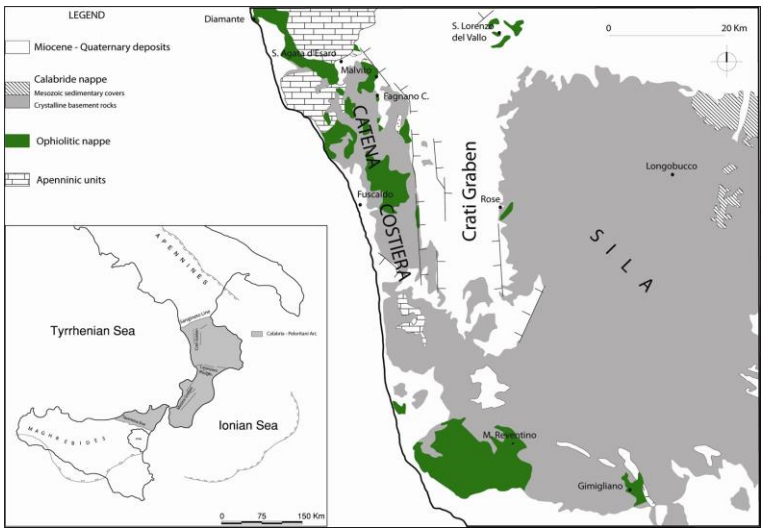

Figure 9. *Geological sketch map of the northern sector of the Calabrian-Peloritani Orogen and ophiolites crop out (Punturo et al., 2015).*

The ophiolitic Units (from the Cretaceous-Paleogenic age) of the Calabrian-Lucan Apennines emerge along the north-eastern side of the Pollino Massif (Figure 10). The subduction of the oceanic crust, below the continental crust of Calabria, between the Upper Cretaceous and the beginning of the Oligocene, led to the construction of an accretionary prism, from the original Neothethyan successions, that include remains of oceanic crust (ophiolites).

The most abundant asbestos variety in serpentinites is chrysotile followed by lizardite, antigorite and polygonal serpentine. In lower amounts, tremolite and actinolite are also present.

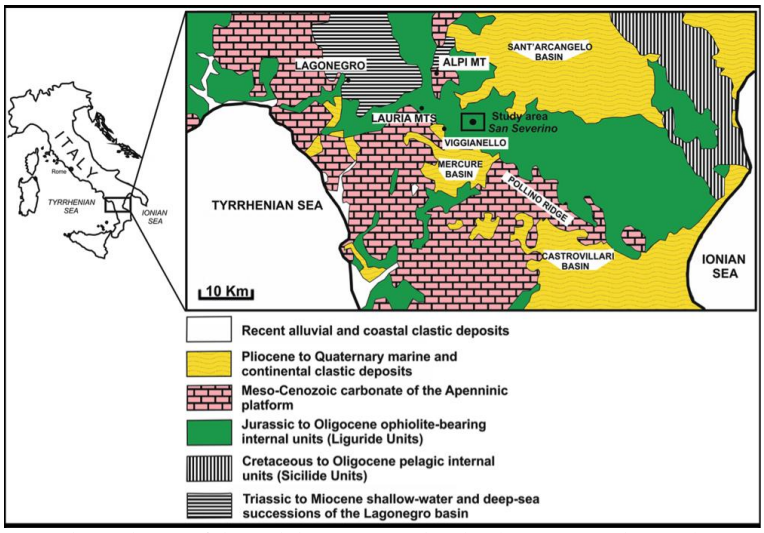

Figure 10. S*chematic geological map of the Calabrian-Lucan border (Punturo et al., 2018).*

Finally, fluoro-edenite (ideally $NaCa_2Mg_5(Si_7Al)O_{22}F_2$), also classified as asbestos, was found both as prismatic and as asbestiform fibres in Monte Calvario on the southwestern flanks of Mt. Etna Volcano (Sicily). Intercalated in the stratigraphic succession exposed in this area, there are massive and stratified ash and scoria flow deposits of the Biancavilla-Montalto ignimbrite. The host rock consists of a locally metasomatised, benmoreitic lava dome and dyke complex and associated autoclastic breccias. Fluoro-edenite crystals occurs within in the altered lava portions and in fractures, as well as in the breccia (Burragato et al., 2005).

4. REGULATORY FRAMEWORK

Asbestos is a known human carcinogen, if inhaled, and this is the reason why it is considered one of the most dangerous and complex factor to face during tunnel excavations and quarries exploitation in asbestos bearing rocks, both for workers' safety and for the disposal of contaminated excavated material. The risk related to the natural occurrence of asbestos, derives from the possible dispersion of asbestos fibres, both for natural processes but also and above all for anthropogenic activities such as mining, drilling, excavation and demolition (Coraglia et al., 2006; Bellomo et al., 2018).

The most important tests in the monitoring field are the following:

- D7200-06: Standard Practice for Sampling and Counting Airborne Fibres, Including Asbestos Fibres, in Mines and Quarries, by Phase Contrast Microscopy and Transmission Electron Microscopy (ASTM, 2006).
- D6281-15: Standard Test Method for Airborne Asbestos Concentration in Ambient and Indoor Atmospheres as Determined by Transmission Electron Microscopy Direct Transfer (TEM) (ASTM, 1998).
- ASTM D7521-16 Standard Test Method for Determination of Asbestos in Soil (ASTM, 2016).

Additionally, the European normative standards are not straightforward about correct reading and counting of fibres in asbestos containing materials. Below are the most significant regulations:

- Commission Directive 1999/77/EC adapting to technical progress for the sixth time Annex I to Council Directive 76/769/EEC on the approximation of the laws, regulations, and administrative provisions of the member states relating to restrictions on the marketing and use of certain dangerous substances and preparations (asbestos).
- Directive 2003/18/EC of the European Parliament and of the Council of 27 March 2003 amending Council Directive 83/477/EEC on the protection of workers from the risks related to exposure to asbestos at work.
- World Health Organization. WHO air quality guidelines, second ed. Asbestos Report on a work group meeting, Copenhagen, Denmark (WHO, 2000).

- Directive 2009/148/EC of the European Parliament and of the Council of 30 November 2009 on the protection of workers against the risks associated with exposure to asbestos.

4.1 Counting criteria and cleavage fragments

A worldwide regulatory and scientific gap concerns the classification criterion of asbestos. Classification systems are generic, subject to bias and not always applicable to amphiboles. In fact, there is not a clear boundary that allows to discriminate which are the fibrous and asbestiform amphiboles (i.e., from their crystallization) and which are coming from the critical dimensions following the comminution of an acicular crystal. In the first case, the amphibole can have a morphology similar to the one of chrysotile (Figure 11 a-b); in the second case, it appears as cleavage fragments (Figure 11 c-d) along the systems of cleavage traces, with dimensions and geometric ratios that however allows the determination as asbestos.

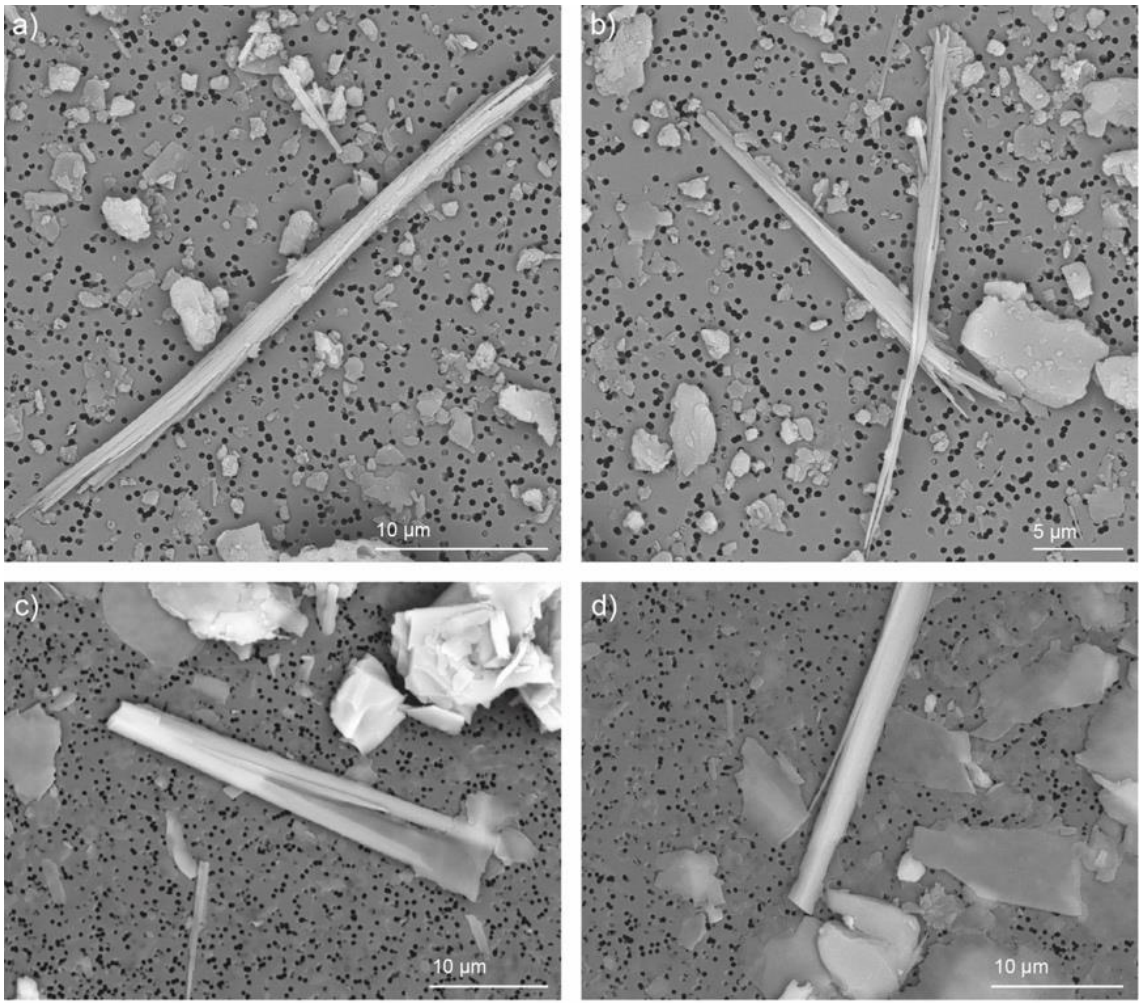

Figure 11. *SEM images. Example of asbestiform (a-b) and non-asbestiform (c-d) amphiboles of the tremolite-actinolite series. HV: 20 kV; Det: BSE.*

Usually, but not always, asbestos and non-asbestos fibres of amphibole group have similar size characteristics, but morphological differences. In general, the non-asbestiform amphiboles have fibres which are rigid and parallel-sided. These fibres have a quadrilateral or polygonal cross section, with variable size distributions of width to length ratios that are dependent upon the mineral type and its geological source.

A great diversity in the size and morphology of particles produced from the serpentine asbestos chrysotile and the fibrous and asbestiform varieties of amphiboles does exist. The morphology of chrysotile asbestos particles is distinctive; it generally consists of more uniformly sized fibril that occur either singly or as bundles. The size and appearance of single chrysotile fibril are unique to this mineral and can help in its identification. However, also non-asbestiform but fibrous varieties of antigorite and lizardite sometimes have an appearance similar to chrysotile. In this case, they cannot be distinguished by microanalysis, as polymorph.

It follows that, prismatic amphiboles and serpentine crystals and cleavage fragments are not yet univocally regulated as asbestos in countries like Italy, Europe, the United States of America and Canada. The approach to quantification and analysis of asbestos in bulk materials is not univocal (Cavariani et al., 2010; Militello et al., 2019). In the national and international regulatory framework, there are mainly two opposite concepts of classification, and therefore variable concern about the particles.

- NIOSH and EPA propose a very cautious approach in favour of exposed workers, therefore the methods of quantification (Method 7400 ‘A’ and ‘B’) of asbestos are much more stringent and strict (NIOSH, 1994). Indeed, any mineral very thin and long, with a high aspect ratio can be called fibrous (Gualtieri, 2017 and references within). The NIOSH, the Occupational safety and Health Administration (OSHA), WHO and EPA, are in favour of including cleavage fragments within fibre counts taking into account length and diameter, as it is sometimes difficult to distinguish amphibole asbestos from prismatic crystals or cleavage fragments, especially if associated (Harper et al., 2012 and cited bibliography).

- The American Society for Testing and Materials (ASTM) restricts the counting field only to those mineral phases whose appearance meets specific characteristics (curvature, flaking, presence of fibrils at the apex of the beam) as those described by NIOSH and length > 10 μm or width <1 μm (Harper et al., 2008, 2012).

4.2 Counting criteria

The classification and the distinction of a particle as either a real asbestiform mineral or a cleavage fragments (non-asbestiform) has a key role in establishing a reliable asbestos hazard scenario.

The evolution of the asbestos hazard is based on counting criteria used to determine the amounted of "regulated/countable fibres", according to WHO, 1997. During grinding, non-asbestos crystal can break along preferred cleavage sheet that may be mistaken for asbestos fibres (Belardi et al., 2018). Nevertheless, different procedures have been proposed for refining the classification of particles as asbestos or fibres originated by preferential cleavage fragments. Moreover, these counting rules are based on individual analytical skill, and misclassifying particles implies a high error rate leading to an overestimation of risk (Van Orden et al., 2008).

Often, asbestiform fibres and cleavage fragments of the same mineral show a significant overlap in the aspect ratio, making it clearly difficult to distinguish among asbestiform fibres and cleavage fragments using aspect ratio alone. Currently, there is no agreement on a means of making such a distinction (Vallero et al., 2009).

According to ANSES (2014), in the current state of knowledge, concerning their health effects, there is no reason to make a distinction between non-asbestiform and asbestiform amphiboles, in particular due to difficulties related to their characterisation and to their differentiations by routine analytical methods.

Many researchers disagree on counting protocols. Most historical exposure databases include only fibres longer than 5 µm. Risk assessment models usually show a large portion of the risk as due to fibres longer than 5 µm and some models suggest that a 10 µm level relates to more than 99% of the adverse health effects. Some risk models also include a factor for fibres less than 5 µm, suggesting that these may have some role in risk assessment, albeit much less than the effect for longer fibres. Table 1 lists only some of the asbestos counting criteria used.

Table 1. *Counting criteria adopted by some authors for asbestos identification procedures. Modified from Militello et al. (2020).*

Reference	Single particle
Stanton et al. (1981)	L > 8 µm; D < 0.25 µm
AHERA method (1987)	A/R ≥ 5:1
EPA (1993)	A/R 20:1-100:1
Berman and Crump (2003)	L > 10 µm; D < 0.4 µm; A/R >25:1
Harris et al. (2007)	D < 0.5 µm; A/R 20:1-100:1
Chatfield (2008)	D < 1.5 µm; A/R > 20:1

Van Orden et al. (2008)	A/R > 5:1
Van Orden et al. (2009)	D < 0.5 μm; A/R > 16:1
Harper et al. (2012)	D <1 μm

Stanton et al., (1981) correlated the asbestos hazard to the occurrence of EMP having size > 8 μm in length and < 0.25 μm in diameter. The AHERA method (Asbestos Hazardous Emergency Response Act) suggested to consider a 5:1 as the minimum aspect ratio. To report further examples, EPA (1993) method noted that the mean aspect ratios for asbestiform fibres ranges between 20:1 to 100:1 (or higher). Conversely, cleavage fragments of the same phases are generally characterised by aspect ratios lower than 20:1 (or less). Berman and Crump (2003) proposed a new risk model protocol by considering particles (not differentiating between asbestiform and non-asbestiform fibres) longer than 10 μm, thinner than 0.4 μm and an A/R > 25:1. Harris et al. (2007) clearly establish the difference between fibres and acicular particles. The first are thin particles (width ≤ 0.5 μm) with parallel sides, smooth surfaces and no discernible crystal faces, characterised by very high (20:1 to 100:1, or higher) aspect ratios and often displaying curvature. Conversely, acicular particles are thin (width ≤ 0.5 μm) with generally moderate (10:1 to 20:1) to high (> 20:1) aspect ratios and developing crystal faces.

Chatfield (2008) proposed a protocol that defined as asbestiform only those fibres with widths ranging from 0.04 μm to 1.5 μm and aspect ratio from 20 to 1000. Accordingly, elongated particles out of these ranges are considered non-asbestiform.

All particles thinner than 1.5 μm and with A/R exceeding 20:1 would be classified as asbestos. In Van Orden et al. (2008; 2009) the asbestos samples average 0.27 μm in width with 90% thinner than 0.5 μm. In contrast, the non-asbestos amphiboles average 0.97 μm wide, with 75% wider than 0.53 μm. The average aspect ratios were 76:1 for asbestos and 16:1 for non-asbestos particles. Furthermore, the authors proposed a multidisciplinary procedure to differentiate between the two by integrating chemical and morphological features at the scale of Transmission Electron Microscopy (TEM). Finally, the method introduced by Harper et al. (2012) is based on microscopic measurements and includes all EMP showing width below 1 μm (Belardi et al., 2018).

Aspect ratio is therefore the main feature used to discriminate asbestiform fibres from cleavage fragment. Several minimum values of aspect ratio have been suggested, ranging from 3:1 to 5:1 to 20:1 or greater. Wylie et al., (1993) showed that the average aspect ratio in asbestos fibres is 8–10 times greater than in non-asbestos particles.

Currently, no agreement is achieved on the bearing of making such a distinction. Some authors consider fibres with length less than 5 μm to be considered hazardous as well. Vallero et al. (2009) argue that the lack of studies on the length of fibres must be monitored: caution would include all

size fractions above 0.5 μm. However, fibres thicker than 3 μm are less concerned as they are less liable to penetrate the lower regions of the lung.

4.3 Italian regulation: open problems in analytical methodologies

In Italy, problems of interpretation, classification and evaluation of asbestos content arose related to the production and processing of excavated soils and rocks (Gaggero et al., 2017). Among the risk assessment protocols specified by regulations governing a reclamation work in Italy, the step of verifying the presence and content of asbestos in bulk materials is a mandatory action that affects the subsequent type of intervention (Legislative Decree (L.D.) 152/2006).

The guidelines issued from the ministerial decrees do not guarantee the compatibility and reproducibility of results among different laboratories, as they lack a precise description for sample preparation and analysis, thereby generating the possibility of variability in the results and therefore in estimates.

The Ministerial Decree (M.D.) 06/09/1994 contains guidelines relating to standards and technical methods for risk assessment, control, maintenance and reclamation of materials containing asbestos present in building structures. Moreover, talks about quantitative determination of asbestos in bulk samples (general aspects of the analytical problem) and quantitative determination of airborne asbestos fibre (concentrations in indoor environments). This decree has now been supplemented by the Decree of the President of the Republic (R.P.D.) 120/2017.

The M.D. 10/8/2012 n. 161 regulates the use of excavated soils and rocks. In Annex 4, which lists the physical chemical characterization procedures and the estimate of environmental qualities, it is established that the samples to be analysed in the laboratory must be free of the fraction greater than 20 mm (to be discarded in the field). So, the analytical determinations must be performed on the particle size of less than 2 mm and the concentration (mg/kg) must be calculated by referring to the weight of the entire sample with a size less than 20 mm, including the lithic skeleton (20 mm – 2 mm). The results of the analysis should be compared with the Contamination Threshold Concentrations (CSC) referred in L.D. 152/2006. For example, the CSC for the asbestos parameter in bulk sample is indicated in 1000 mg/kg and M.D.161/2012 establishes that the asbestos content must be lower than 1000 mg/kg to re-use excavated materials as by-products.

However, parameters indicated by M.D. 161/2012 are not considered "precautionary" by the Regional Environmental Protection Agencies (ARPA), as they do not provide an estimate of the total fibres potentially released by a rock. Therefore, it is more prudent to follow the M.D. 06/09/1994, that indicate to refer to the weight of the entire sample with grain size below 20 mm.

The analysis of asbestos content is required as a basis for classifying geomaterials and for providing information regarding their disposal. To evaluate the qualitative (presence/absence of asbestos) and quantitative (the concentration of asbestos by weight) aspects of asbestos content, the International Organization for Standardization (ISO 22262-2:2014 (EN)) has prescribed the use of several techniques (optical and electron microscopy and gravimetry) either singly or in combination. In contrast, Optical Microscopy (OM) has been recommended as the primary technique for identification in the regulations of several countries (Lee et al., 2008). Several analytical techniques within OM have traditionally been used and include visual evaluation, Stereomicroscopy (STM), Phase-Contrast OM (PCOM) with the use of Polarized light (Pol), chromatic dispersion, and point counting (Cavariani et al., 2010).

The M.D. 06/09/1994 proposes the use of the following techniques for the determination of asbestos in bulk samples:

1) PCOM, X-Ray Diffractometry (XRD) and Fourier Transform Infrared Spectroscopy (FTIR) techniques for the quantitative determination of asbestos when the content exceeds 1% by weight.
2) Electron microscopy techniques, such as SEM coupled with EDS and TEM, for quantitative information on asbestos when the content lies between 0.01% and 1% by weight. In particular, the SEM–EDS technique can detect asbestos concentrations between 100 ppm (0.01%) and 10,000 ppm (1%) or higher, providing quantitative results for asbestos contents between 1000 and 10,000 ppm and semi-quantitative results for contents of <1000 ppm (0.1%) and >10,000 ppm.

4.3.1 Constraints and limitations on sample preparation

It can be inferred that methods described in the ministerial decrees are just guiding procedures for the detection and quantification of asbestos fibres and lack a precise coding of sample preparation. If the procedures for the detection and quantification of asbestos fibres are replicable, precise specifications regarding sample preparation are lacking. These regulations, in fact, do not consider heterogeneity of the rock/deposits, sampling method, the mode and duration of comminution, initial fibre concentration and possible formation of new fibres after comminution, a fundamental step for the preparation of sample, thus, not guaranteeing intra and inter-laboratory reproducibility.

Moreover, once the representative sample is issued from the outcrop or deposit in the field, the analysis is carried out on a small subsample, which must be representative of the material of the sample (i.e., ensuring that the subsample reflects all grain size classes and fabric types of the

macroscopic sample) (Turci et al., 2015). The type and duration of milling depend on the hardness of the material. Milling can transform the material (Bloise et al., 2018; Baietto et al., 2019) by modifying the size and the number of asbestos fibres that are subsequently counted using microscopy techniques, or by altering the integrity of the crystalline structure that is detected using XRD (ISO 2009; Wylie & Candela, 2015). Such constraints involve close attention during the milling phase regarding to its duration and the properties of the milled material.

A further limitation is that the analysis is performed on a limited portion of the subsample where dimensions, grain size distribution, number, and types (e.g., bundles, clusters, and fibrils) of asbestos fibres are observed (Cavariani et al., 2010). This requires that the analysed parts of the subsample are representative of the subsample itself.

4.3.2 Comminution methods

Mechanical comminution is the reduction of solid materials from an average particle size to a smaller average size. Size distribution and shape of the final products depend on the nature of the minerals (and therefore on the lithotype), but also depend on grinding conditions and type of mill. The type and duration of grinding, controlled by rock hardness, can deeply transform the material itself by changing the size, and hence the number of fibres that are counted under microscopy (Cavariani et al., 2010) as well as their pristine crystallinity (Bloise et al., 2018).

In addition, no worldwide regulation suggests what instrument should be used to grind the samples, to be subsequently analysed to quantify the presence of asbestos in excavated soils and rocks.

For instance, Cossio et al., (2018) used the Jaw Crusher Retsch BB 200 equipped with stainless steel breaking jaws and variable openings to obtain a size reduction from < 90 mm down to < 2 mm. Chatfield (2018) crushed by agate mortar and pestle the amphibole-containing material for TEM investigations (ISO 13794 (1999)). In Baietto et al., (2019), samples were ground in an agate jar closed with a sealing gasket lid (model number 952/2 from Humboldt-Wedag).

Disk pulveriser, plate grinder cross beater, freezer mill or ball mill are also used. Moreover, Salamatipour et al. (2016). showed that wet grinding preserved fibre integrity and originated individual fibrils with high aspect ratio, whereas dry grinding broke fibres, primarily creating fibre bundles with smaller aspect ratio.

Therefore, grinding is an extremely delicate stage and is often the reason for the scarce reliability of quantitative determinations based on counting of the number of fibres in asbestos containing materials (Cavariani et al., 2010).

5. MATERIALS AND METHODS

5.1 Materials

The samples under study were selected because of their variety and conspicuous presence of fibrous but not asbestiform amphiboles of the tremolite-actinolite series, as well as the three polymorphic varieties of the serpentine, however associated with host rocks with very different mineralogical and petrographic characteristics. In fact, the sample set (Table 2) consists of various lithotypes belonging to metamorphic units spanning from oceanic to continental crust sequences characterised by different petrological evolution. Due to the considerable variety of minero-petrographic characteristics (which will be described in chapter 6), the entire sample set was used in specific investigations of this PhD work. Therefore, in the following chapters it will be specified which part of the sample set was selected for a given study.

Table 2. *Samples and their provenance.*

Sample	Lithotype	Provenance
F1	Amphibole vein in ophicalcite	Ligurian Apennines (Italy)
F2	Amphibole vein in serpentinite	Ligurian Alps/Apennines (Italy)
F3	Amphibole vein in serpentinite	Ligurian Apennines (Italy)
P1	Amphibole-bearing metagabbro	Ligurian Apennines (Italy
P2	Amphibole-bearing dolomite	Swiss Alps
P3/A5	Actinolite schist	Ligurian Alps (Italy)
A1	Actinolite schist	Ligurian Alps (Italy)
A2	Amphibole-bearing vein	Swiss Alps
A4	Amphibole vein in serpentinite	Ligurian Apennines (Italy
S2	Amphibole vein in serpentinite	Aosta Valley (Italy)
S3	Metabasalt with plagiogranite vein	Piedmont (Italy)
S4	Pyroxenite cut by talc and actinolite vein	South Africa
A3/S1	Serpentinised peridotite with lizardite vein	Piedmont (Italy)

To address the study of the minerals of the amphibole group, 13 samples were selected, 3 with characteristics of asbestos (F1, F2 and F3) and 9 in the prismatic, acicular and fibrous varieties (P1, P2, P3/A5, A1, A2, A4, S2, S3, S4). While for the study of serpentine polymorphs, the A3/S1 sample was sampled in the Lanzo Massif in Piedmont.

5.1.1 Serpentinites

Samples F2, F3, A4, S2 and A3/S1 are serpentinites (Figure 12). Sample F1 is a vein isolated from an ophicalcite.

Figure 12. *Close up photographs of analysed samples: F1, amphibole vein in ophicalcite; F2, amphibole vein in serpentinite; F3, amphibole vein in serpentinite; A4, serpentinite with actinolite; S2, serpentinite with tremolite vein; A3/S1, serpentinised peridotite.*

Although the ultramafic system is chemically relatively simple, serpentinites are characterised by several microstructures that reflect different conditions of pressure and temperature, different extent of deformation and different types of fluids circulating at different moments in their evolutionary history. The host rocks are predominantly fine-grained. The contact of the vein with the host rock is clear and only rarely a reaction/alteration selvedge is observed.

The analysed serpentinites are crossed by metamorphic, mono- or polymineralic veins. Several generations of crosscutting veins associated by one or more fibrous phases, but mainly by fibrous and not asbestiform amphiboles of the tremolite/actinolite series have been recognised.

Most veins are composite fibres veins, but both syntaxial and antitaxial patterns of fibre growth occur as well (Gaggero et al., 2006; 2013).

In the F2 sample the geometry of the fibres indicates that fracture has been filled during an extension kinematics (syntaxial growth) and cutting (crack and seal). In this case, fibres are perpendicular to vein walls and bend towards the centre (Gaggero et al., 2006; 2013). Samples F1, F3, A4, S2 and A3/S1, instead show antitaxial veins (the fibre bundles are straight at the centre of the vein and folded to the proximity of the wall-rock), suggesting that vein fills are externally derived and indicating that "crack-seal "mechanism is responsible for this geometry.

Moreover, samples F1 and F2 have veins where the translucent fibre bundles are very flexible and soft. In F1 the fibres do not exceed one centimetre in length while the F2 sample records fibres

with lengths of decimetres and more at the scale of the outcrop. Samples A4 and S2 are characterised by the prismatic/acicular varieties of amphiboles. They contain straight and rigid fibres, of centimetre size. These varieties are sometimes so abundant that they can be considered the main constituents of the lithotypes in question. The F3 sample at the scale of the hand sample shows the presence of stiff and elongated fibres which however flake easily when touched, these are a woven mesh also rich in calcite and chlorite.

As regards sample A3/S1, the fibrous lizardite (10 cm in length), of green-grey colour, shows rigid and compact bundles of fibres. It is a serpentinite with some relics of the peridotitic protolith. Between the host rock and the vein, millimetre thick chrysotile vein filling is present.

5.1.2 Amphibole vein-bearing dolomite

Characterised by a coarse-grained (A2) or very fine (P2) matrix of dolomite and calcite (Figure 13). They present prismatic to highly asbestiform varieties of amphiboles that vary in colour between white and grey.

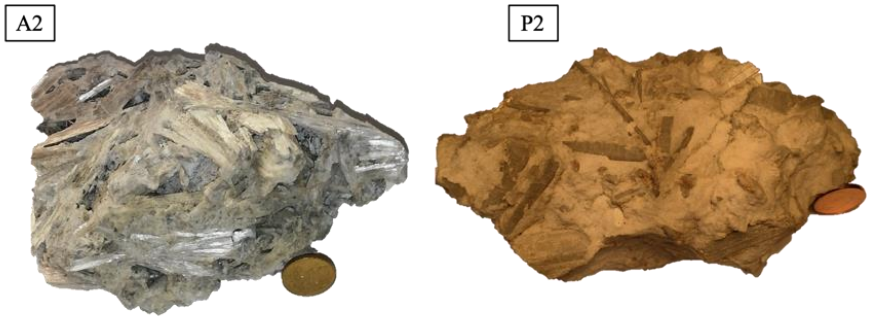

Figure 13. *Close up photographs of analysed samples: A2, amphibole-bearing vein; P2, amphibole-bearing dolomite.*

The fibres of variable length (centimetre) are straight and rigid (not flexible). The fibres appear translucent, in fibrous, granular or columnar aggregates. The tremolite and calcite veins are systematically close to calc-schists and therefore linked to the presence of CO_2-rich fluids.

5.1.3 Actinolite schists

Samples A1 and P3/A5 represent Actinolite schists. The veins are almost monomineralic, characterised by intense green colour (Figure 14).

Figure 14. *Close up photographs of analysed samples: A1, P3/A5 actinolite schists.*

The length of the fibres herein varies from millimetres to centimetres. They are acicular (it is possible to observe extremely fine components), rigid and never occur in bundles.

5.1.4 Metagabbro and Metabasalt

P1 and S3 are respectively a metagabbro and a metabasalt (Figure 15).

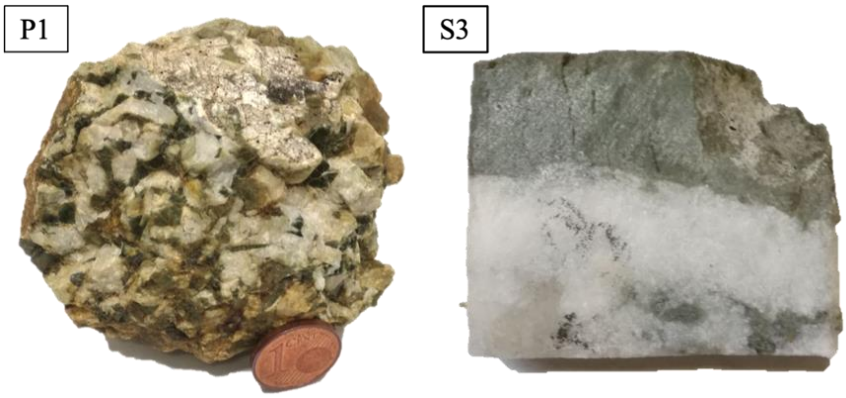

Figure 15. *Close up photographs of analysed samples: P1, amphibole-bearing metagabbro; S3, metabasalt with plagiogranite vein.*

These two samples contain significant amounts of elongated acicular amphiboles of micrometric dimensions. In the S3 sample the elongated and flexible amphiboles are distributed perpendicular to the contact between the metabasalt and the plagiogranite vein.

5.1.5 Pyroxenite

Sample S4 is a pyroxenite. This sample was selected because at the submicroscopic level it is characterised by a vein rich in potassic edenite but also by amphiboles of the tremolite and actinolite series (Figure 16).

Figure 16. *Close up photographs of analysed samples: S4, pyroxenite cut by talc and actinolite-filled vein.*

The amphiboles are arranged perpendicular to the length of maximum elongation of the vein and have an aspect that varies from acicular to fibrous.

5.1.6 Soil and rocks from Sestri-Voltaggio Zone

These samples were selected due to the assessed presence of asbestos in all lithotypes, a necessary condition for the use of the two decree protocols.

The samples were issued from outcrops along the Sestri–Voltaggio Zone (Central Liguria, Northern Italy) and are representative of metamorphic rocks (serpentinite, metabasalt, and calc-schist/metargillite) and sedimentary rocks/detrital (argillite, debris material, and soil) derived from an ophiolite succession and its cover (Figure 8).

Samples were taken from the following Units (from oldest to youngest). Meta-argillites (Late Triassic–Early Jurassic) belong to the Monte Gazzo–Isoverde tectono–metamorphic Unit, including carbonatic lithotypes (dolomites and recrystallised dolomitic limestones) intercalated with metapelites and marly limestones (Figure 17a); serpentinite and serpentine schist (Middle Jurassic) from the Cravasco–Voltaggio Unit, comprising variably metamorphosed, cataclastic chrysotile- and antigorite-bearing serpentinite (Figure 17b); metabasalts (Late Jurassic) from the Monte Figogna Unit, consisting of massive or more commonly brecciated pillow lavas that were subsequently recrystallised under pumpellyite–actinolite facies conditions during the Alpine event (Figure 17c); calc-schists (Cretaceous) from the Busalla Flysch Unit, consisting of grey/black shales with alternating crystalline limestone and/or schistose metapelites affected by low-grade metamorphism (Figure 17d); debris covers, Pliocene breccia, and conglomerates associated with marly clays, marls, siltstones, and fine sandstones (Figure 17e); and Quaternary soil-detritus composed of sand–silt matrix, clasts, and breccias with ophiolitic elements (Figure 17f).

Figure 17. *Microphotographs (80× magnification) of: (a) meta-argillites; (b) serpentinite; (c) metabasalts; (d) calc-schists; (e) debris and (f) soil (from Militello et al., 2019b).*

5.2 Methods

The mineral-petrographic characterization of serpentinites and other lithotypes cut from metamorphic veins (mainly consisting of asbestiform minerals of the serpentine group, but also of EMPs of the amphibole group) is affected by the difficulty of recognizing the different fibrous minerals through the investigation under optical microscope, because of their morphological and compositional similarity, and of the frequent accretions between two or more phases.

Therefore, the samples chosen for the PhD project were observed and studied using more than one technique, such as optical microscopy (OM), SEM/EDS, TEM/EDS and Raman spectroscopy. Moreover, microstructural relationships in the host rock and in the veins were evidenced. Finally, the Synchrotron Radiation X-ray Microtomograph (SR-μCT), was addressed, an unconventional technique for the characterization of NOA.

5.2.1 Scanning Electron Microscopy

SEM-EDS was used for the qualitative (morphological and chemical) and quantitative characterization of the veins. This is one of the best known and most used surface analytical techniques. Through the interaction of the electron beam with the sample, it allows to obtain images of the surface topography of samples in high resolution, with excellent depth of field.

Thin polished sections, coated with graphite were analysed by SEM-EDS TESCAN 3 XML (TESCAN, Brno, Czech Republic) installed at the Electron Microscopy Laboratory at the Earth, Environment and Life Sciences Department (DISTAV), University of Genoa (Italy). Qualitative and quantitative analyses were performed (the preparation protocol will be described later). SEM makes possible morphological investigations under higher magnifications (up to 10,000X) with coupled in situ microanalysis to obtain compositional information. The instrumental conditions used were: 20 kV of accelerating voltage (HV). The elemental analysis (counting time 30 seconds) of the minerals was carried out by energy dispersive X-ray spectroscopy (Oxford Instruments, AZtec 2.4).

5.2.2 Micro-Raman

Micro-Raman spectroscopy is an *in situ* analysis that allows the identification of fibrous phases, providing information on the different vibrational modes of molecules. In particular, this technique has the advantage of being able to use the sample as is, by positioning it on the stage of the microscope, or the same thin sections prepared for the analyses in optical microscopy can be used. Micro-Raman scattering measurements were conducted with a Horiba Jobin-Yvon Explora_Plus single monochromator spectrometer (HORIBA, Longjumeau, France) (with a grating of 2400 groove/mm) equipped with an Olympus BX41 microscope (HORIBA, Longjumeau, France), installed at the Earth, Environment and Life Sciences Department (DISTAV), University of Genoa (Italy). Raman spectra were excited by the 532 nm line. The spectrometer was calibrated to the silicon Raman peak at 520.5 cm^{-1}. The spectral resolution was ~ 2 cm^{-1} and the instrumental accuracy in determining the peak positions was ~ 0.56 cm^{-1}. Raman spectra were collected in the spectral ranges of 100–1100 cm^{-1} and 3000–3800 cm^{-1} for 15 s, averaging over 10 accumulations.

Micro-Raman spectroscopy allowed to recognize the serpentine polymorphs. This technique is efficient and reliable, to draw comparisons and ground for quantitative analyses.

5.2.3 Transmission Electron Microscopy

The Transmission Electron Microscopy (TEM) associated with the microanalysis system implements the previous techniques, reaching atomic resolutions that allow the recognition of the different minerals of the serpentine sample and of all types of amphiboles. The TEM was performed

using a Jeol JEM 1400 Plus (Tokyo, Japan) working at 120 kV, equipped with a double tilt holder to check the morphology of the samples and to obtain structural data by Selected Area Electron Diffraction (SAED) installed at the Department of Biology, Ecology and Earth Sciences, University of Calabria (Cosenza, Italy). Moreover, Energy Dispersive X-ray Spectrometry (EDS) performed using the Jeol allowed us to obtain Analytical Electron Microanalyses (AEM). In order to discriminate the mineral chemistry of asbestos fibres, three-point analysis were carried out on each single fibre. For TEM investigations, a small aliquot of the sample was ground using an agate pestle and mortar in isopropyl alcohol and then sonicated; this powder was then deposited onto a copper mesh grid coated with 200 Å carbon film.

5.2.4 Synchrotron Radiation X-ray Microtomography

This technique allows to reconstruct the 3D structures of a sample preserving its original structure as it is not destroyed in the preparation phase. Therefore, it can help to better observe the arrangement of the fibres in the three dimensions.

The samples chosen for microtomography were cut in the form of a parallelepiped with a square base (2×0.5 cm^2) and illuminated by a polychromatic X-ray beam (white beam configuration) in transmission geometry. The contribution of low energies in the beam spectrum was suppressed by applying 1 mm Si + 1 mm Al filters. The SR-µCT installed at the SYRMEP beamline of the Elettra synchrotron laboratory (Trieste, Italy) was performed with a fixed sample-to-detector distance of 200 mm and collected, for each sample, 1800 projections over a total scan angle of 180° with an exposure time per projection of 2s. The employed detector was a 16 bit, air-cooled, sCMOS camera (Hamamatsu C11440 22C) (Hamamatsu, Hamamatsu City, Japan) with a 2048×2048 pixel chip and an effective pixel size set at 1.95^2 m^2, yielding a maximum field of view of ca. 3.2^2 mm^2. Since the lateral size of the samples was larger than the field of view of the detector, microtomographic scans were acquired in region of interest mode (Maire et al., 2014). The 2D tomographic slices were reconstructed using the Syrmep Tomo Project (STP) house software suite (Brun et al., 2017), which allowed the application of different filters in order to reduce ring artefacts caused by detector inhomogeneity (Brun et al., 2013). A single-distance phase-retrieval algorithm (Paganin et al., 2002) based on the transport of intensity equation (TIE) was applied to the sample projections to improve the consistency of the morphological analysis. Combining phase-retrieval and filtered back-projection algorithms (Herman, 1980) allowed obtaining the 3D distribution of the complex refraction index of the imaged samples. This process reduces the edge-enhancement effect at sample borders, at the same time preserving the morphology of the smallest features. The obtained 3D volumes were

then segmented by manual thresholding. Three-dimensional renderings were obtained by VGStudio Max 2.2 software (Volume Graphics, Heidelberg, Germany).

5.3 Quantitative analysis protocol

5.3.1 Sample preparation

For safe handling of the sample, the operator is equipped with nitrile gloves and FFP3 mask, furthermore the operations took place exclusively under a hood with absolute filters installed at the FIBRES Clean Laboratory of the University of Genoa. This is a room working under depression and equipped with 4 levels of safety devices for the operator.

First, each sample was observed at the stereoscope for a preliminary petrographic and mineralogic characterization on a macroscopic scale. Then bulk sample (500 g) previously dried, was divided into four subsamples each weighing 125 g still representative of the bulk sample (i.e., more heterogeneous and including all the components).

Selected samples were subjected in parallel to two preparation protocols in parallel:

1) According to M.D. 06/09/1994 (total asbestos) which involves performing the analytical determination on a significant fraction of < 100 μm obtained by milling of a representative subsample with a grain size of ≤ 20 mm.

2) According to M.D. 161/2012 which establishes to perform the analytical determination on the grain size fraction < 2 mm and to relate the concentration to the entire sample including the skeleton (particle size fraction between 20 mm and 2 mm). Even in this case the fraction < 2 mm must be grinded to reach particle size < 100 μm.

Samples without the fraction greater than 2 mm were prepared only according to M.D. 06/09/1994.

Therefore, in both protocols, the material has to be grinded in order to pass through the sieve < 100 μm. Milling was carried out by a Retsch BB50 jaw crusher. Accurate cleaning of the jaw crusher by compressed air and milling of a neutral sample (quartz sand) between samples was carried out to avoid contamination. In order to standardize the preparation method, as much as possible, the samples, despite having different geo-mechanical characteristics, were ground to an equal speed of 750 rpm and a spacing between the jaws of 0.2 mm (± 0.1). The time intervals used to reach the

powder were different in relation to the hardness of the lithotype. After milling, the powder was weighed.

For each sample, 10 mg of powder were sampled, weighed by analytical balance (RadwagAs 220.R2), and suspended in 100 mL of deionised water. To improve the dispersion of the solution, the sample was left in an ultrasonic bath for 10 min. Using a vacuum filtration system, a known aliquot of the prepared dispersion containing ~1 mg of powder was deposited on a 47-mm-diameter polycarbonate membrane filter with a porosity of 0.8 µm. Subsequently, a quarter of the filter was cut out and fixed on an aluminium stub using a conductive glue (carbon tape). The filter was made conductive with a 25–50 nm layer of Au by cathodic sputtering (Quorum Q150T ES).

A flow diagram showing the main steps of the two procedures and the differences between them is presented in Figure 18.

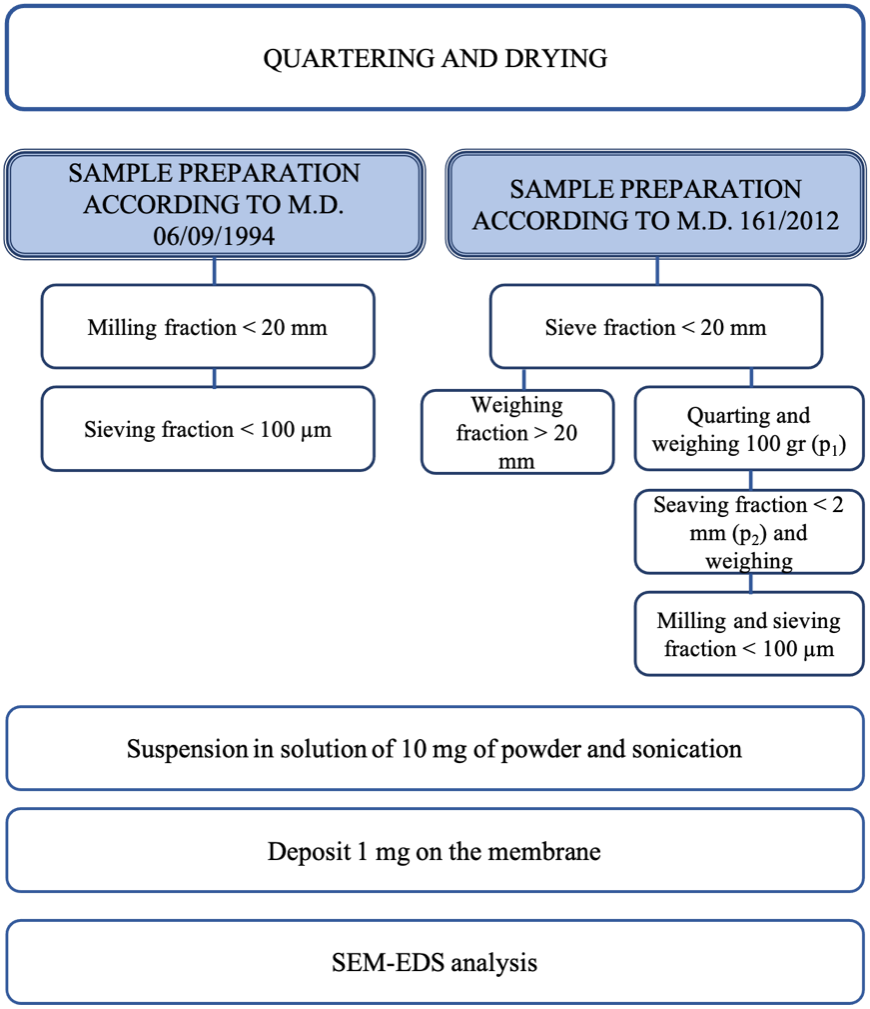

Figure 18. *Flow diagram of the sample preparation steps according to M.D. 06/09/1994 and M.D. 161/2012.*

5.3.2 Quantitative Analysis by Scanning Electron Microscopy

In order to calculate the concentration of asbestos fibres it is necessary to count and measure accurately all the fibres present in more than one reading field of the filter (the number of reading fields must be statistically significant). Samples were analysed using a working distance of 11 mm, 2000× of magnification and 20 kV energy of the incident beam. An area of 2 mm^2 (108 fields) in each subsample was measured, avoiding the overlap of read fields. Furthermore, for fibres that did not lie completely in the read-fields, only those parts included within the fields were measured.

According to M.D. 06/09/1994, the calculation of fibre weight was performed using densities of 2.6 g/cm^3 for chrysotile and 3.0 g/cm^3 for amphibole. Asbestos concentration C (mg/kg) in the sample was calculated as follows:

$$C = \frac{A \cdot (p_c + p_a)}{n \cdot a \cdot P} \cdot 10^6$$

$p_a = da \cdot \sum_j vj =$ total weight of amphibole fibres (mg)

$p_c = dc \cdot \sum_j vi =$ total weight of chrysotile fibres (mg)

Where:

A = effective filter area (mm^2)

a = reading field area (mm^2)

n = number of fields examined

P = total sample weight deposited on the filter (mg)

da = density of amphiboles ($gr/cm^3 = mg/mm^3$)

dc = density of chrysotile ($gr/cm^3 = mg/mm^3$)

vj = volume of the i-th fibre of amphiboles (mm^3)

vi = volume of the i-th fibre of chrysotile (mm^3)

Whereas according to the M.D. 161/2012, the concentration of asbestos is calculated on the fraction size < 2 mm. In detail is then determined by dividing the fraction of asbestos < 2 mm fraction (p_2) from the mass of the sample ≤ 20 mm (p_1), that is, the lithic skeleton material.

$$Asbestos\, mg/kg = \frac{C \cdot p_2}{p_1}$$

$p_1 =$ sample weight < 20 mm (mg)

p_2 = sample weight < 2 mm (mg)

For each asbestos concentration value, there is an analytical error associated with the method that depends on:

1) The statistics of the sampling of the fibres when reading the filter. In fact, the number of the sampled fibres on a given surface has a Poissonian distribution if the fibres are distributed randomly on the filter.
2) The width of the grain size spectrum of the fibres contained in the sample. The grain size spectrum of asbestos fibres produced in the grinding of a sample generally is well described by a lognormal distribution).

The error is therefore given by:

$$\frac{\Delta C}{C} \approx \frac{1}{\sqrt{N}} + \frac{\sqrt{\frac{(f - f_i)^2}{N(N-1)}}}{f}$$

where C is the concentration of asbestos in the sample, N is the number of fibres identified (the equation is significant only if N is sufficient to be within the limit of large numbers (≥30)), f is the mean weight of asbestos fibres (N) identified (mg), and f*i* is the weight of each single fibre of asbestos.

Although this technique has the great advantage of allowing the morphological investigation of the sample, the quantitative evaluation of asbestos fibres by means of SEM has the following limitations. The count of the fibres is extremely subjective due to the operator's ability to distinguish all the fibres present in the reading field and because SEM-EDS does not allow to recognize polymorphs. It is therefore impossible to distinguish, for example, chrysotile (considered asbestos by Law n. 257/92) from fibrous antigorite (not considered asbestos by Italian law).

6. MINERALOGICAL AND PETROGRAPHIC CHARACTERIZATION

All samples were observed under a polarizing microscope to study their microstructure and to identify the different paragenesis, with particular regard to amphiboles and the minerals of the serpentine group with asbestiform and non-asbestiform fibrous aspect. Table 3 summarizes the techniques used and the biological assays performed on each sample.

Table 3. *Analytical techniques used for each sample.*

ANALYTICAL TECNIQUE	SAMPLE												
	F1	F2	F3	P1	P2	P3/ A5	A1	A2	A3/ S1	A4	S2	S3	S4
	OM	OM	OM	OM	OM	OM	OM	OM	OM	OM	OM	OM	OM
									SR-µCT		SR-µCT	SR-µCT	SR-µCT
	SEM-EDS	SEM-EDS	SEM-EDS	SEM-EDS	SEM-EDS	SEM-EDS	SEM-EDS	SEM-EDS	SEM-EDS	SEM-EDS	SEM-EDS	SEM-EDS	SEM-EDS
									TEM-EDS		TEM-EDS	TEM-EDS	TEM-EDS
									µ-Raman				
			In vitro test	*In vitro* test	*In vitro* test	*In vitro* test	*In vitro* test	*In vitro* test	*In vitro* test	*In vitro* test			

6.1 Amphibole asbestos vein in ophicalcite – Sample F1

Sample F1 is represented by a vein of ophicalcite. Calcite matrix (Figure 19 a-b) occurs in elongated/fibrous and saccharoid textures (only in some parts). Deformed serpentinite lenses (possible remnants of the protolith texture) are dispersed in the carbonate matrix (Figure 19b). The elongated prismatic amphibole, whose optical characteristics correspond to actinolite, is included in variably sized and lens-shaped aggregates of antigorite (Figure 19b).

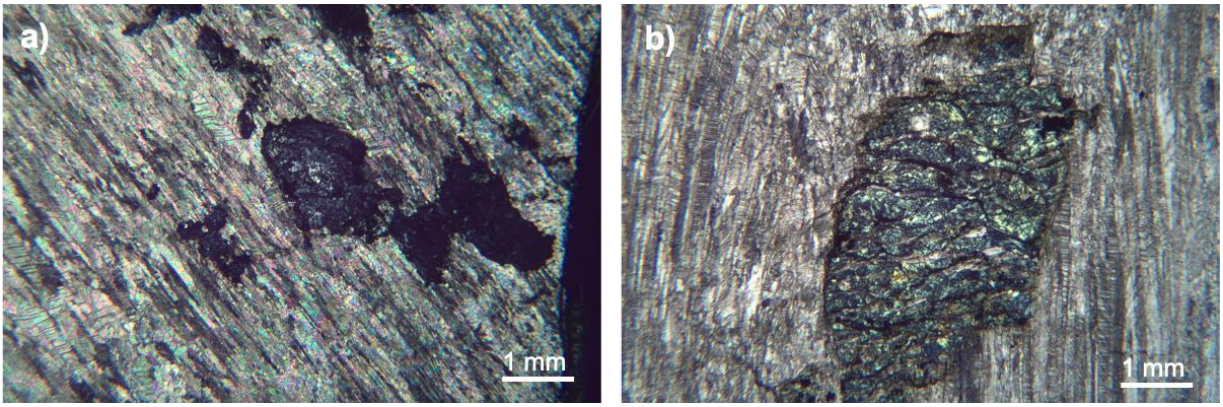

Figure 19. *Microphotograph of the vein associated to the ophicalcite. The vein consisting of antigorite serpentinite + amphibole nodules embedded in foliated calcite matrix (cross polarised light; Mag: 250x).*

Under SEM, the boundary between antigorite-amphibole nodules is evidenced in Figure 20 a-b. Figure 20b shows a detail of the serpentine nodules which vary in size and shape. At 500x of magnification in Figure 20c, and at 2000x in Figure 20f, the morphology of the serpentine results characterised by a plastic deformed aspect. The habit of amphibole is prismatic to stubby, with some exceptions (Figure 20e, centre) where fibres (length not exceeding 20 microns) with a low length/width ratio are observed.

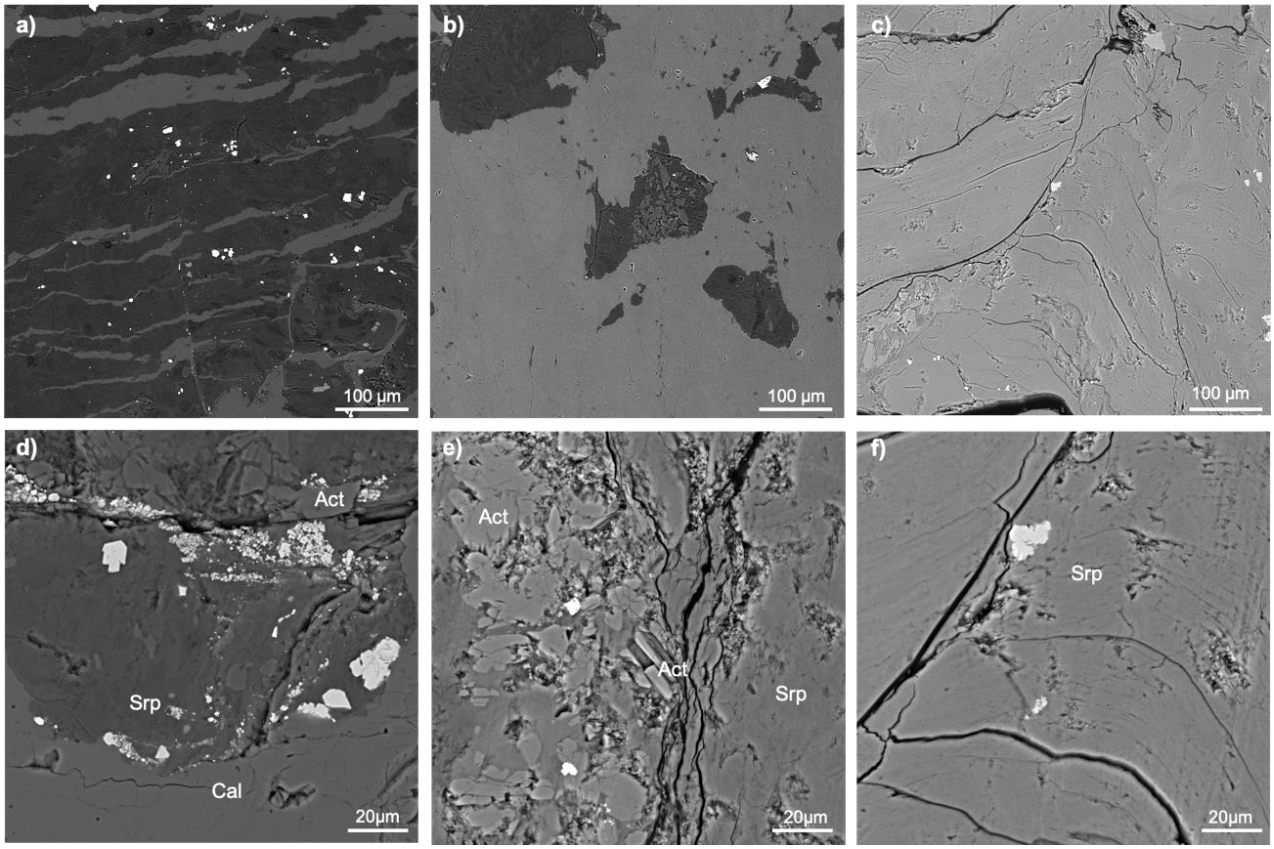

Figure 20. *SEM images from polished thin section of sample F1. Detail of the serpentinite nodules and associated calcite (a); serpentinite nodules immersed in the calcite matrix (b); deformed serpentinite (c); detail of the serpentinite nodule with prismatic and acicular amphiboles + oxides (d-e); detail of fractured and deformed serpentinite nodule (f). MAG: 500x in a, b, c and 2000x in d, e, f (HV: 20 kV; Det: BSE).*

6.2 Amphibole asbestos vein in serpentinite – Sample F2

Sample F2 is a serpentinite that preserved some mineralogical and structural relics of the peridotite protolith. The lizardite massive matrix, with mesh structure (Figure21a), is cut by sub-millimetric veins filled with chrysotile. Peridotite relics are represented by pristine clinopyroxene together with idioblastic magnetite. The contact between the host rock and the vein is clear and marked throughout the sample (Figure 21a). Figure 21b shows the amphibole-bearing vein. Fibres,

growing perpendicular to the serpentinite contact, are very elongated, slightly bent and build a dense and continuous mesh.

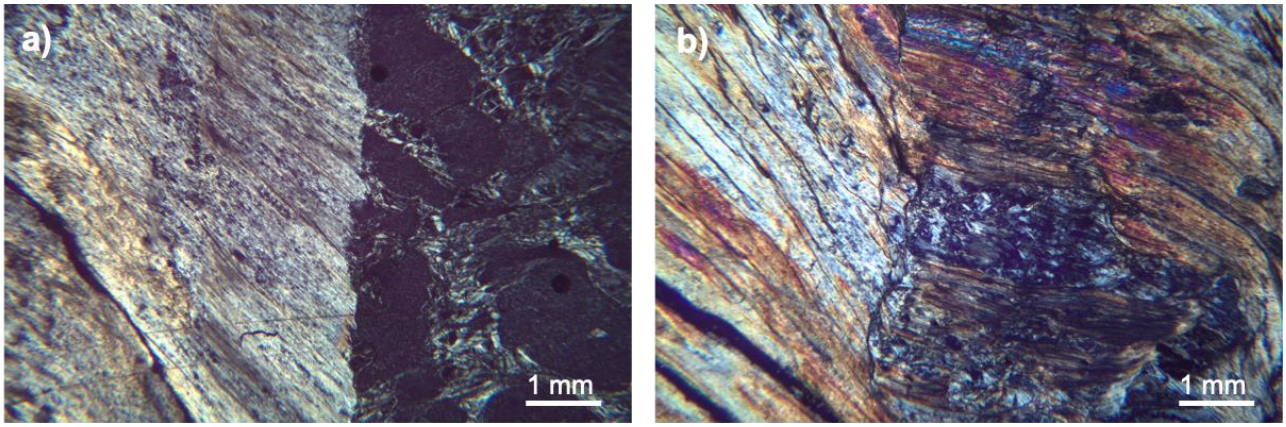

Figure 21. *Microphotograph of the contact between actinolite-tremolite vein and the lizardite-serpentinite. In the rock matrix (right part), serpentine aggregates with mesh structure (a); Detail of the actinolite-tremolite vein (b) (cross polarised light; Mag: 250x).*

Under SEM (Figures 22 a-c), the amphibole vein sometimes enters the serpentinite texture. This is clearly visible in Figure 22d where the amphibole developed inside the host rock. The habit is highly fibrous rigid bundles shows very high length/width ratios (Figures 22 e-f).

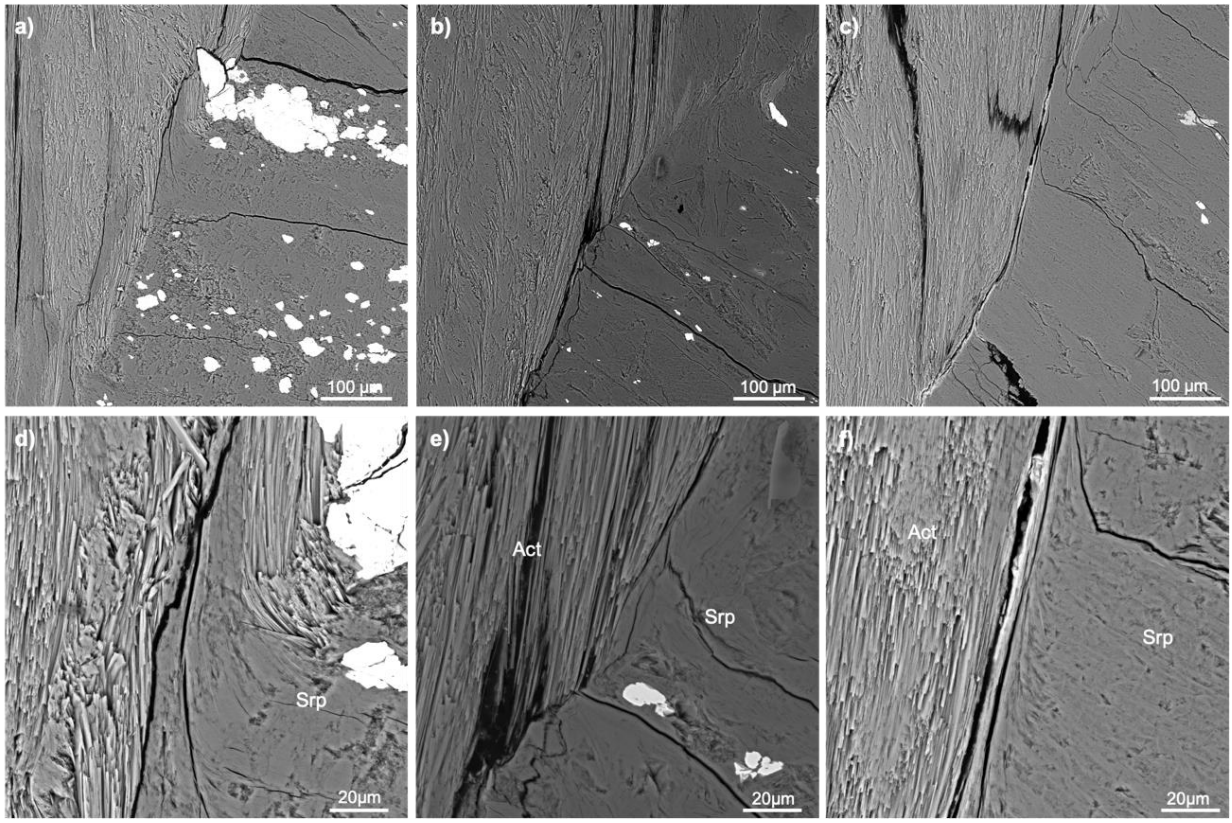

Figure 22. *SEM images from polished thin section of sample F2. In all the images, detail of the contact between the vein and the serpentinite. The amphibole is rigid, acicular and compact. MAG:500x in a, b, c and 2000x in d, e, f (HV: 20 kV; Det: BSE).*

6.3 Amphibole asbestos vein in serpentinite – Sample F3

Sample F3 is a serpentinite cut by a large (decimetre thick) amphibole-rich veins of the tremolite-actinolite series (Figures 23a-b). Chromiferous chlorite and spinel make a felt like texture. Amphibole habit is acicular to highly fibrous.

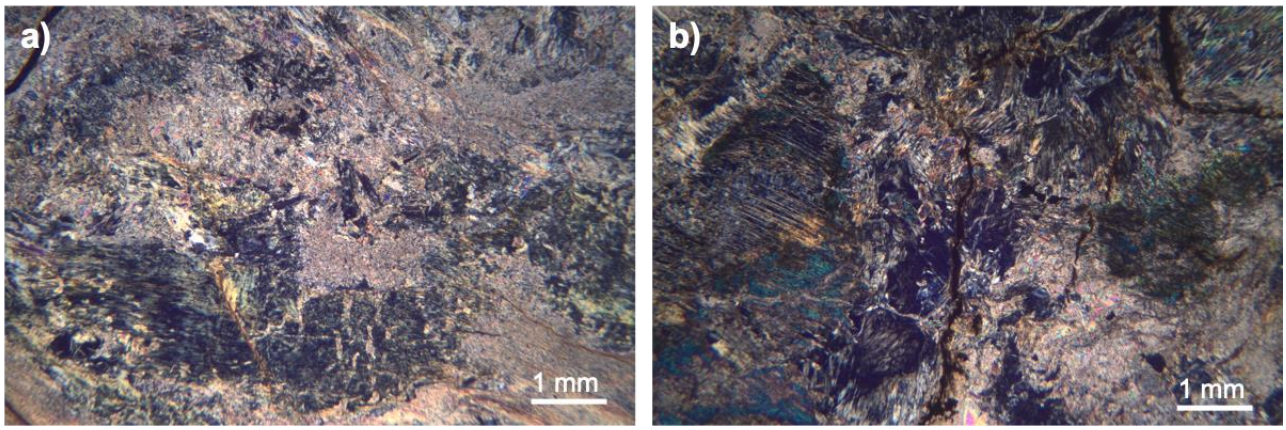

Figure 23. *Microphotograph of the actinolite/tremolite vein in contact with serpentinite. Detail of the intergrowth between amphibole and chlorite inside the vein (a-b) (cross polarised light; Mag: 250x.*

Elongated amphiboles with acicular to highly fibrous habit was also confirmed by SEM (Figure 24). In detail, the amphibole stretches, inside the chlorite mesh, both longitudinally and transversely (Figures 24a-b). In Figure 24e, the soft fibres also show tufts with frayed apexes.

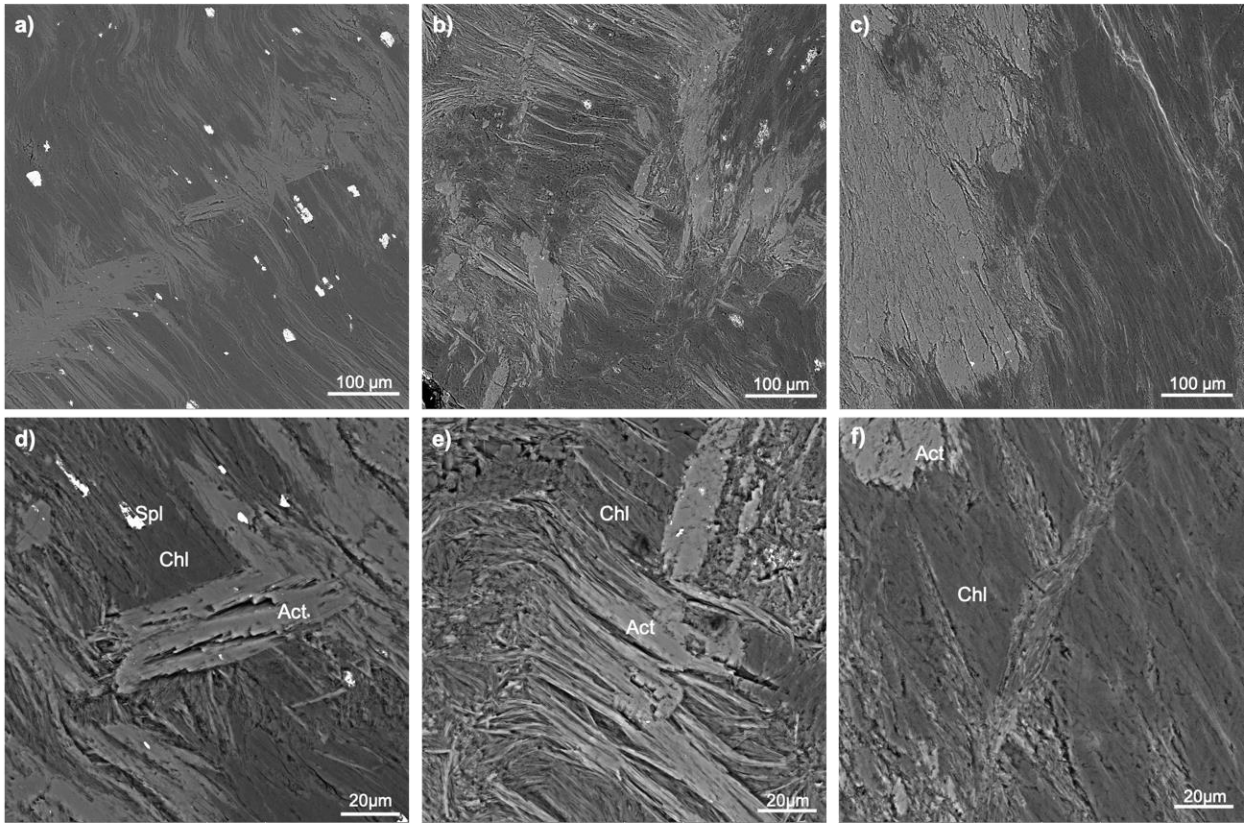

Figure 24. *SEM images from polished thin section of sample F3. Evidence of transverse and longitudinal dispersion of the amphibole veins within a predominantly chlorite matrix (a-c); detail of amphibole tufts ranging from acicular to highly fibrous (d-f) (HV: 20 kV; Det: BSE).*

6.4 Amphibole-bearing metagabbro – Sample P1

Sample P1 is a metagabbro. The sample shows an isotropic blocky texture composed by large grains of plagioclase, chlorite and clinopyroxene. Clinopyroxenes are immersed in alteration products of plagioclase. Amphibole developed at the contacts between clinopyroxene and plagioclase.

Unfortunately, the strong alteration caused the collapse of the sample and due to its small volume, it was not possible to investigate it by optical microscopy or by SEM. The analysis of the amphiboles was carried out on the powders (Figures 25 a-c).

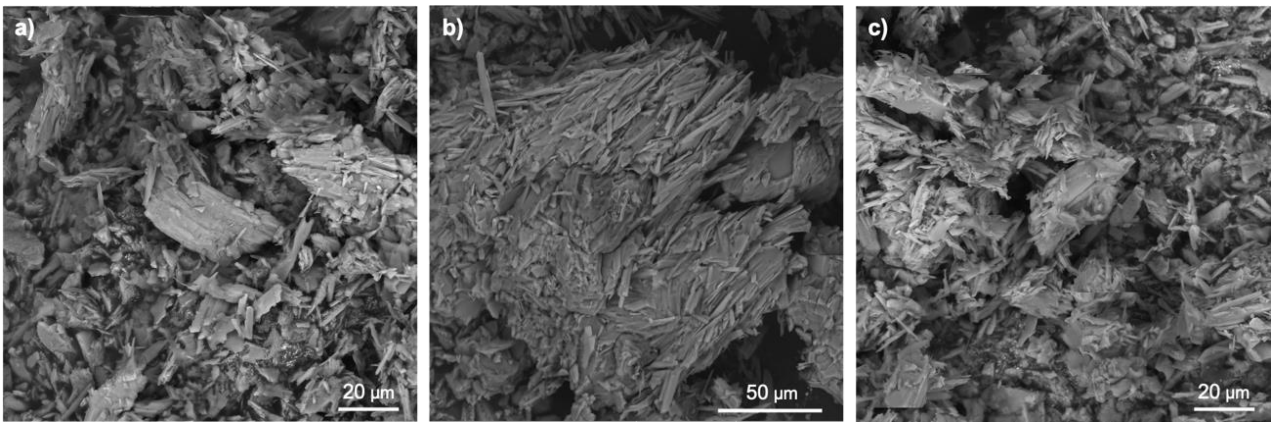

Figure 25. *SEM images of sample P1. Detail of isolated fragments of platy-acicular amphiboles (Mag: 2000x; HV: 20 kV; Det: BSE).*

Fibrous terminations show cleavage and formation of isolated smaller fibres. Amphibole also occurs as prismatic-to-acicular crystals with width exceeding 5 µm.

6.5 Amphibole-bearing dolomite – Sample P2

Sample P2 is a dolomite with large tremolite crystals. The rock is made of granoblastic mosaic. Tremolite has an idioblastic, stubby prismatic habit (Figure 26a).

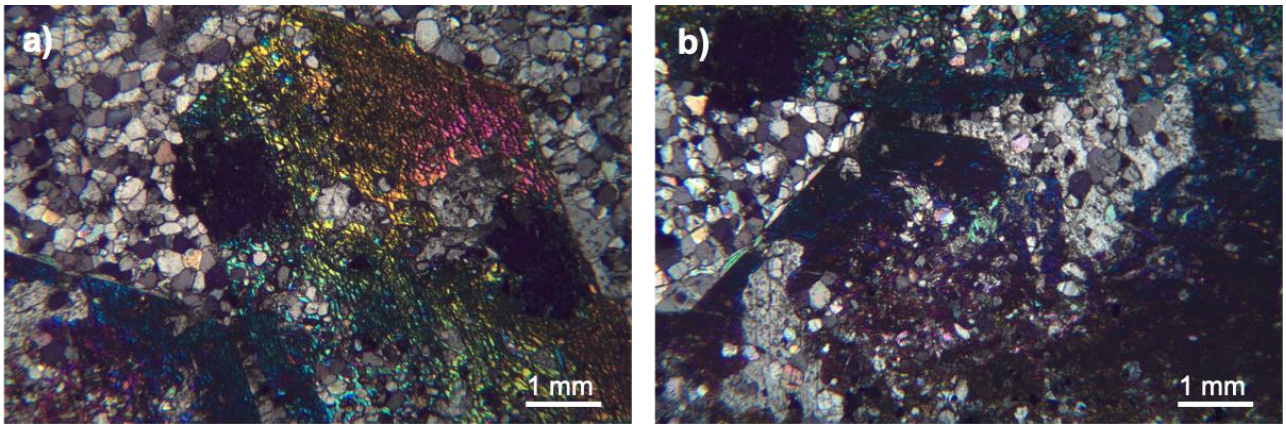

Figure 26. *Microphotograph of granoblastic dolomite and prismatic tremolite (cross polarised light; Mag: 250x).*

SEM investigation evidenced talc veins in the proximity of amphibole (Figures 27 a, b, d). Calcite tends to recrystallize at the boundaries between dolomite and prismatic tremolite (Figures 27e-f).

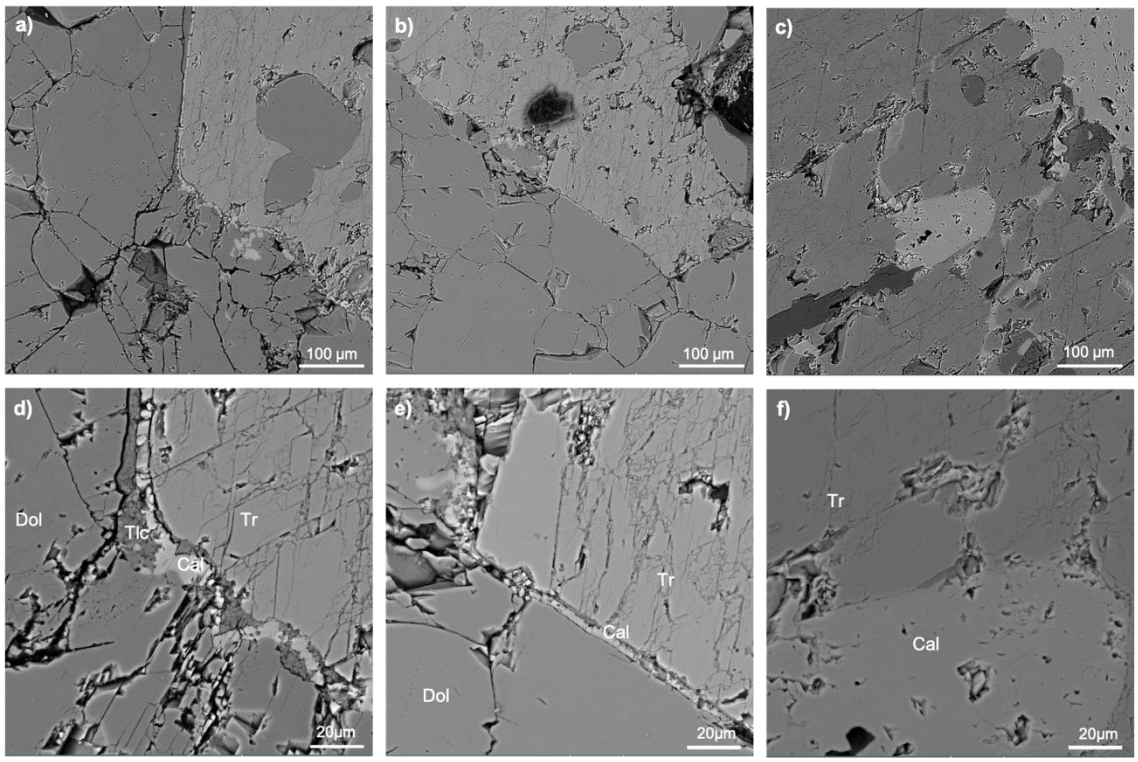

Figure 27. *SEM images from polished thin section of sample P2. Textural relationships between dolomite and prismatic tremolite (a-c); presence of talc and interstitial calcite between dolomite and tremolite (d-f). Mag:500x in a, b, c and 2000x in d, e, f (HV: 20 kV; Det: BSE).*

6.6 Actinolite schist – Sample P3/A5

Sample P3/A5 is an actinolite schist (Figure 28), predominantly composed of mm sized nematoblastic amphibole of the tremolite-actinolite series associated with fine grained chlorite and idioblastic titanite. Subordinate Fe oxide occur with minor granoblastic quartz. The amphibole is

mostly acicular with a very high length to width ratio, but also as prismatic habit (Figure 28b) prismatic grains are also present (Figures 29e, and 29d).

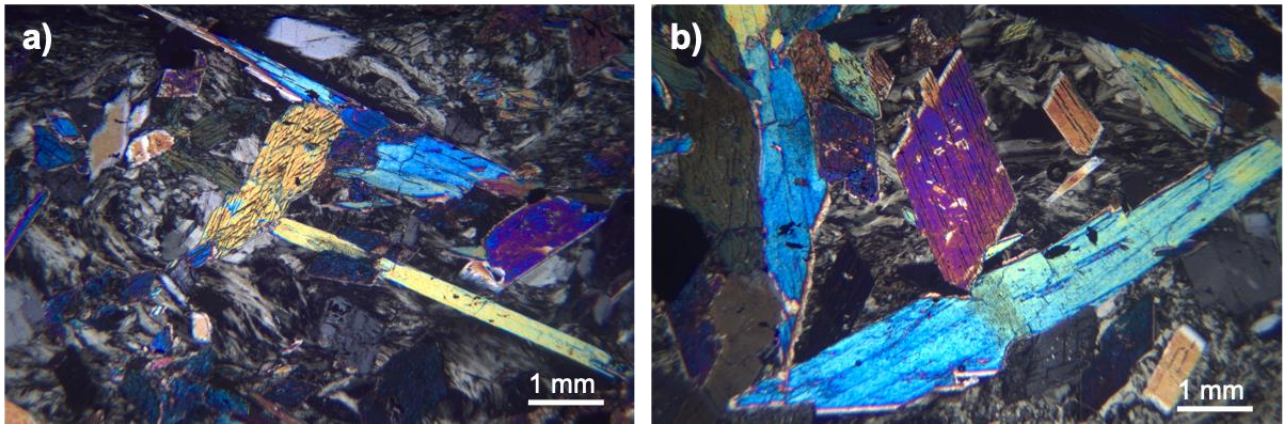

Figure 28. *Microphotograph of the actinolite schist (a). Detail of basal section and acicular actinolite (b) (cross polarised light; Mag: 250x).*

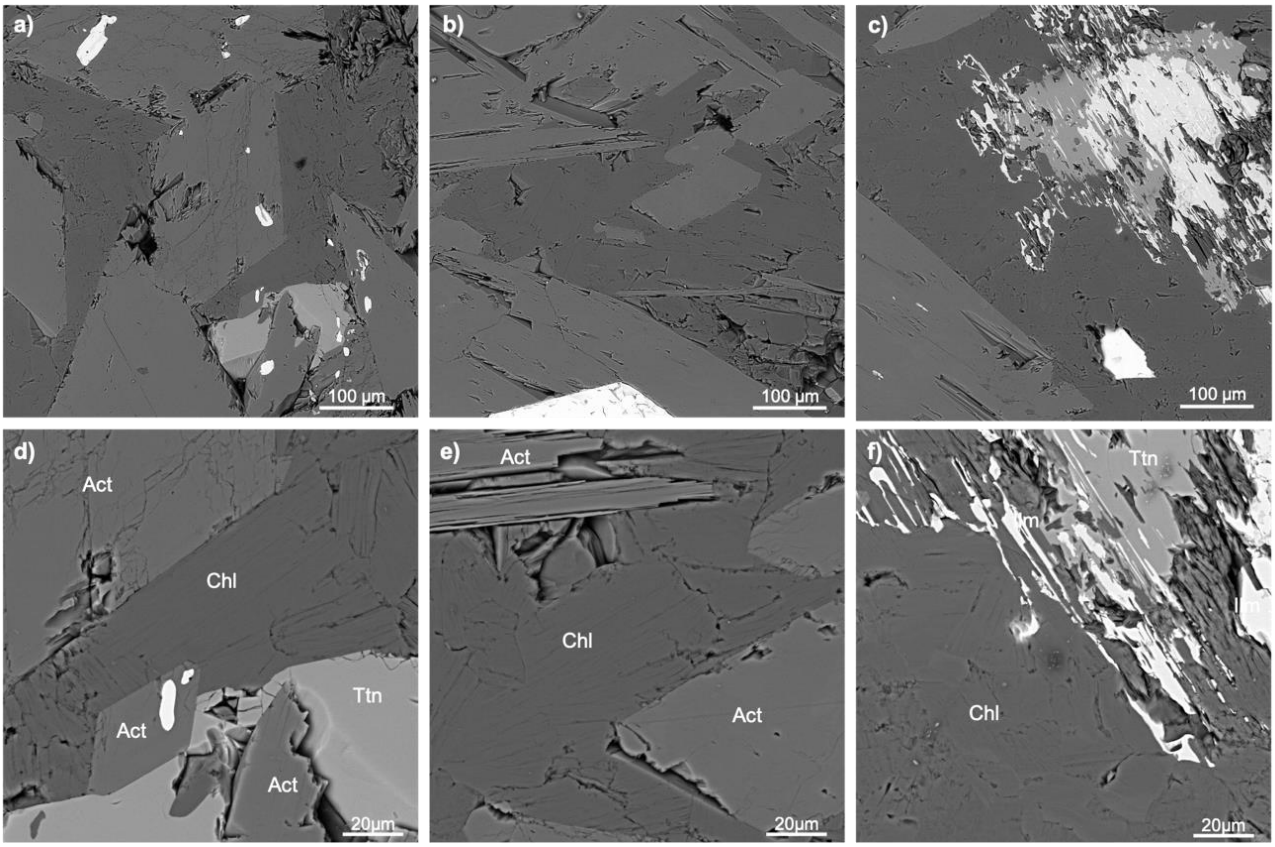

Figure 29. *SEM images from polished thin section of sample P3/A5. Overview of the textural relationships of paragenesis crystals (a-c); basal section of a prismatic amphibole (d); elongated chlorite wrapping around acicular amphibole (e); detail of the textural relationships between chlorite, ilmenite and titanite (f). MAG:500x in a, b, c and 2000x in d, e, f (HV: 20 kV; Det: BSE).*

6.7 Amphibolite-bearing vein – Sample A1

Sample A1 is an actinolite schist with a decimetre thick vein of actinolite (Figures 30a-b). The sample is characterised by medium-fine-grain size, and is essentially made up of chlorite, actinolite

and epidote with variable amounts of albite, quartz and calcite. The mineral assemblage is the expression of a mafic protolith. The elongated fibres of actinolite are acicular and associated with euhedral titanite wrapped in lamellar chlorite (Figure 30b).

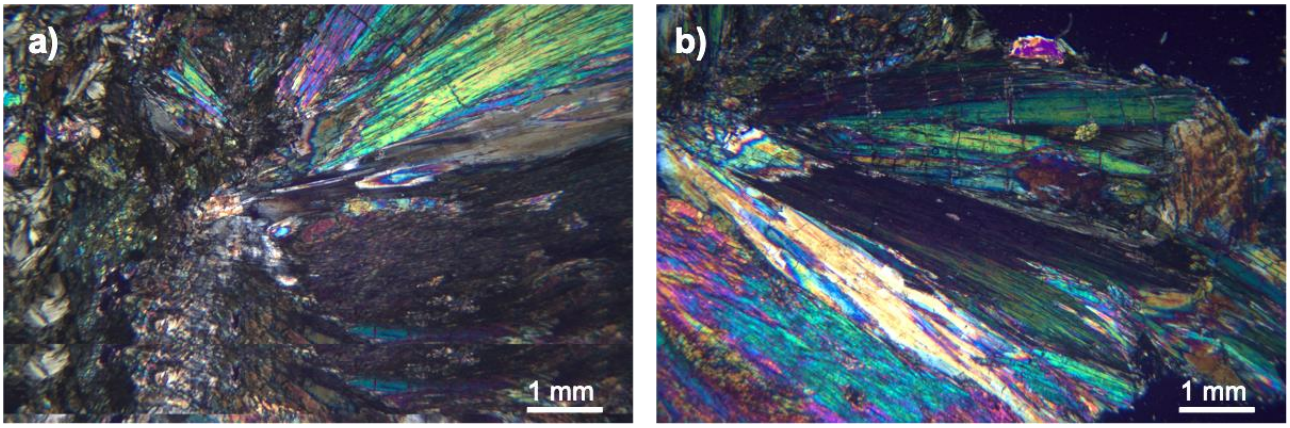

Figure 30. *Microphotograph of the actinolite schist (a). Detail of acicular amphiboles with high length:width ratio (b) (cross polarised light; Mag: 250x).*

Under SEM, chlorite and plagioclase evidence indentate boundaries. Actinolite shows massive aggregates of rigid, and free of cleavages habit. The most acicular variety is reported in Figure 31e.

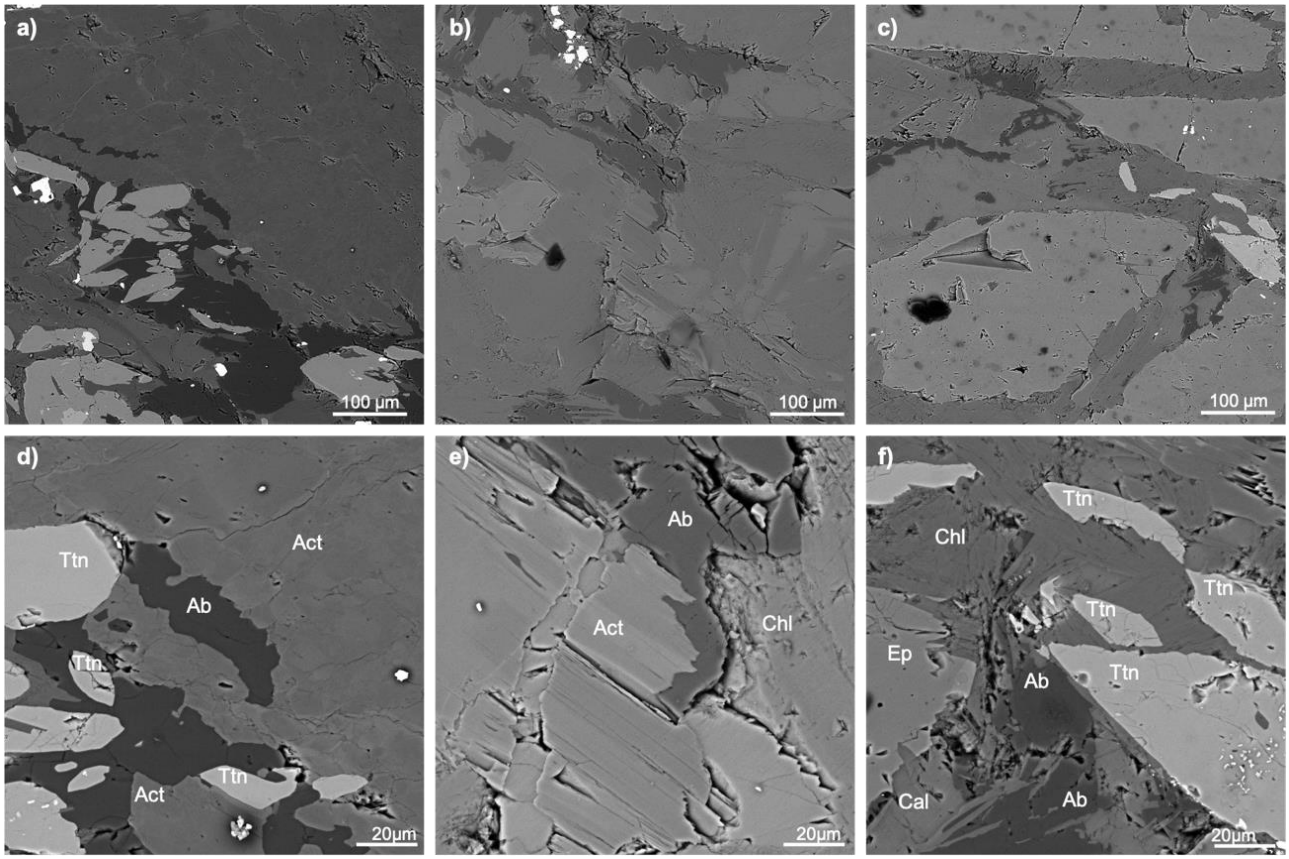

Figure 31. *SEM images from polished thin section of sample A1. Overview of the textural relationships (a-f); basal section of a prismatic amphibole (d); elongated acicular amphibole (e). MAG:500x in a, b, c and 2000x in d, e, f (HV: 20 kV; Det: BSE).*

6.8 Amphibole-bearing vein – Sample A2

This sample is composed by calcite and amphiboles. Minor talc, quartz and sometimes dolomite within calcite occur (Figure 32b). Lamellar talc developed interstitial between calcite and amphiboles of the tremolite-actinolite series. The latter with evident cleavage is stubby and prismatic, with very low ratio of length and width (Figures 32a-b).

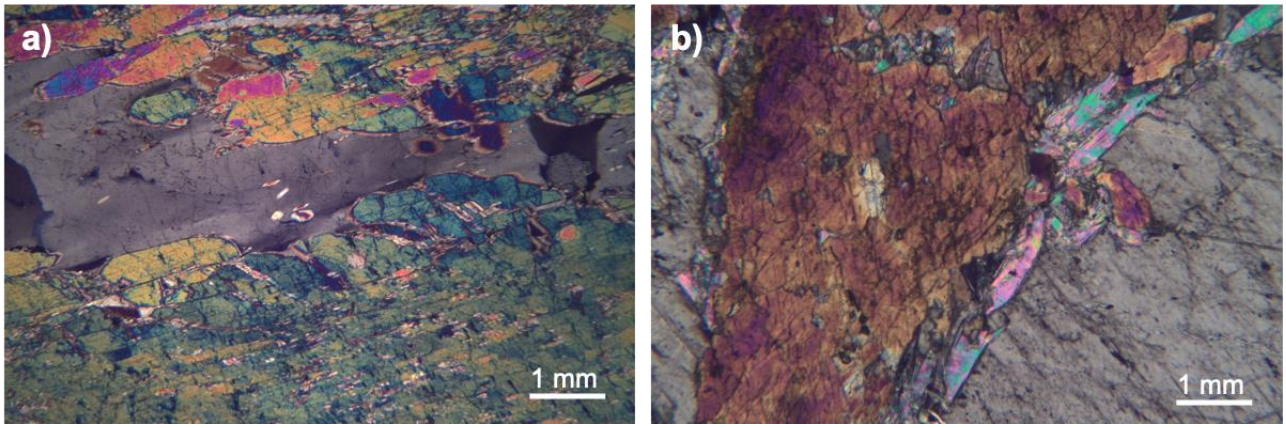

Figure 32. *Microphotograph of calcite and prismatic tremolite in vein (a). Detail of tremolite surrounded by lamellar talc (b) (cross polarised light; Mag: 250x).*

The amphiboles, characterised by high degree of fracturing, are mostly prismatic (Figures 33d-f).

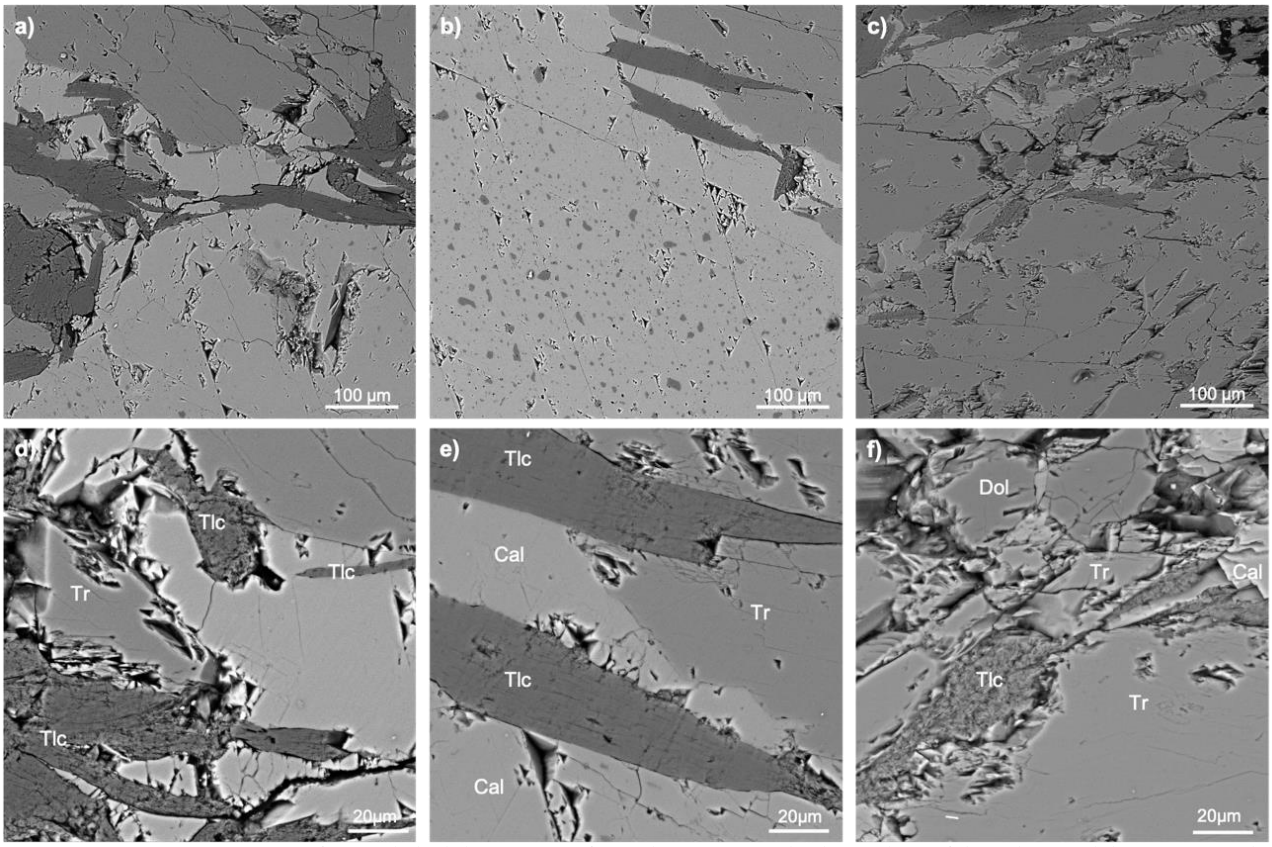

Figure 33. *SEM images from polished thin section of sample A2. Textural relationships of the calcite + dolomite vein rich in elongated prismatic tremolite. MAG:500x in a, b, c and 2000x in d, e, f (HV: 20 kV; Det: BSE).*

6.9 Serpentinised peridotite with lizardite vein – Sample A3/S1

Sample A3/S1 is a serpentinised peridotite cut by a fibrous/acicular lizardite-filled vein. Most of the host-rock is made up of antigorite and is very rich in Fe-oxides (mainly magnetite). Extensional veins with chrysotile/antigorite filling contain relics of pyroxenes (diopside) with prismatic habit and kinked cleavages. Within the diopside, small veins filled of fibrous talc were developed (Figure 34a). Late serpentine veins develop parallel or perpendicular to the walls of the host fractures (Figure 34b). Therefore, all the three serpentine polymorphs occur in the sample.

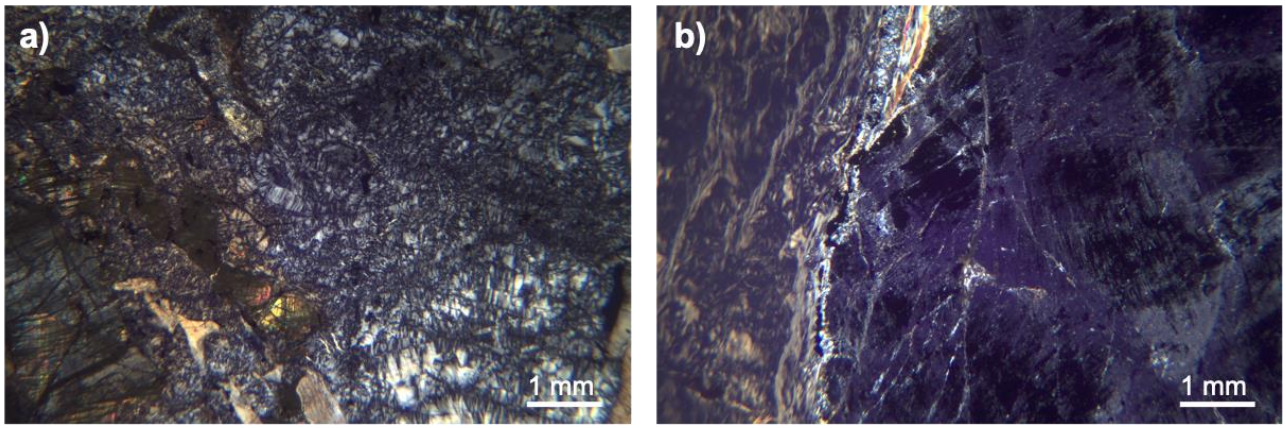

Figure 34. *Microphotograph of the massive antigorite serpentinised peridotite and clinopyroxene relics (a); from the left to the right: Contact between the lizardite vein, the chrysotile microvein and the host rock (b) (cross polarised light; Mag: 250x).*

To unravel the sub-microscopic mineralogy of serpentine polymorphs, the first characterization was by μ-Raman. Two analysis spots were performed on the vein/rock interface and in the vein. Analysis spot 1 (shown in Figure 35b) is represented by lizardite (Figures 35a-b) and the interface between the vein and the host rock (analysis spot 2 in Figure 35d) is filled with chrysotile (Figures 35c-d).

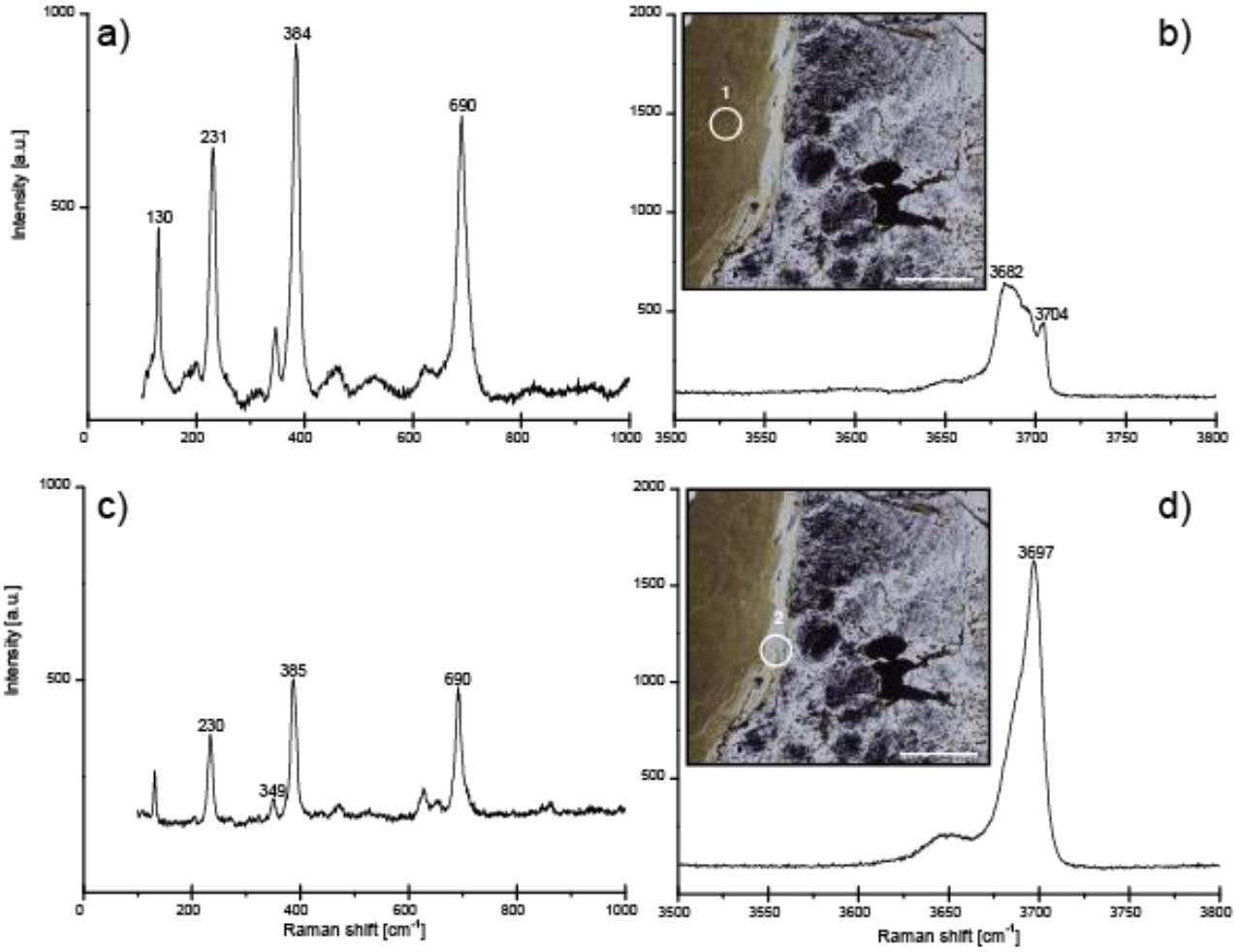

Figure 35. *Raman spectra in the low-wavenumber and high-wavenumber regions of lizardite (a and b respectively) and chrysotile (c and d respectively). Photomicrographs show the positions of the spots where the spectra were acquired; scale bar: 0.2 mm (from Militello et al., 2019a).*

The region of low-wavenumber (150–1000 cm^{-1}) corresponds to the vibrational mode of the crystal lattice and the vibrations of Si–O_4; contrariwise, in the high-wavenumber region is displayed the stretching vibration behaviour of the OH group (3500–3800 cm^{-1}). The low-wavenumber region is sometimes ambiguous because a little modification of the chemical composition could modify the intensity of the peak as well as the vibrational wave number and its intensity. Therefore, the distinction of the serpentine polymorphs is based on the vibration of the OH group, which is very sensitive to the variation of the geometry of the layers (Petriglieri et al., 2015). In our case, the lizardite (Figure 35a) has very intense peaks at 690, 384 and 231 cm^{-1}; however, the peaks at 3682 and 3704 cm^{-1} are discriminating (Figure 35b). The chrysotile (Figure 35c) shows peaks at 230, 385 and 690 cm^{-1}, while the OH group shows the main peak at 3697 cm^{-1} (Figure 35d) with a small hump of lower intensity.

Under SEM morphological details of the polymorphs are evidenced (Figures 36 a and d), such as the long bands of magnetite (Figure 36b), the preserved orthopyroxenes from the protolith (Figures 36 c and f), and the contact between the three polymorphs (Figures 36 e-f).

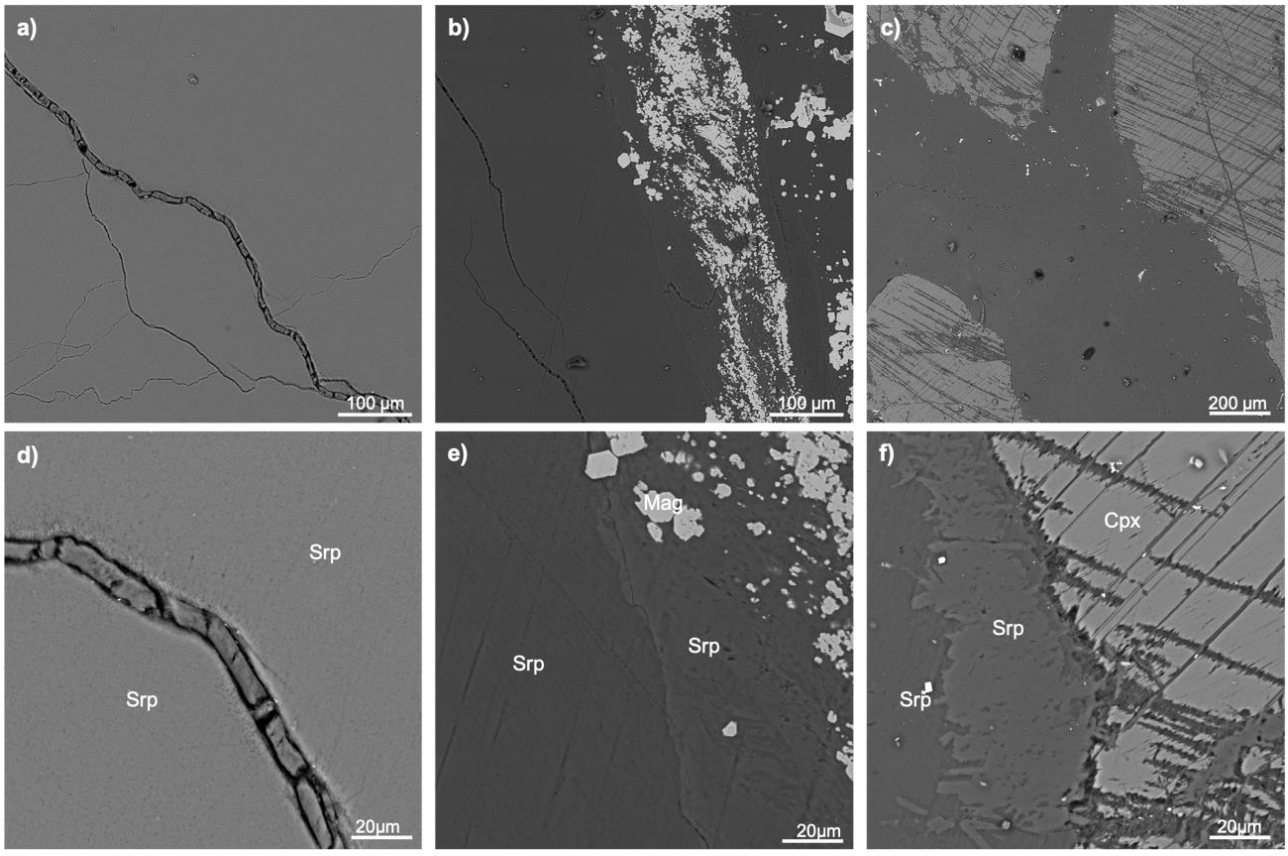

Figure 36. *SEM images from polished thin section of sample A3/S1. Serpentinised peridotite (a) with elongated bands of magnetite (b) and clinopyroxene relics (c and f). Detail of the contact between the serpentinised peridotite and the lizardite vein (d-e). MAG:500x in a, b, c and 2000x in d, e, f (HV: 20 kV; Det: BSE).*

Although the *in situ* composition and speciation were determined using µ-Raman, OM and SEM, habit and fibre morphology of chrysotile were further investigated by transmitted electron microscopy.

TEM investigations showed structural varieties of chrysotile, lizardite, and antigorite, both in platelets and fibres. Chrysotile consists of bundles of long and flexible fibrils with a hair-like appearance (Figure 37). The chrysotile fibres were often curved, and the length of some fibres may be longer than 2 µm.

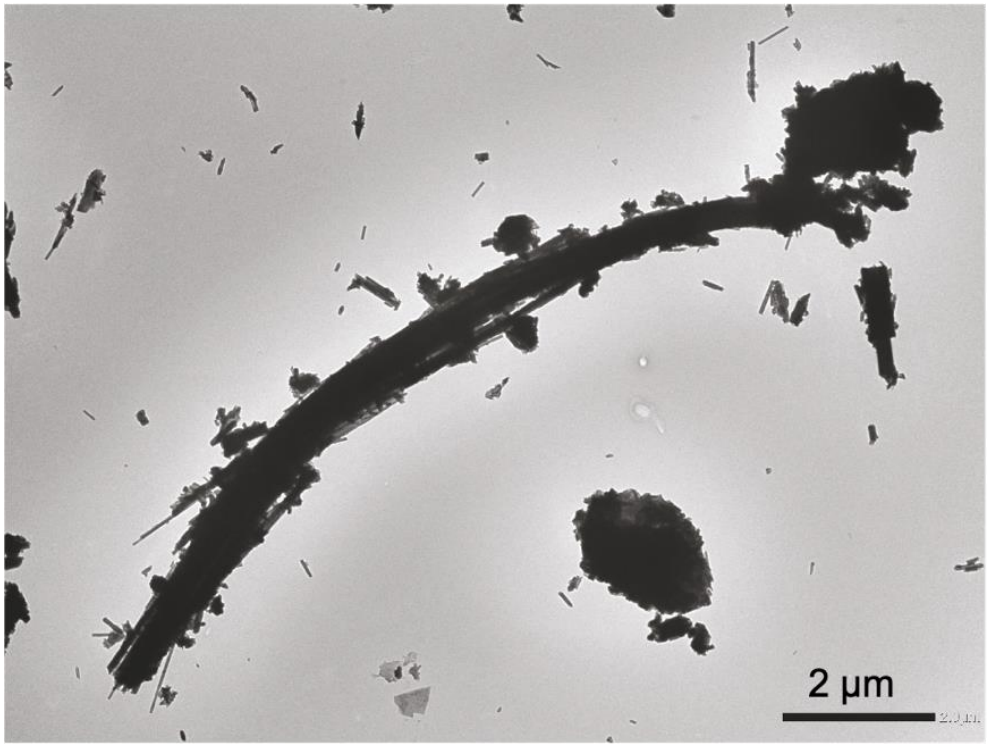

Figure 37. *TEM image. Bundle of chrysotile fibres (from Militello et al., 2019a).*

TEM analyses of single fibres showed cylinder and rarely conical morphologies (Figures 38 a-b). The central empty core lies along the entire fibre length, sometimes with some interruptions, with outer and inner diameters of about 40 and 8 nm, respectively. In some fibres the outer walls of the chrysotile are very thin, and the core is wide. In rare occasions, chrysotile grew with a proto-chrysotile morphology (Figure 38c) (Bloise et a., 2017). The proto-chrysotile morphology is the precursor of the cylindrical morphology of chrysotile (Bloise et al., 2017b; Yada & Lishi, 1977). The polygonal serpentine fibres often have a diameter larger than 100 nm (Figure 38d) as measured in the (100) cross-section. The other polymorphs (lizardite and antigorite) mostly have a platy morphology and

thus are identified as non-asbestiform. The fibrous antigorite was rarely detected. The bundle sides have a smooth and nearly constant diameter along the length.

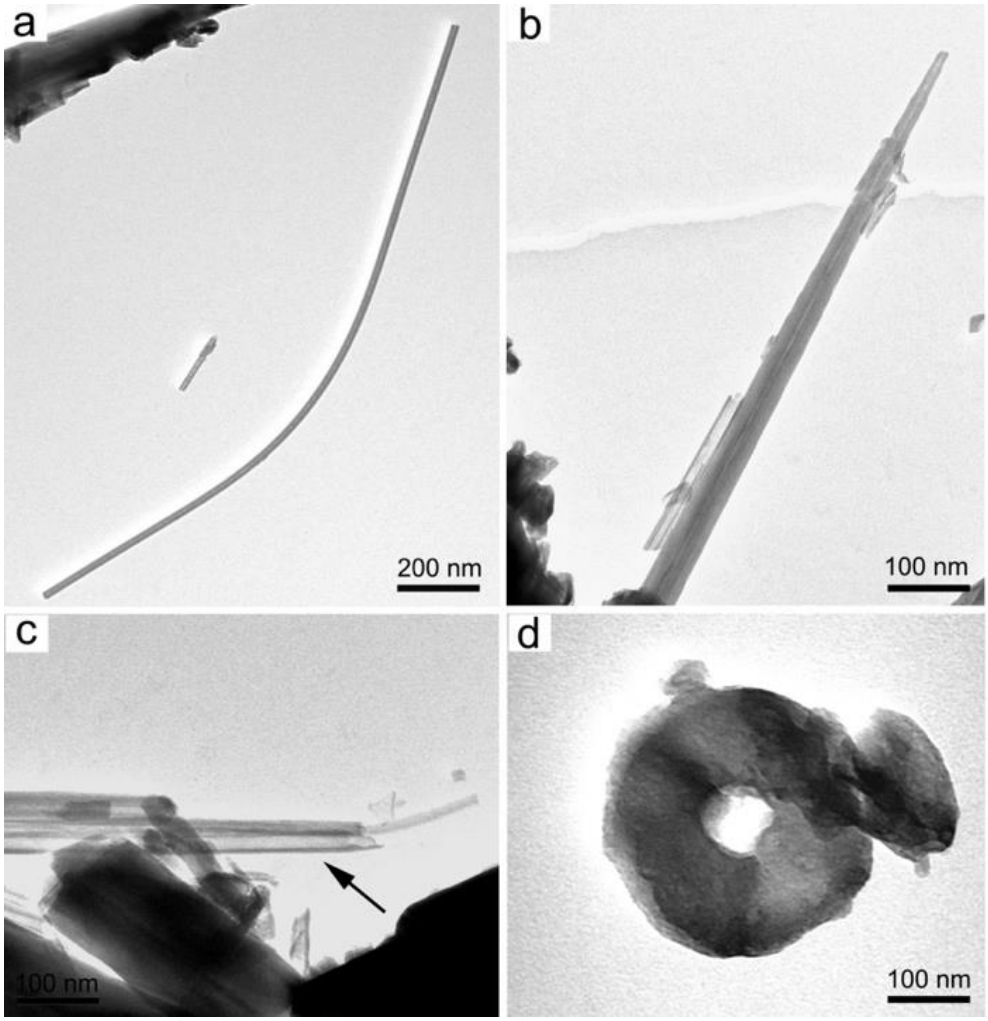

Figure 38. *TEM image of: (a) a thin cylindrical chrysotile; (b) conical chrysotile with not-interrupted empty core; (c) poorly shaped proto-chrysotile (black arrow); (d) cross-section of [100] polygonal serpentine (from Militello et al., 2019a).*

The lamellar/fibrous morphology of lizardite makes it a mineral of interest from an environmental point of view and therefore potentially dangerous, even if not classified as asbestos.

6.10 Serpentinite with amphibole vein – Sample A4

Sample A4 is a serpentinite with an amphibole-rich vein. It is a serpentinite with few relics of the peridotite protolith and has an intertwining structure consisting of antigorite lamellae, elongated and interpenetrated with each other (Figure 39a). The thin veins (mainly filled with calcite and talc) present in serpentinite are often not cutting but follow lines of weakness and can cut the textural elements. The amphibole is elongated to highly fibrous (Figure 39b). The millimetre-thick amphibole fibres lie sub-parallel in contact with the host rock, have an elongated aspect not easily distinguishable.

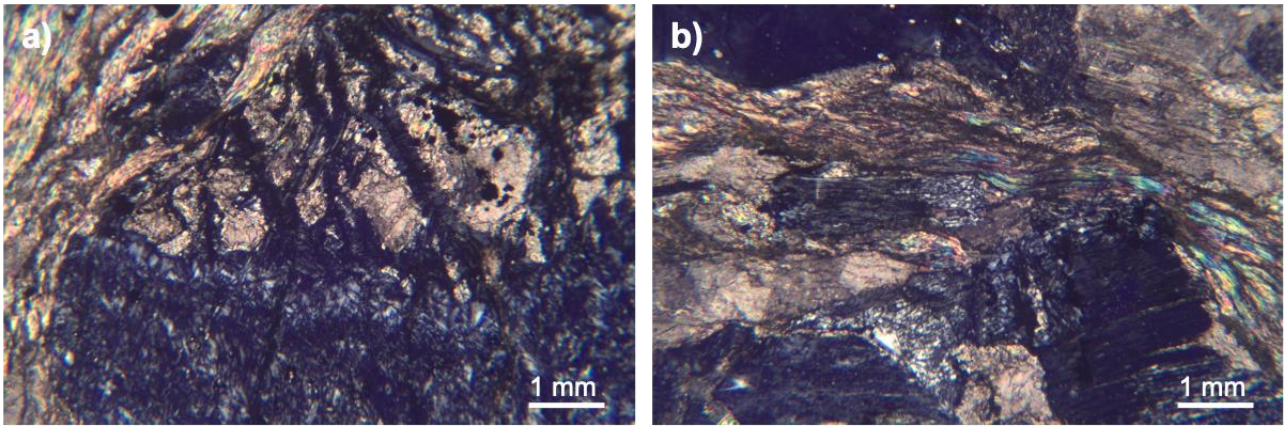

Figure 39. *Microphotograph of the contact between tremolite-actinolite amphibole with a predominantly fibrous habit vein and antigorite and magnetite aggregates of the rock matrix) (a-b) (cross polarised light; Mag: 250x).*

Under low magnification (500x), the contact between the vein and the serpentinite is clear (Figure 40c). In detail, at 2000x magnification, the amphibole has an acicular/fibrous habit, is intercalated in talc and calcite and serpentine nodules (Figures 40 e-f).

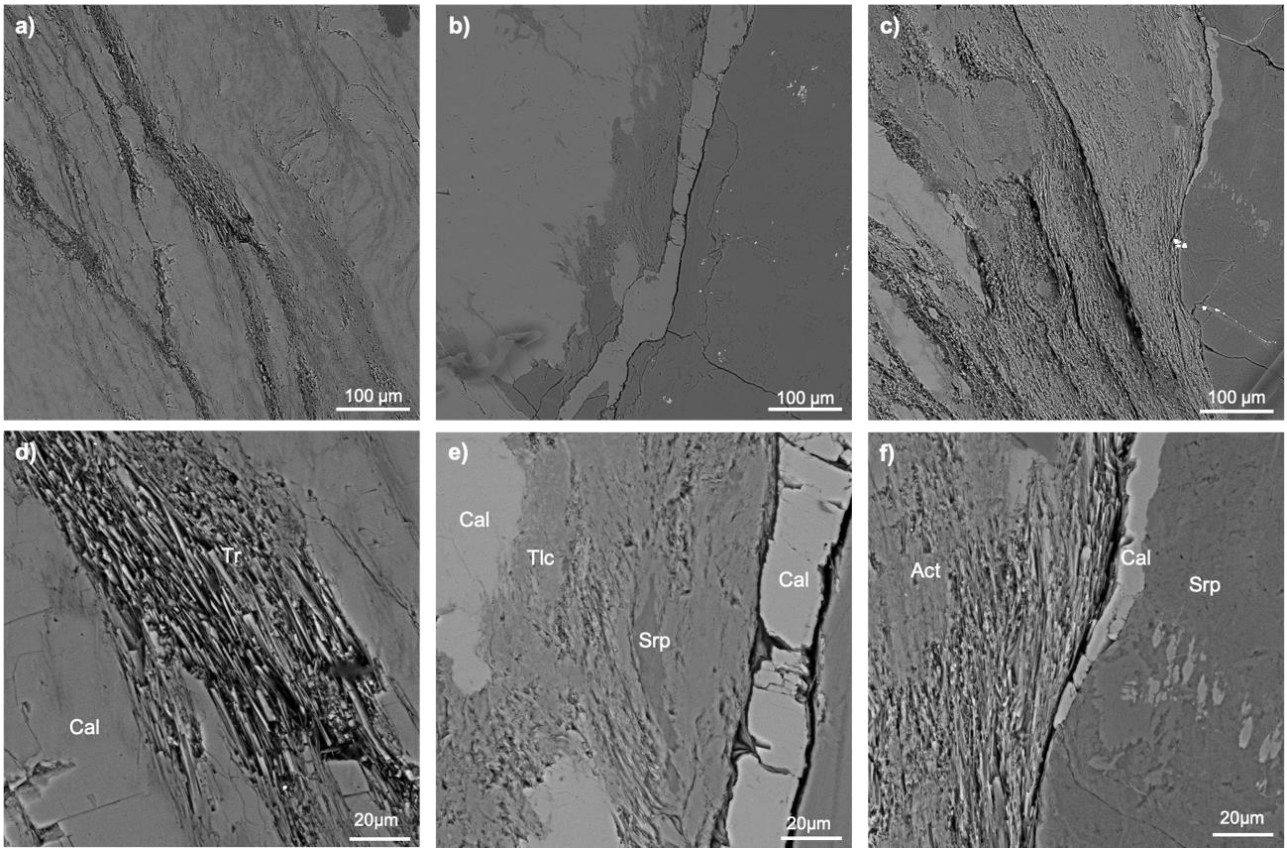

Figure 40. *SEM images from polished thin section of sample A4. Detail of the amphibole vein of the tremolite-actinolite series (a); contact between the vein and the serpentinite (c-d) diffused in a calcite filled micro-vein (b, e-f). MAG:500x in a, b, c and 2000x in d, e, f (HV: 20 kV; Det: BSE).*

6.11 Serpentinite with amphibole vein – Sample S2

Sample S2 is a serpentinite cut by an amphibole bearing vein. The vein mainly contains acicular and more or less fibrous tremolite-actinolite amphiboles associated with diopside, dolomite, calcite, clinochlore and Fe-oxide (Figure 41a). In addition, the sample is very rich in chrysotile/fibrous antigorite affected by kink deformation. The grain size of amphibole is variable, from very fine (0.03 mm in length) up to a 4 mm in length; the habit is acicular, although fibrous samples with high aspect ratio are also present (Figure 41b).

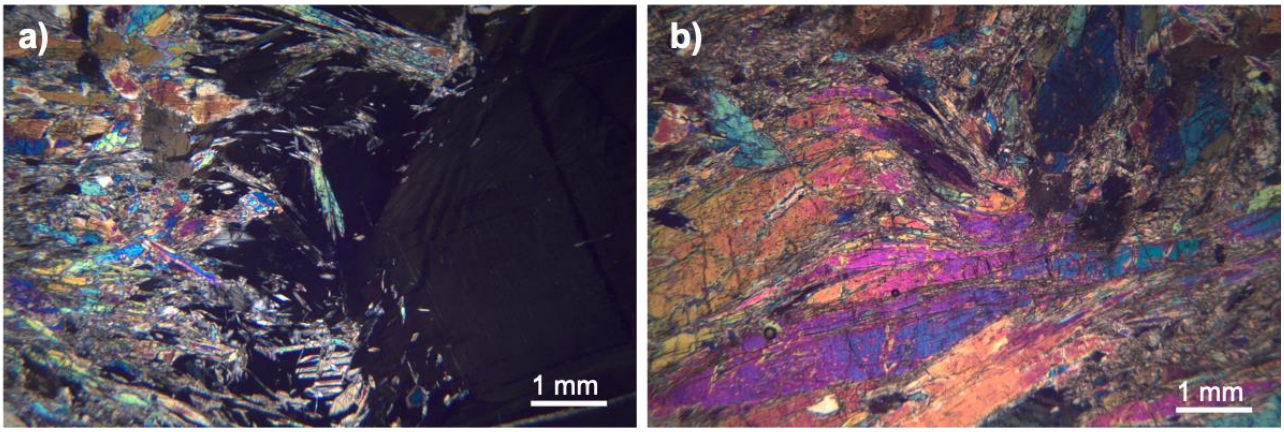

Figure 41. *Microphotograph of the actinolite-tremolite-rich vein (a); detail of the fibrous to elongated prismatic acicular/fibrous amphiboles (b) (cross polarised light; Mag: 250x).*

Under higher magnifications, amphibole of the tremolite-actinolite series occur in a prismatic and acicular (Figures 42 c, d) habit with crystalline termination and well-defined edges or corners.

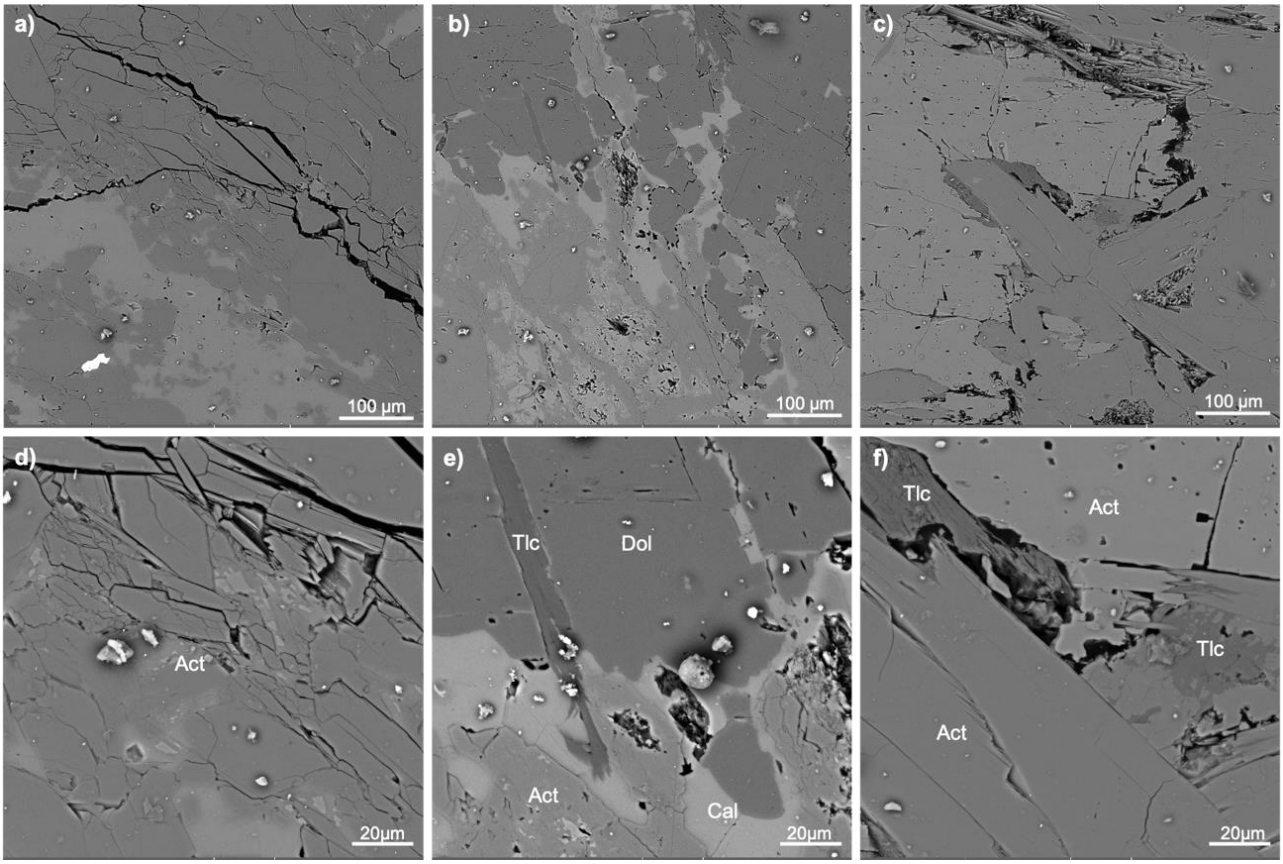

Figure 42. *SEM images from polished thin section of sample S2. Actinolite-tremolite rich-vein (a-f). Example of prismatic amphibole (b, d) and acicular amphibole (c, f). MAG:500x in a, b, c and 2000x in d, e, f (HV: 20 kV; Det: BSE).*

The fibrous asbestiform habit was confirmed by SEM and TEM, evidencing bladed grains similar to asbestos fibres (Figs. 43 and 44).

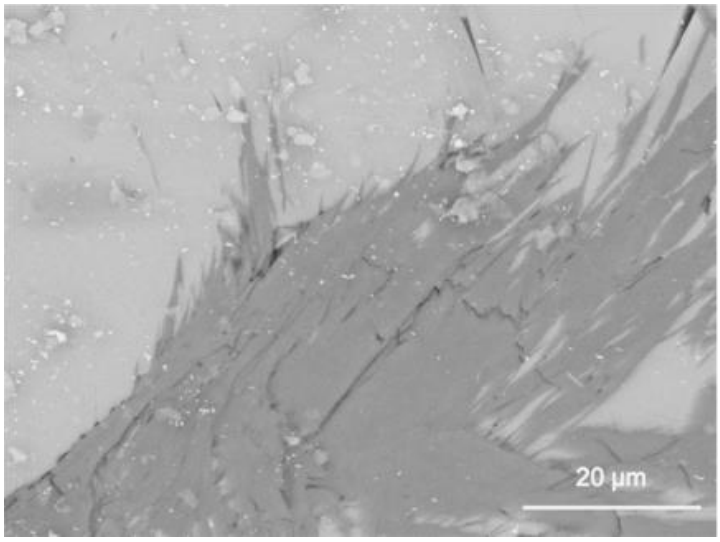

Figure 43. *High magnification (5000x) detail of a fibrous tremolite bundles (HV: 20 kV; Det: BSE).*

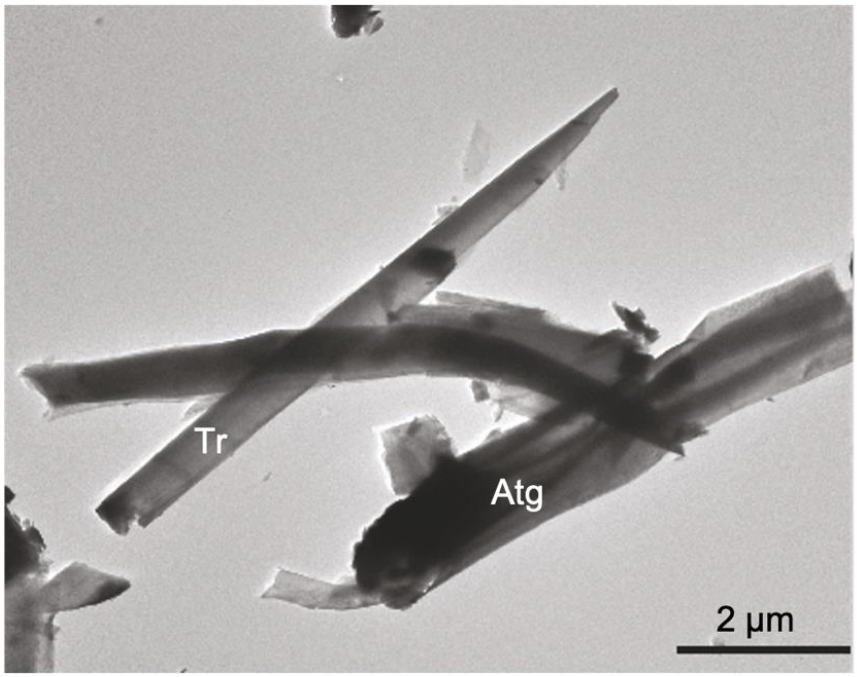

Figure 44. *TEM image. Tremolite + fibrous antigorite (from Militello et al., 2019a).*

Tremolite shows the strain-shaped morphology with parallel sides and regular termination. Sometimes the longitudinal splitting of the fibres parallel to (110) cleavage surfaces into thin fibrils is observed (Fig 45 a-b). The fibres length is generally > 6 µm with a width of < 0.2 µm. However, cleavage fragments of tremolite are also present (Fig 45 c). Antigorite and lizardite also occur, together with minor fibrous antigorite.

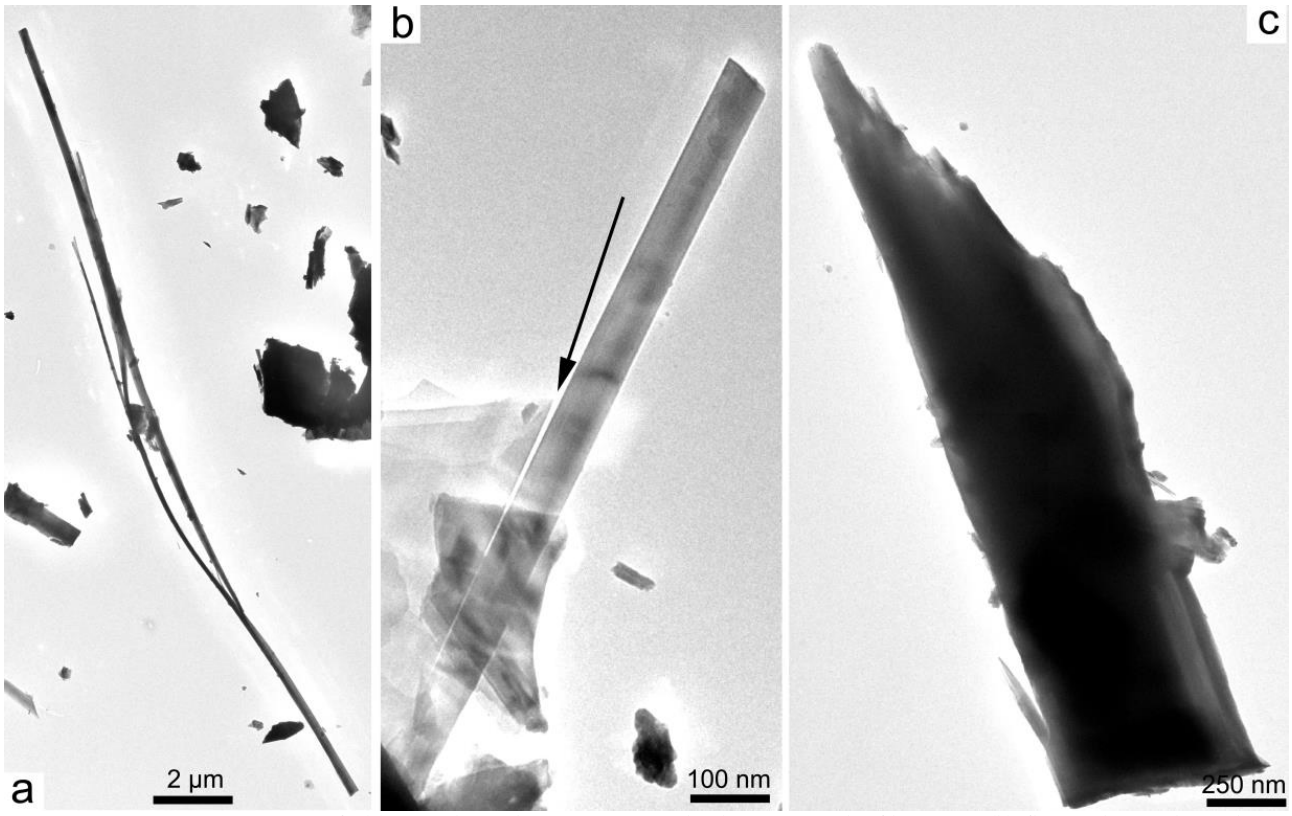

Figure 45. *TEM image of: (a) tremolite asbestos in perpendicular view to the fibre axis; (b) flattened tremolite splitting longitudinally into thinner fibrils; (c) prismatic single crystals of tremolite (cleavage fragment) (from Militello et al., 2019a).*

6.12 Metabasalt with plagiogranite vein – Sample S3

Sample S3 is a metabasalt with intersertal texture where skeletal albite and acicular/prismatic and occasionally fibrous actinolite occur. The rock is cut by a granoblastic plagiogranite vein formed mainly by primary plagioclase, secondary calcite and actinolite (Fig 46 a-b). Quartz, albite, and calcite are the vein filling phases. Acicular or fibrous actinolite occurs either at the selvedge of the vein or are scattered in the basalt groundmass, which is rich in skeletal plagioclases and acicular actinolite. Titanite is a common accessory phase.

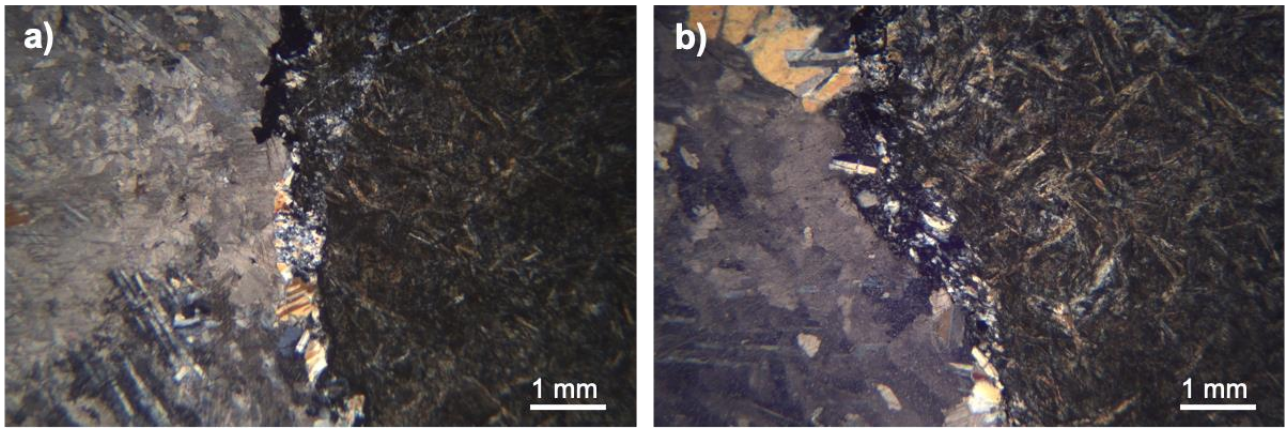

Figure 46. *Microphotograph of the contact between coarse-grained plagiogranite and fine-grained metabasalt with intersertal microstructure (a-b); Detail of a micro-vein filled by acicular/fibrous actinolite (b) (cross polarised light; Mag: 250x).*

Amphiboles, sometimes as fibril bundles, are generally included in plagioclase (Fig 47). Acicular and very elongated actinolite occur at the contact between metabasalt and plagiogranite vein (Figure 47e). The acicular morphology tends to thin out at the tips, which are often needle-like, with a generally moderate aspect ratio (10:1).

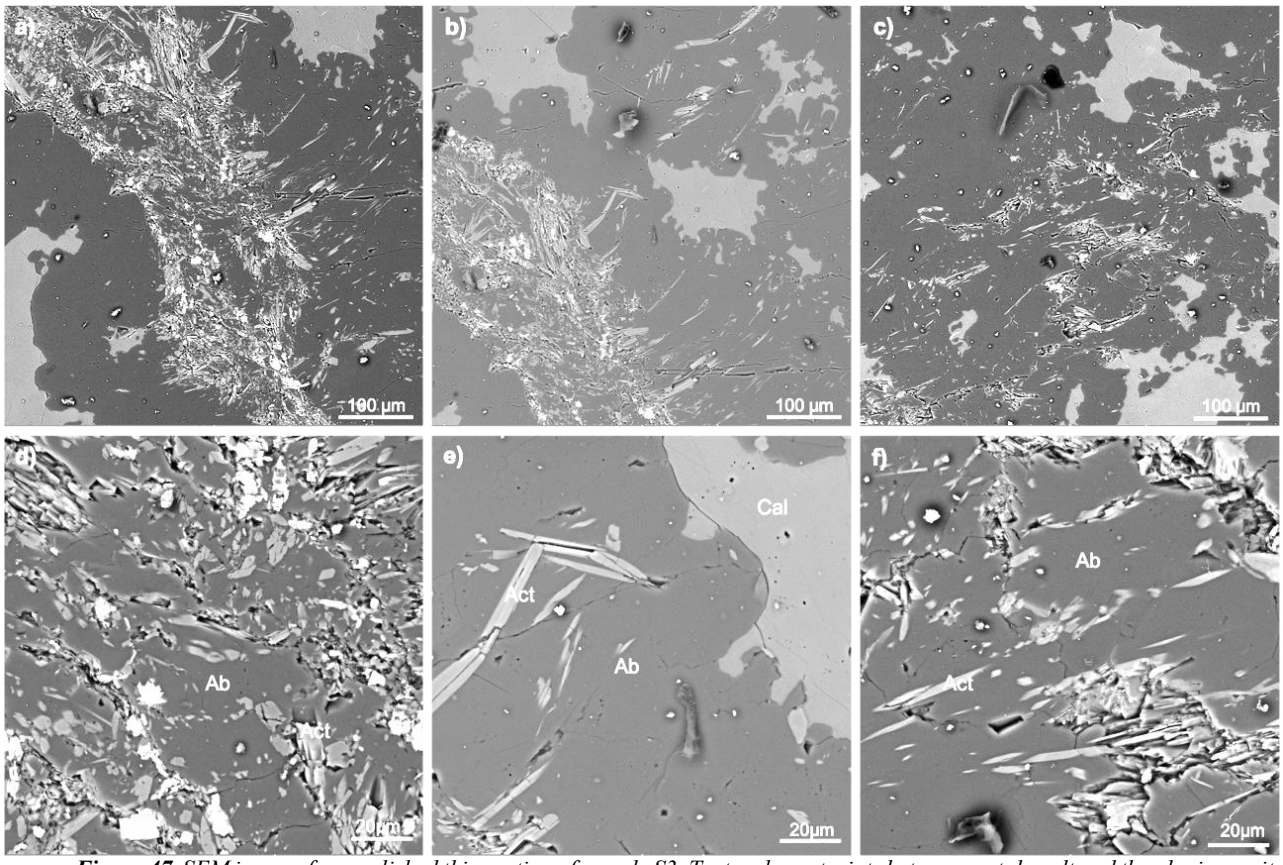

Figure 47. *SEM images from polished thin section of sample S3. Textural constraints between metabasalt and the plagiogranite vein (a-c); detail inside the metabasalt with reference to the elongated acicular amphiboles (d-f). MAG:500x in a, b, c and 2000x in d, e, f (HV: 20 kV; Det: BSE).*

TEM investigations showed amphibole fibres with a rugged surface and irregular sides, suggesting an origin in a cleavage fragment (Figures 48 a-b).

According to the crystals/chemical data obtained by EDS/TEM, the elongated particles of amphiboles were classified as actinolite, since they had a value of Si ranging from 7.90 to 7.99 atoms per formula unit (a.p.f.u.) and a $Mg/(Mg+Fe^{2+})$ value > 0.9 a.p.f.u. (Hawthorne et al., 2012). Furthermore, low concentrations of very short chrysotile fibres were also identified.

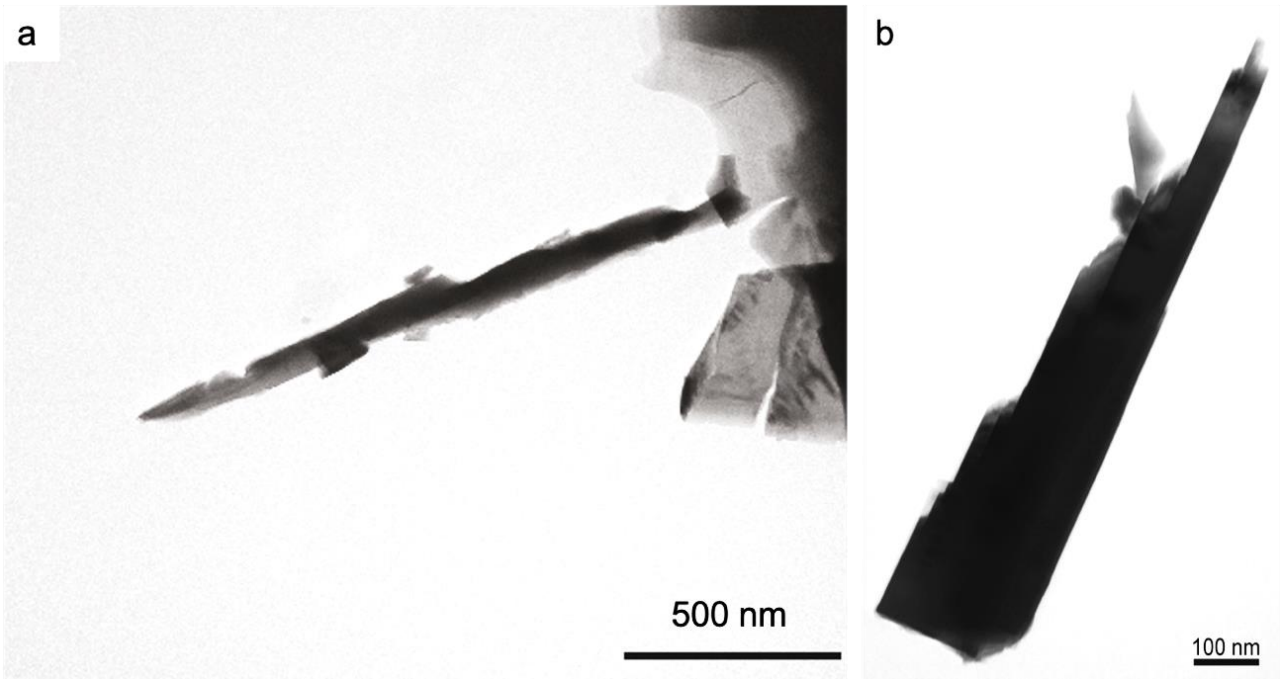

Figure 48. *TEM image. Acicular actinolite (a); crystals of tremolite (cleavage fragment) note the irregular sides (b) (from Militello et al., 2019a).*

6.13 Pyroxenite cut by talc and actinolite vein – Sample S4

Sample S4 is a pyroxenite cut by millimetre-thick veins of the fibrous/acicular form of the actinolite-tremolite series associated with talc; the protolith is a metasomatized metagranitoid (Figures 49 a-b). This sample is a recrystallised cumulus rock and is mainly composed of clinopyroxene (diopside) with a mosaic texture overprinting the orthocumulus phase, subhedral potassic edenite as an inter-cumulus phase and local cataclastic, rare orthopyroxene, actinolite, interstitial mica (phlogopite), quartz and apatite as accessory minerals and finally trace spinel. The diopside is cut by talc micro-veins, and sometimes associated with titanite, ilmenite and actinolite. The rock hosts a large vein, filled with actinolite, talc, calcite and chrysotile/antigorite with a finer grain size than clinopyroxene. Both fibrous and acicular habits are present. In the cataclastic band, actinolite has an average grain size from 0.04 mm up to 0.4 mm and potassic edenite has an average grain size from 0.06 to 0.3 mm, whereas the orthopyroxene is a fine-grained unresolvable aggregate.

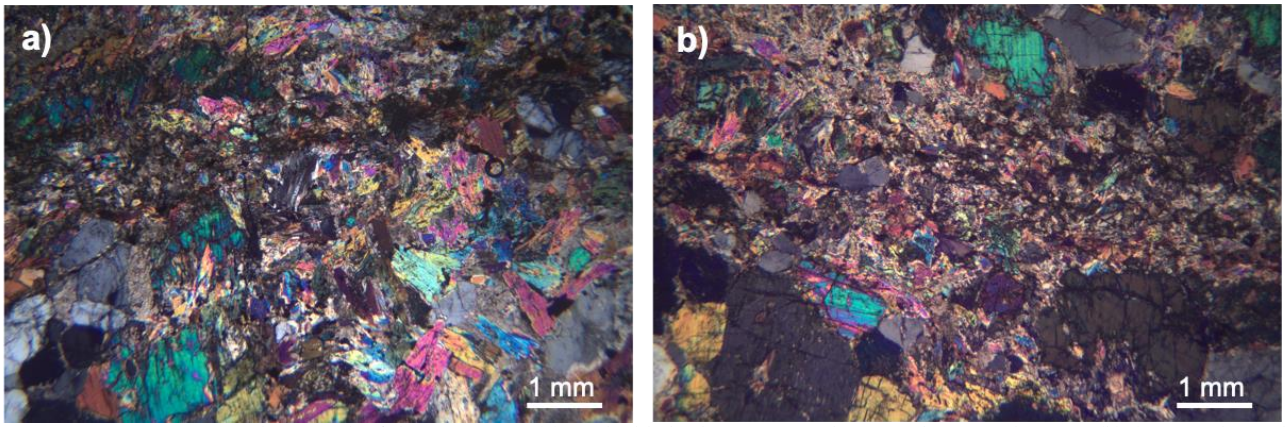

Figure 49. *Microphotograph of the pyroxenite (a); embedded talc, potassic edenite and ± actinolite vein (b) (cross polarised light; Mag: 250x).*

Under SEM the amphibole is the main constituent of the vein is potassic edenite (with fibrous habit) which forms a 3D network with talc vein (Figure 50). Actinolite is rare and has an acicular habit with a low length-to-width ratio.

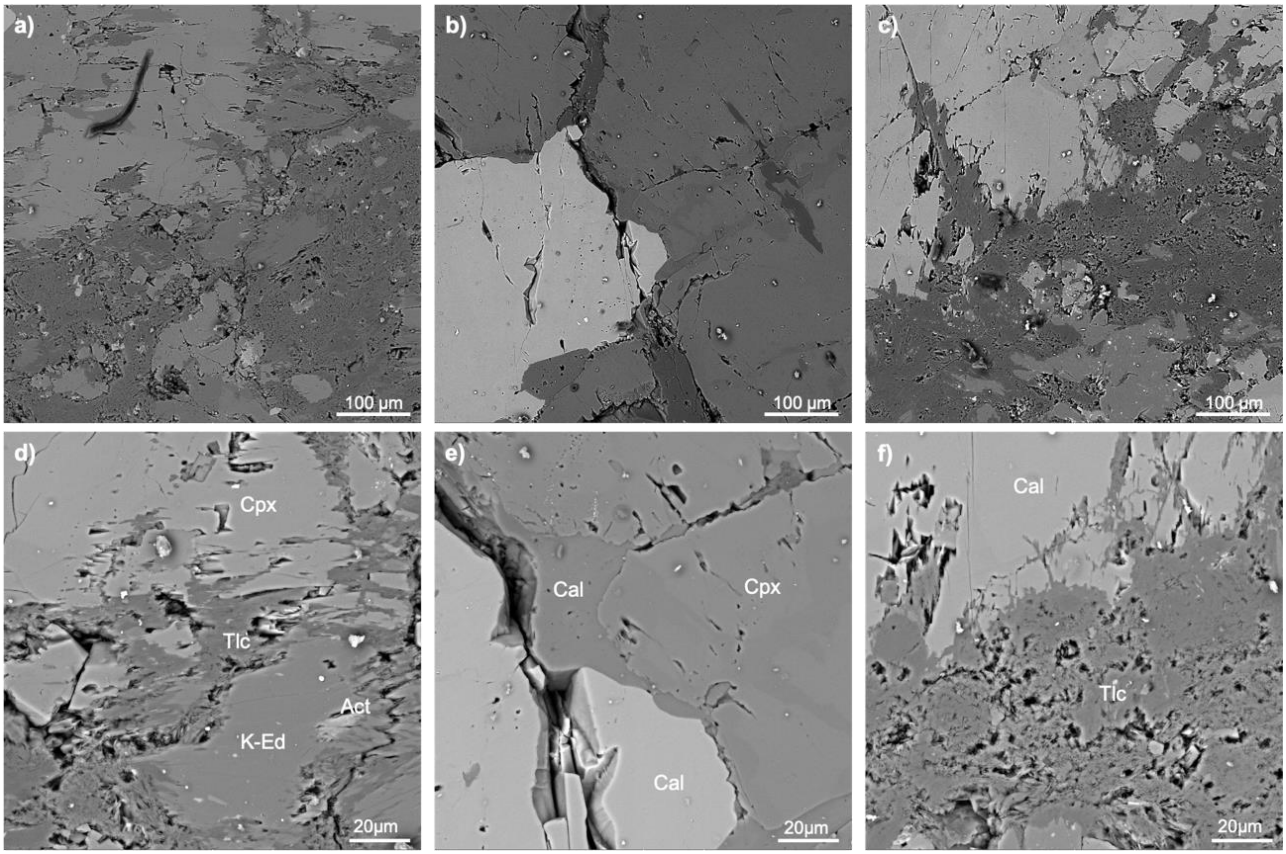

Figure 50. *SEM images from polished thin section of sample S4. Contact between the pyroxenite and the cutting vein (a-c); blasts of talc and calcite between the pyroxenite and the vein rich in potassic edenite ± actinolite, (d-f) are detected. MAG:500x in a, b, c and 2000x in d, e, f (HV: 20 kV; Det: BSE).*

Fibres and elongated particles assemblage detected by TEM/EDS in the following sample were: actinolite, tremolite, cleavage fragments of tremolite and chrysotile. Actinolite exhibits a lath-shaped morphology (Figure 51) as well as asbestos tremolite (Figure 52a).

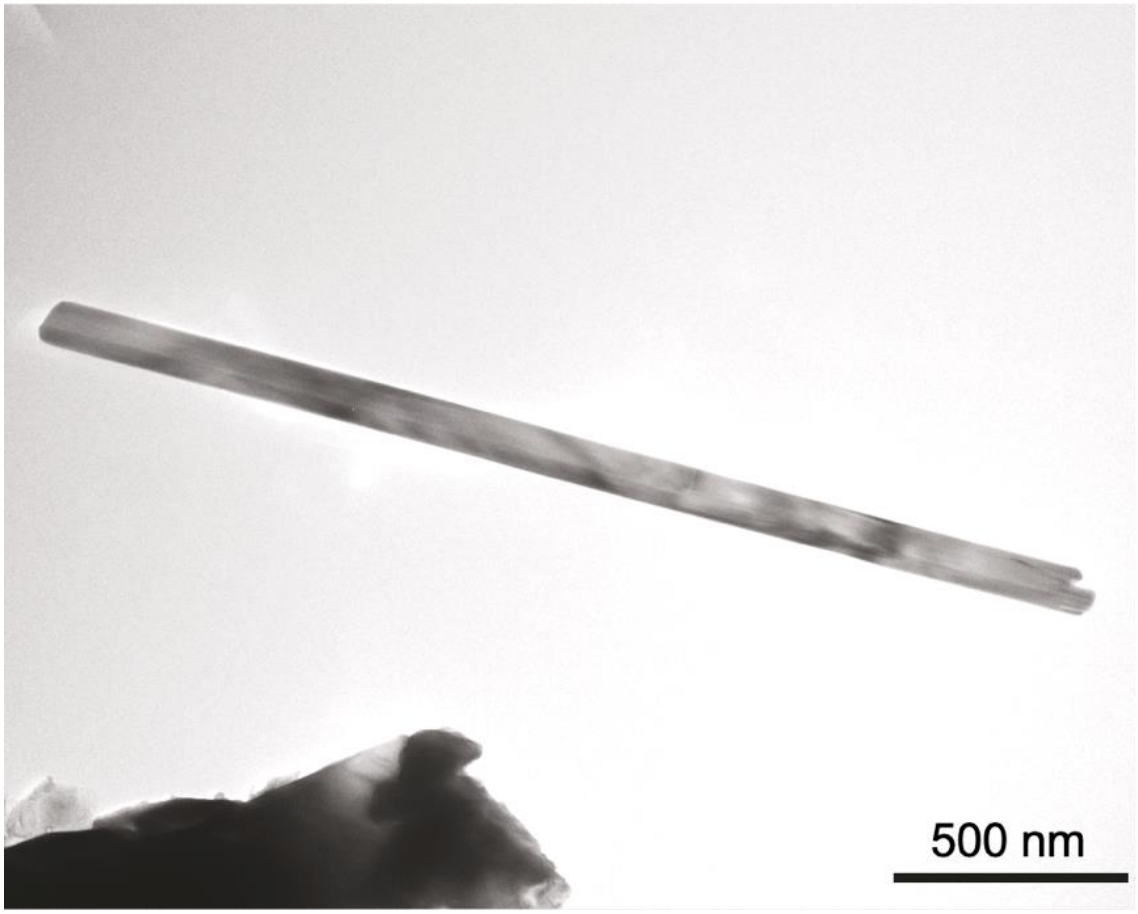

Figure 51. *TEM image. Fibrous actinolite (from Militello et al., 2019a).*

On the other hand, in the same samples, tremolite classified as “non asbestiform” has been observed (Figure 52b). In fact, according to literature data (Van Orden et al., 2008; Belluso et al., 2017), asbestiform habit is confirmed by the typical square terminations of the fibrils, whereas tremolite on Figure 52b better accounts for an origin in a cleavage along the z axis of tremolite, as suggested by the oblique tip of the fibre, projection of the polygonal cross section of the double chain building. Chrysotile, rarely detected in this sample, showed a cylindrical shape.

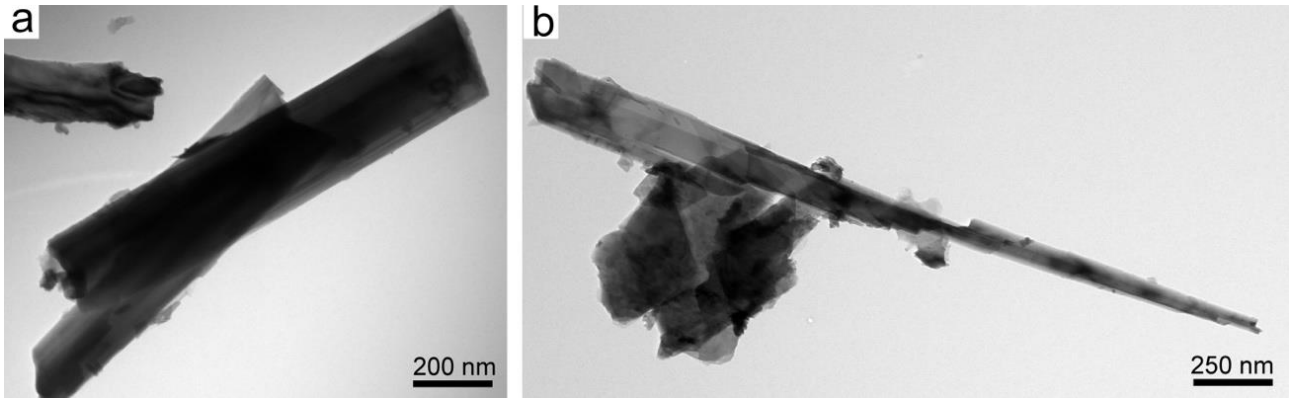

Figure 52. *TEM image of: (a) tremolite as viewed perpendicular to the fibre axis; (b) single crystals of tremolite (cleavage fragment), note the irregular sides. The wider end displays an initial split into two-three fibrils (from Militello et al., 2019a).*

According to the literature (Belluso et al., 2017; Van Orden et al., 2008) the asbestiform habit is confirmed by the typical square terminations of the fibrils, whereas the sample better accounts for an origin in the cleavage along the z axis of the tremolite, as suggested by the oblique tip of the fibre and the projection of the polygonal cross-section of the double chain building.

6.14 Mineral chemistry

For each spot, EDS/SEM analyses were performed with the following working conditions: 2500x of magnifications, 15 of beam intensity, back scattered electrons as detectors and 60 seconds as time of analysis.

According to the classification of amphiboles proposed by the IMA in 2012 (Hawthorne et al., 2012), the analysed samples possess amphiboles all belong to the subgroup of calcium amphiboles. Considering the classification of calcium amphiboles according to the classification of Leake (1997), almost all of the samples fall within the amphiboles of the tremolite-actinolite series with the exception of sample S3 which is classified as magnesium-hornblende (Figure 53).

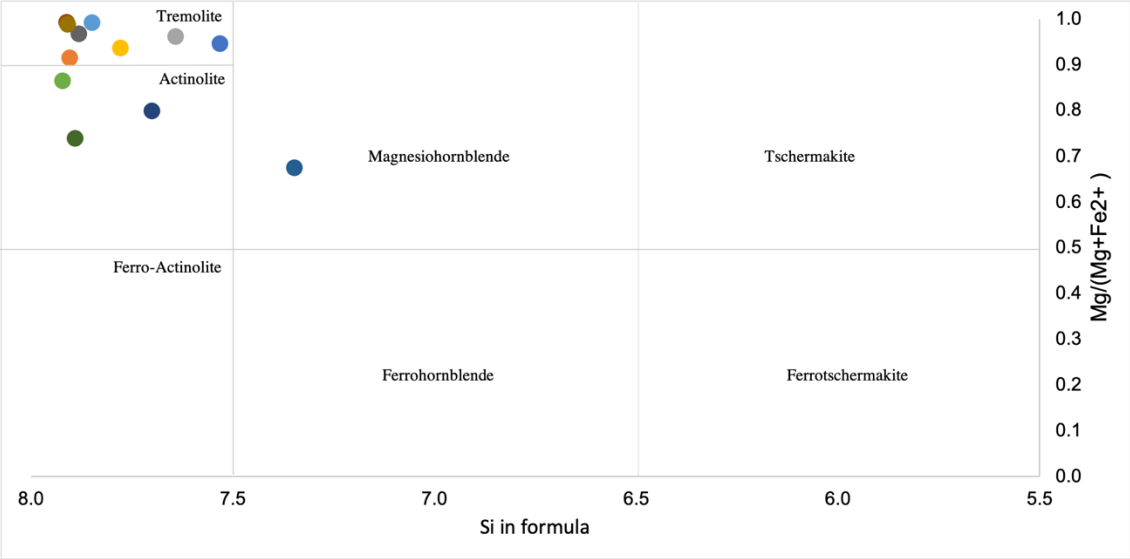

Figure 53. *classification of the calcic amphiboles (from Leake et al., 1997).*

Chemical compositions listed in Table 4 indicate that amphiboles belong to the tremolite-actinolite series, while the amphibole of spot 2 of sample S4, is classified as potassic-edenite.

Table 4. *Average compositions of asbestiform and non-asbestiform amphiboles.*

Samples	**F1**	**F2**	**F3**	**P1**	**P2**	**P3/A5**	**A1**	**A2**	**A4**	**S2**	**S3**	**S4 Spot 1**	**S4 Spot 2**
Oxides (wt%)													
SiO_2	54.66	57.19	55.55	56.49	59.06	56.67	54.97	58.39	57.37	57.85	50.85	55.84	57.41
TiO_2	0.16										0.61		0.15
Al_2O_3	3.15	0.33	2.31	2.72	0.52	0.97	4.75	0.33	0.42	0.19	5.11	1.07	0.26
Cr_2O_3	0.55		0.21	0.18	0.16	0.20			0.53	0.17		0.18	
MnO	0.13	0.31	0.15	0.10		0.30	0.35		0.17		0.40	0.32	0.18
FeO	2.34	4.34	2.75	5.21	0.36	7.04	8.20	0.30	2.43	1.55	13.01	10.75	1.85
NiO	0.16					0.25			0.19				
MgO	23.09	22.21	23.27	21.72	25.71	20.21	17.28	24.99	23.26	24.16	14.77	17.08	24.02
CaO	13.18	12.79	13.00	10.44	14.12	10.70	10.24	13.77	13.19	13.61	12.80	12.88	9.74
Na_2O	0.41	0.51	0.74	1.01	0.07	1.28	1.97	0.07	0.16	0.09	0.57	0.46	2.46
K_2O		0.36		0.05		0.11	0.07	0.08					2.28
F													1.64
Formula Assignments													
T (ideally 8 a.p.f.u.)													

Si	7.53	7.91	7.64	7.78	7.85	7.92	7.70	7.91	7.88	7.91	7.35	7.89	7.89
Al	0.47	0.05	0.36	0.22	0.08	0.08	0.30	0.05	0.07	0.03	0.65	0.11	0.04
T subtotal	8.00	7.96	8.00	8.00	7.93	8.00	8.00	7.97	7.95	7.94	8.00	8.00	7.95
C (ideally 5 a.p.f.u.)													
Ti	0.02										0.07		
Al	0.04		0.02	0.22		0.08	0.49				0.22	0.07	
Cr	0.06		0.02	0.02	0.02	0.02			0.06	0.02		0.02	
Ni	0.02					0.03			0.02				
Mn^{2+}												0.04	
Fe^{2+}	0.12	0.42	0.19	0.30		0.66	0.91		0.16	0.06	1.53	1.27	0.08
Mg	4.74	4.58	4.77	4.46	4.98	4.21	3.61	5.00	4.76	4.92	3.18	3.60	4.92
C subtotal	5.00	5.00	5.00	5.00	5.00	5.00	5.00	5.00	5.00	5.00	5.00	5.00	5.00
B (ideally 2 a.p.f.u.)													
Mn^{2+}	0.02	0.04	0.02	0.01		0.04	0.04		0.02		0.05		0.02
$Fe2^{+}$	0.15	0.08	0.13	0.30	0.04	0.17	0.06	0.03	0.12	0.12	0.04		0.14
Mg					0.11			0.05					
Ca	1.84	1.89	1.86	1.54	1.85	1.60	1.54	1.92	1.86	1.88	1.91	1.95	1.44
Na				0.15		0.20	0.37					0.05	0.41
B subtotal	2.00	2.00	2.00	2.00	2.00	2.00	2.00	2.00	2.00	2.00	2.00	2.00	2.00
A (from 0 to 1 a.p.f.u.)													
Ca	0.11	0.01	0.06		0.16			0.08	0.08	0.11	0.07		
Li													
Na	0.11	0.14	0.20	0.12	0.02	0.15	0.17	0.02	0.04	0.02	0.16	0.08	0.25
K		0.06		0.01		0.02	0.01	0.01					0.40
A subtotal	0.22	0.21	0.26	0.13	0.18	0.17	0.18	0.11	0.13	0.14	0.23	0.08	0.65
O (non-W)	22.00	22.00	22.00	22.00	22.00	22.00	22.00	22.00	22.00	22.00	22.00	22.00	22.00
W (ideally 2 a.p.f.u.)													
OH	2.00	2.00	2.00	2.00	2.00	2.00	2.00	2.00	2.00	2.00	2.00	2.00	1.29
F													0.71
W subtotal	2.00	2.00	2.00	2.00	2.00	2.00	2.00	2.00	2.00	2.00	2.00	2.00	2.00

In detail, samples F1, F2, F3, P1, P2, A2, A4 and S2 possess amphiboles close to the tremolite end-member with a $Mg/(Mg+Fe^{2+})$ ratio ≥ 0.9, whereas samples P3/A5, A1, S3 and S4 have a chemical composition close to actinolite end-member with a $Mg/(Mg+Fe^{2+})$ between 0.5 and 0.9.

The iron content of actinolite amphiboles ranges from 7.04 to 13.01 wt%. Tremolite amphiboles have calcium values similar to actinolite ones and vary from 10.44 to 13.61 wt%, whereas have higher magnesium values (21.72-24.99 wt%). In general, it was revealed a few percent substitution of tetrahedral Al in the Si site, and minor replacements of Mg for Fe.

In sample A3/S1, one spot was analysed in the lizardite vein (spot 1) and one in the host rock (spot 2). The recalculations were performed with full side occupancy (the H_2O site was also filled). In the site "spot 1" a low replacement of Al and Fe for the Mg in the octahedral sites was evidenced. In the site "spot 2" in addition to Al and Fe, a very low replacement of Mn and Ni for the Mg in the octahedral sites was detected (Table 5).

Table 5. *Average compositions of serpentines.*

Sample	A3/S1 Spot 1	A3/S1 Spot 2
Oxides (wt%)		
SiO_2	42.84	43.75
Al_2O_3	2.13	2.10
FeO	1.87	1.85
MnO	0.12	0.18
MgO	40.08	39.65
NiO	0.16	0.20
Total	100.13	100.77
Si	1.99	2.01
Al	0.12	0.11
Fe^{2+}	0.07	0.07
Mn	0.00	0.01
Mg	2.77	2.72
Ni	0.01	0.01

The structural formula for serpentine "spot 1" is $(Mg_{2.77}Fe_{0.07}Al_{0.12})(Si_{1.99})O_5(OH)_4$ and for the serpentine of the "spot 2" is $(Mg_{2.72}Al_{0.11}\ Fe_{0.07}Mn_{0.01}\ Ni_{0.01})(Si_{2.01})O_5(OH)_4$.

7. 3D ROCK IMAGING BY SYNCHROTRON RADIATION X-RAY MICROTOMOGRAPH

Only suitable samples of the dataset (A3/S1, S2, S3, S4) were selected for this investigation. In addition to the conventional techniques (OM, SEM-EDS and TEM), an original methodological approach was addressed through the SR X-ray μCT. This semi-destructive technique can help to better observe the arrangement of the fibres in the three dimensions and help the comparative description of cleavage.

Sample A3/S1 underwent microtomographic analysis but did not provide effective information and was subsequently discarded. The high and almost equal density of the mineralogical phases, the consequent low-density contrast and lack of voids or fractures determined an almost total absorption of the X-rays and prevented the collection of significant information. Even the occurrence of magnetite, whose high density absorbed most of the radiation, obscured the other phases.

Conversely, the other three samples exhibited good discrimination. Sample S2 was cut for tomographic scanning. Starting from single slices of tomography (Figure 54b), obtaining images of the 3D arrangement and the geometric relationships between the fibre-bearing volumes and the massive rock. In particular, a diopside and tremolite-rich vein was evidenced, where the tremolite fibres are stretched (dashes); around there, dolomite and clinochlore are in contact.

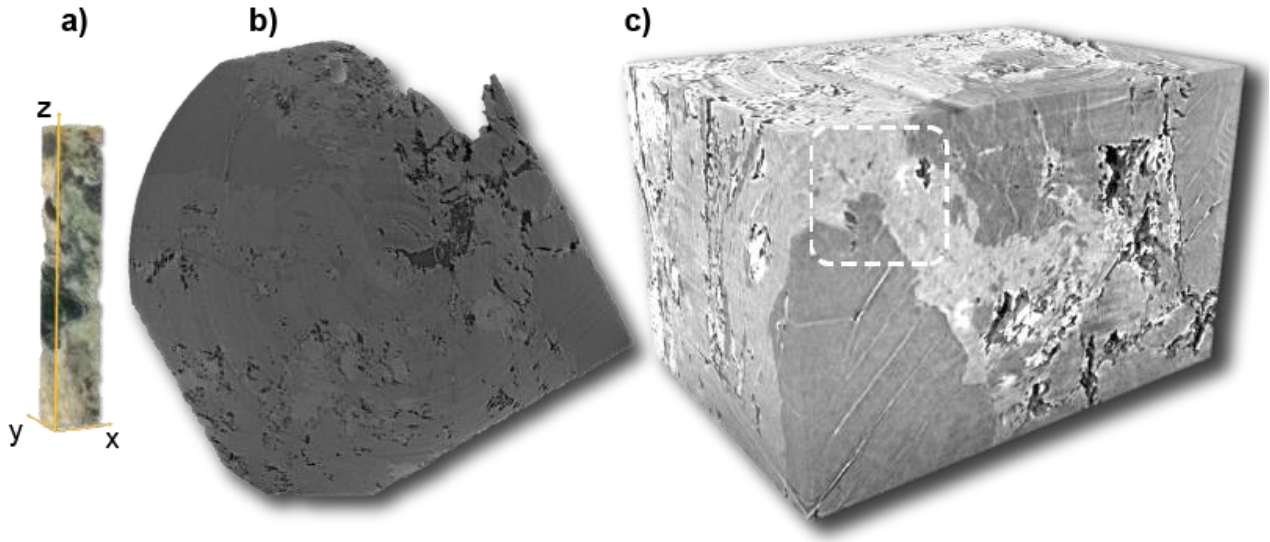

Figure 54. *Sample 2 (S2). (a) Sample cut for tomographic scanning; (b) example of one single slice generated (1800 scans in total); (c) volume rendering (7.7 mm3) obtained by Synchrotron Radiation X-ray microtomography (rendering performed using the commercial software VGStudio Max 2.0).*

In the slice (Figure 54 b), the actinolite overgrows the plagiogranite and the plagioclase inside the metabasalt. The 3D reconstruction reveals the texture and the rugged contact between the

metabasalt and the plagiogranite. As is particular evident in Figure 55 (b), sometimes fibrils and acicular crystals are associated.

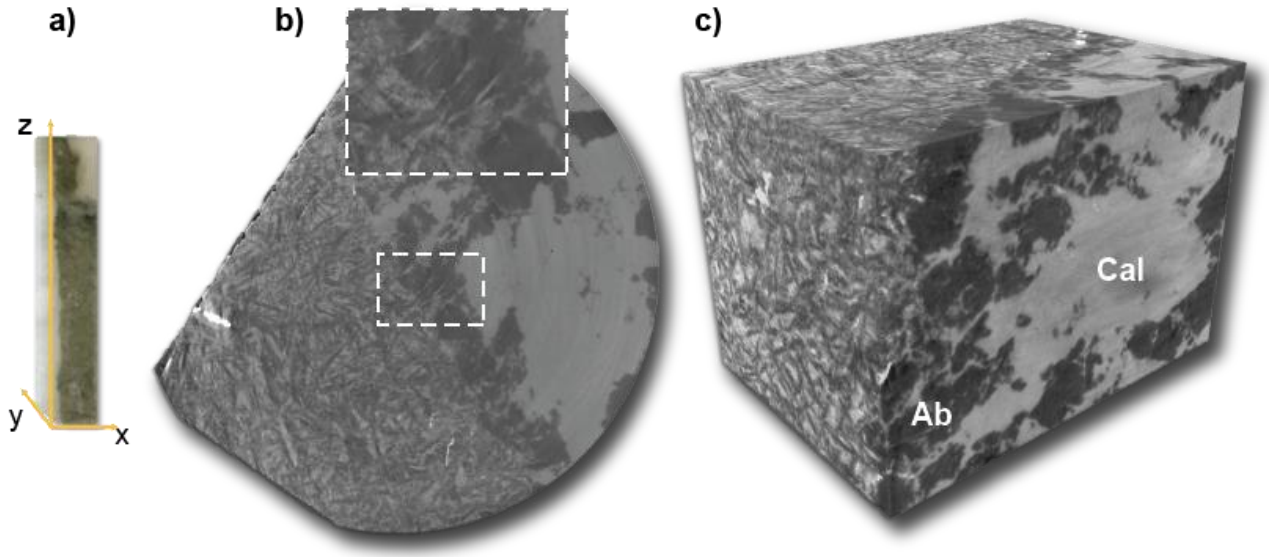

Figure 55. *Sample 3 (S3). (a) Sample cut for tomographic scanning; (b) example of one single slice generated (1800 scans in total); (c) volume rendering (7.5 mm3) obtained by Synchrotron Radiation microtomography (rendering performed using the commercial software VGStudio Max 2.0).*

The elaboration of the synchrotron data showed that the veins rich in talc and actinolite cut the sample (Figure 56). This was also evident from the low-magnification SEM image, and from the vein direction and texture shown in both the 2D axial slice and 3D rendering.

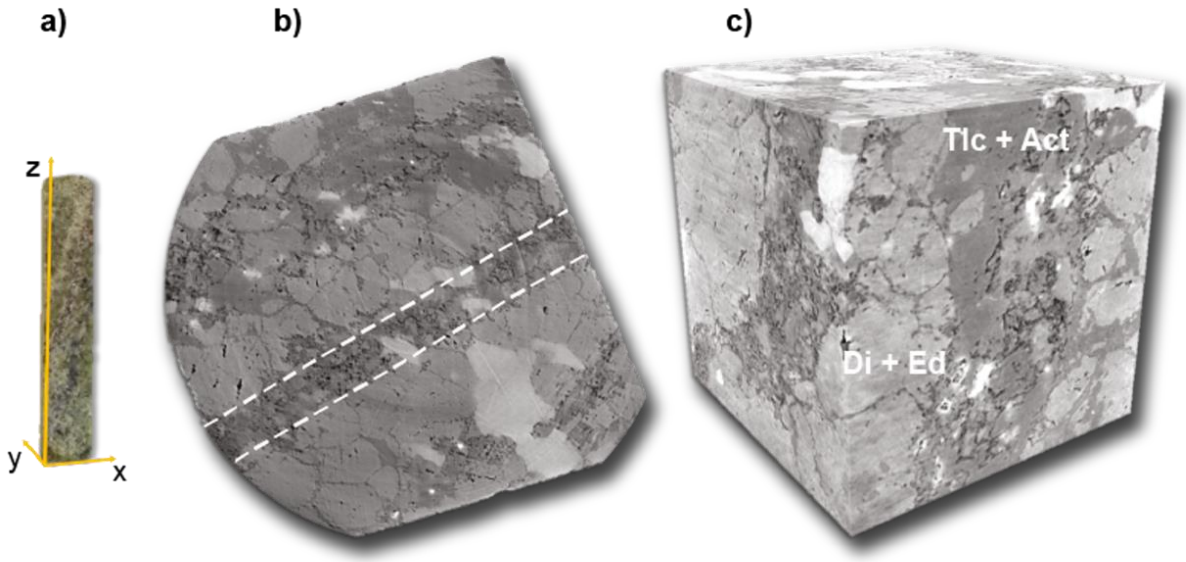

Figure 56. *Sample 4 (S4). (a) sample cut for tomographic scanning; (b) example of one single slice generated (1800 scans in total); (c) volume rendering (7.4 mm3) obtained by Synchrotron Radiation X-ray microtomograph (rendering performed using the commercial software VGStudio Max.*

8. EFFECT OF COMMINUTION ON ASBESTIFORM AND NON-ASBESTIFORM AMPHIBOLES

The aim of this part of the project was to investigate samples containing amphiboles with fibrous or acicular/prismatic habit. After analysis under OM and SEM in order to characterize them from a petrographic point of view and in their textural variations, it was later observed by SEM the change of the particles geometry and morphology after different time length of comminution. Samples F1, F2, F3 are the best representative amphiboles with asbestiform aspect. Samples P1, P2 and P3 represent the most appropriate selection of samples with fibrous but non-asbestiform aspect.

Before the comminution, preliminary analyses in a 3D piece of sample (Figure 57) were carried out by SEM-EDS. In F1, F2 and F3, amphiboles occur as bundles formed by flexible fibrils, stretched and parallel each other.

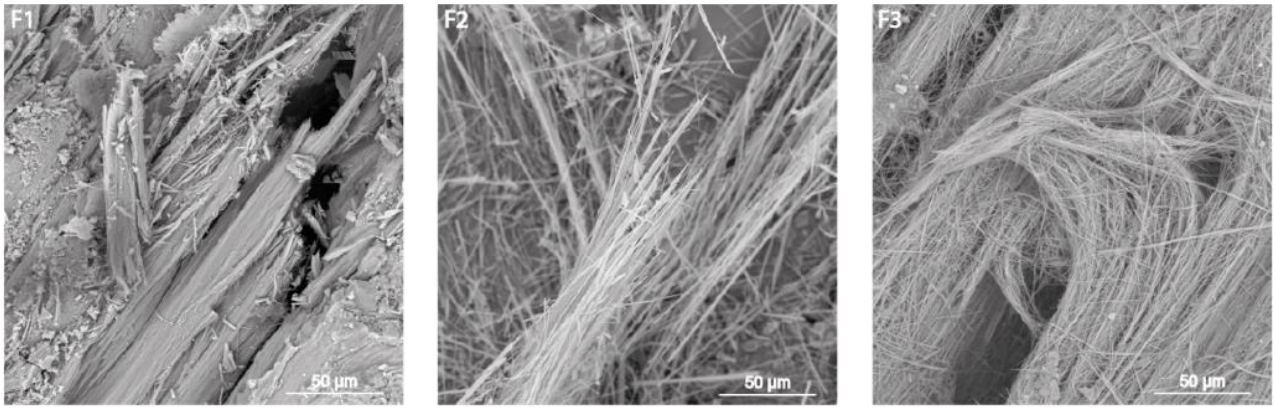

Figure 57. *SEM images of isolated fragments of asbestiform (F1, F2, F3) amphiboles (HV: 20 kV; Det: BSE).*

In P1, P2 and P3, amphiboles occur as prismatic/acicular crystals with the planar surfaces leading to separation like splinters with the geometric ratios of fibres (Figure 58).

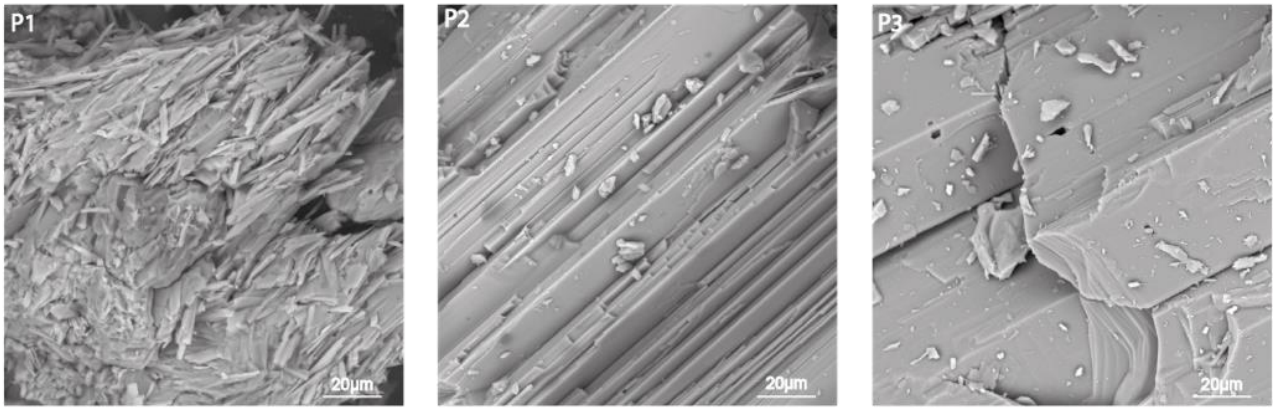

Figure 58. *SEM images of isolated fragments of non-asbestiform amphiboles (P1, P2, P3) (HV: 20 kV; Det: BSE).*

8.1 Sample preparation

Each sample was divided into three aliquots of 3 g each (weighed by analytical balance RadwagAs 220.R2) and mechanically milled at three different time intervals (30 seconds, 120 seconds, 300 seconds respectively), at constant speed (Speed 2) with the Retsch-Mill McCrone micronizer, equipped with a hermetically sealed case containing up to 48 small agate cylinders. The case is shaken so that the agate cylinders gently grind the sample. The samples were then manipulated under a laminar flow hood and prepared according to the procedure prescribed by the decree (all. 1 - Quantitative determination of asbestos in bulk samples) for analyses by SEM (Paragraph 5.3).

Preliminary analyses were made under SEM at 1000x magnification. The measurements of the fibres and therefore the counts were made at 2000x magnification, by analysing an area of 2 mm^2, in accordance with the guidelines in the Italian M.D. 06/09/1994.

The morphology and geometric features were analysed and measured for each sample. Both length and diameter were measured for each particle. Afterwards, a comparison of lengths, widths and aspect ratio was carried out.

8.2 Data elaboration and results

Asbestiform amphiboles show average aspect ratio values ranging from 15:1 to 65:1 (Figure 59). The median ranges between 30:1 to 35:1 (more than 30%).

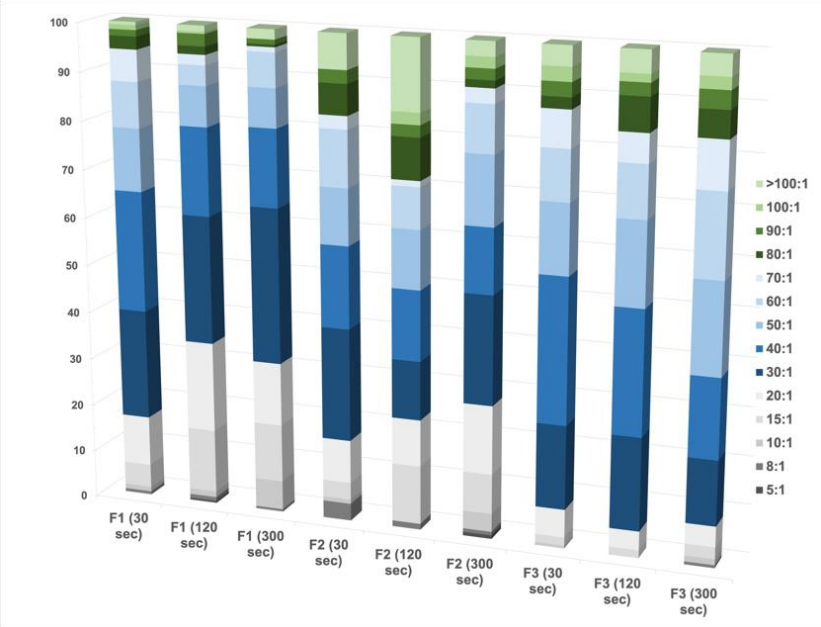

Figure 59. *Illustrative histograms of the frequency (expressed as a percentage) of the different length: width ratios of the particles present in the samples (F1, F2 and F3) for the three different grinding times (30, 120 and 300 seconds).*

In order to check the statistical reliability of the data, the one-way Analysis of Variance (ANOVA) was carried out, verifying the internal variability within each group. Statistical significance was assessed at a p-value < 0.05. Provided that the p-value was lower than 0.05, a statistically significant difference was evidenced for the three groups. A summary of means, standard deviations for the aspect ratio of the particles and the statistical data is shown in table 6.

Table 6. *Number of particles (N) detected in the different samples at different grinding times. Values represent mean of each aspect ratio (A/R Mean), standard deviation (SD) and P-value.*

Milling time	Sample	N	A/R mean (µm)	SD	P-Value
30 sec	F1	305	37.24	18.89	< 0.05
	F2	111	44.05	30.14	
	F3	173	44.54	24.12	
120 sec	F1	240	30.91	20.28	< 0.05
	F2	82	52.28	40.63	
	F3	307	47.18	26.20	
300 sec	F1	198	29.86	19.08	< 0.05
	F2	133	38.58	31.14	
	F3	164	48.95	25.88	

Generically, a slight deviation of the 30 sec time length curves from the other ones is evidenced. By extending the time of grinding, a comparison between the trends of the other two groups shows no significant difference (Figure 60).

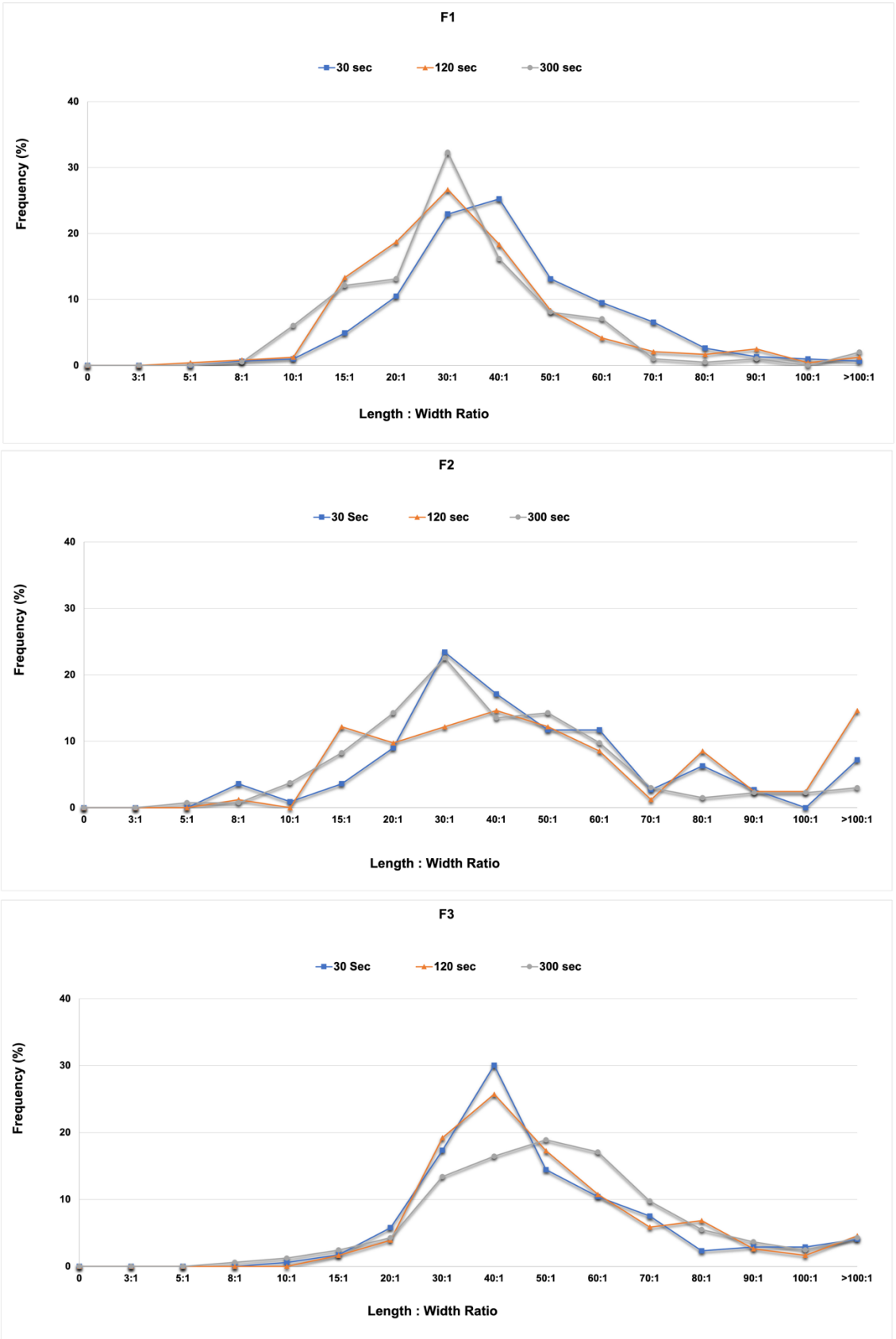

Figure 60. *Comparison of the aspect ratio distribution, in the three different intervals of grinding times, of asbestiform (F1, F2, F3) amphiboles.*

The length but also the diameter of the asbestiform amphiboles tends to decrease in the early stages of comminution.

Non-asbestiform amphiboles demonstrate (Figure 61) average aspect ratio values ranging from 3:1 to 20:1, with prevalent frequency 8:1 (~45%).

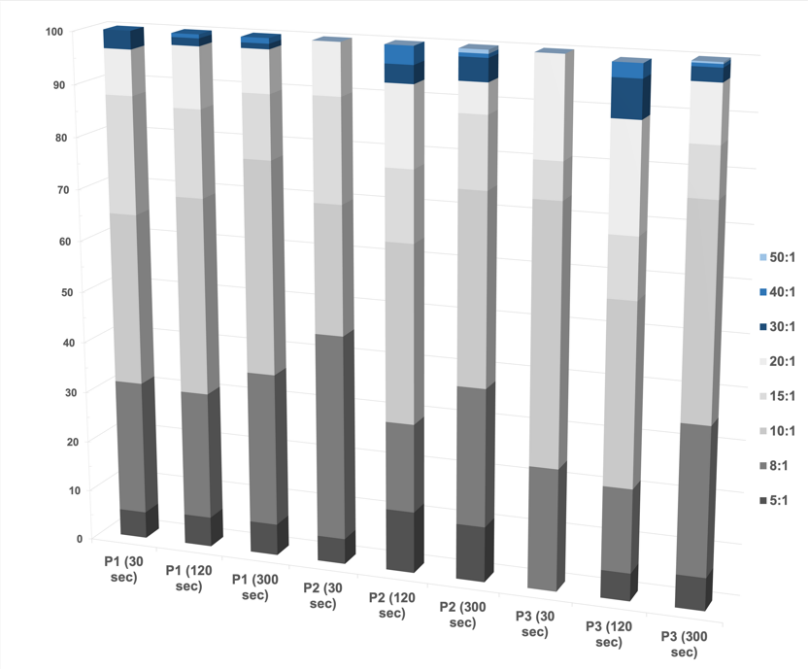

Figure 61. *Illustrative histograms of the frequency (expressed as a percentage) of the different length: width ratios of the particles present in the samples (P1, P2, P3,) for the three different grinding times (30, 120 and 300 seconds).*

Only samples with non-asbestiform amphiboles (P1-P2-P3), ground for 30 and 300 seconds, have a p-value higher than 0.05, which means there are no statistically significant differences. A summary of means, standard deviations for the aspect ratio of the particles and the statistical data is shown in table 7.

Table 7. *Number of particles (N) detected in the different samples at different grinding times. Values represent Mean of each aspect ratio (A/R Mean), standard deviation (SD) and P-value.*

Milling time	Sample	N	A/R mean (µm)	SD	P-Value
30 sec	P1	57	7.01	3.32	> 0.05
	P2	20	6.46	2.57	
	P3	42	7.02	2.57	
120 sec	P1	136	6.83	3.13	< 0.05
	P2	58	7.53	4.54	
	P3	111	9.11	6.81	
300 sec	P1	97	6.44	2.99	> 0.05
	P2	138	6.73	4.67	
	P3	313	6.77	3.72	

Generically, a slight deviation of the 30 sec time length curves from the other ones is evidenced. By extending the time of grinding, a comparison between the trends of the other two groups shows no significant difference (Figure 62).

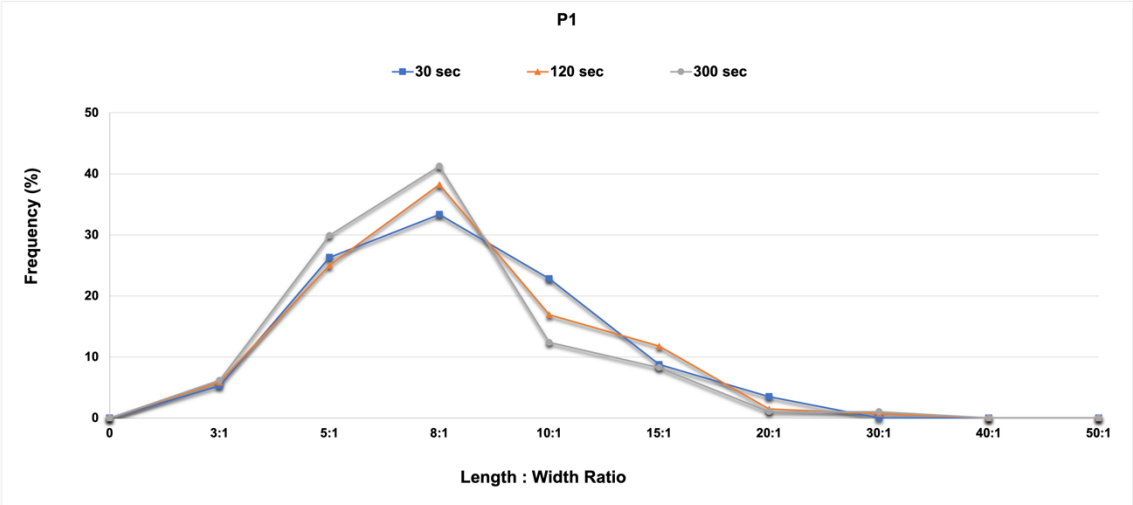

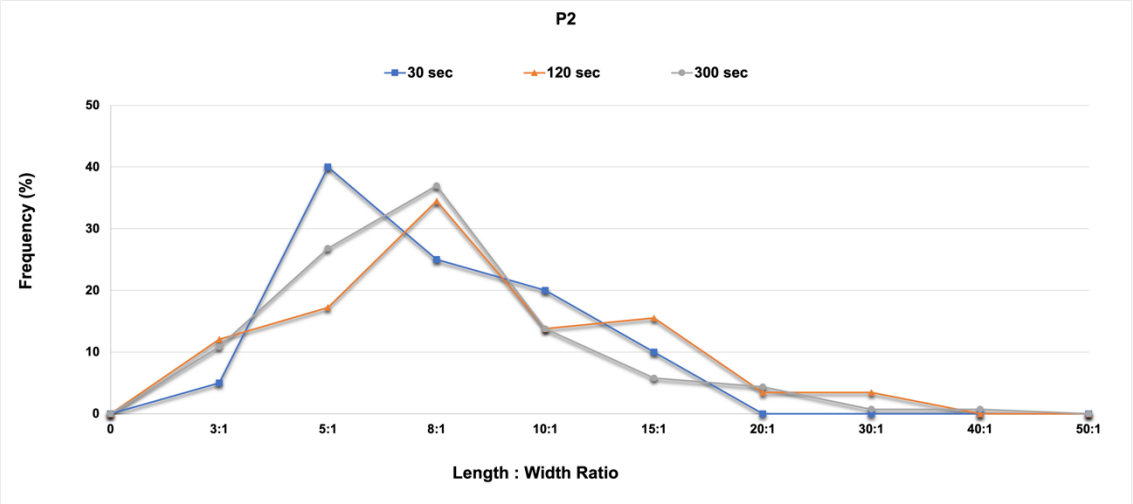

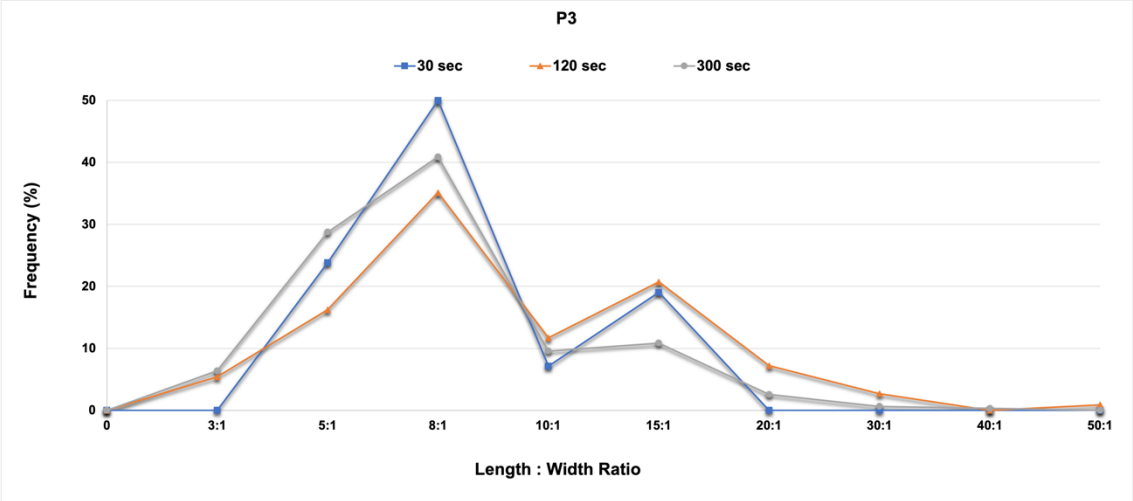

Figure 62. *Comparison of the aspect ratio distribution, in the three different intervals of grinding times, of non-asbestiform (P1, P2, P3) amphiboles.*

The length of the prismatic tremolite varies rather uniformly throughout the milling process.

8.3 Comparison of asbestiform and non-asbestiform amphiboles

Furthermore, for each grinding time, the granulometric range of the fibres was determined.

As the grinding time increases, asbestiform amphiboles tend to have a more homogeneous distribution (Figure 63) in terms of width.

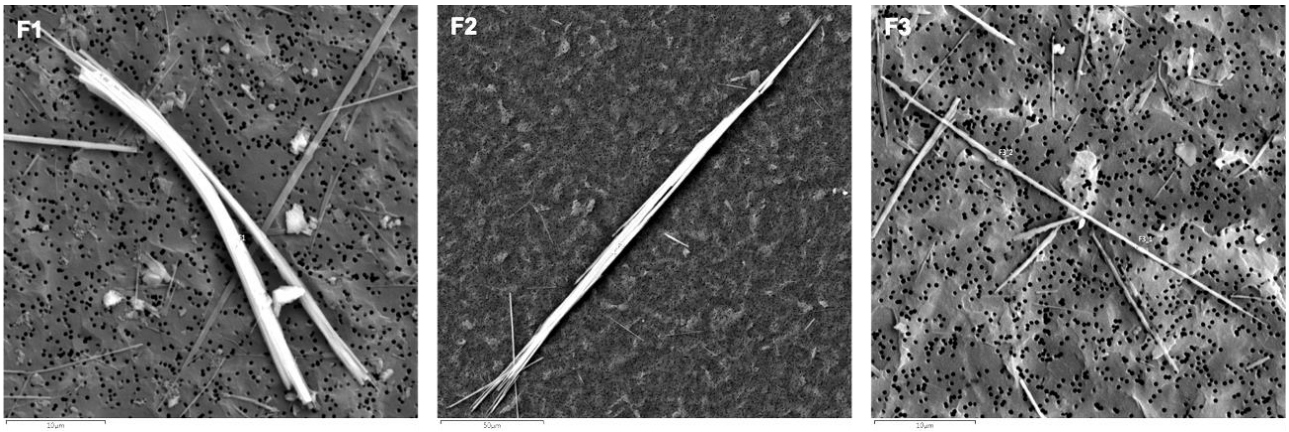

Figure 63. *SEM images of asbestiform amphibole fibres (F1, F2, F3) (HV: 20 kV; Det: BSE and EDS).*

The number of countable fibres decreases, because many turned below the detectable dimensions at 2000x of magnification (fibrils reached a diameter even lower than 0.2-0.1 μm). As a rule, length does not seem affected by the milling, therefore it tends to remain more or less constant.

Conversely, in the case of non-asbestiform amphiboles, at increasing grinding time, a greater dispersion of width is evidenced (Figure 64).

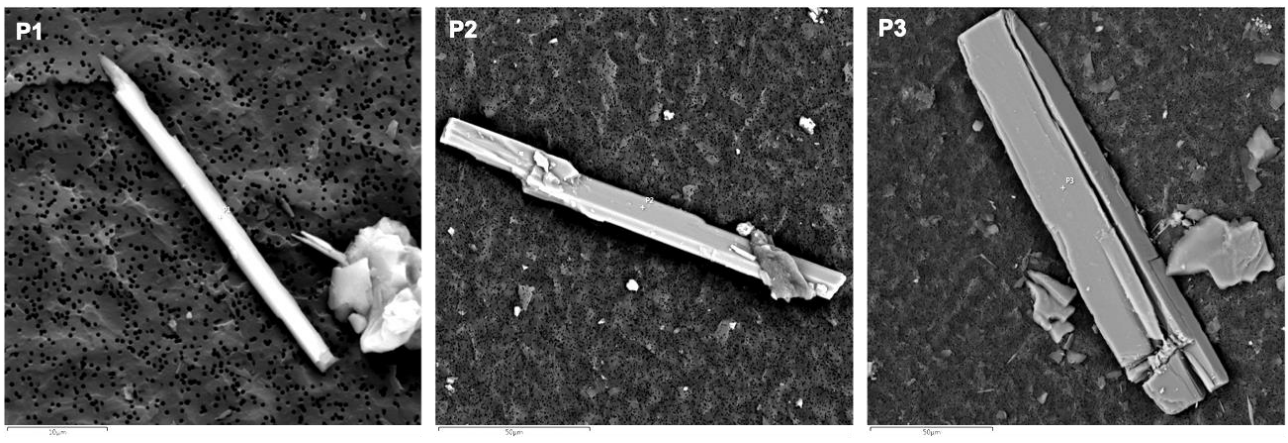

Figure 64. *SEM images of non-asbestiform amphibole fibres (P1, P2, P3) (HV: 20 kV; Det: BSE and EDS).*

The number of fibres increases after longer milling time because they separate, producing cleavage fragments. However, the particles shorten considerably in length but also in the diameter, as the width is not below 0.6-0.5 µm.

In non-asbestiform samples, after 30 sec of milling, some fragments were not counted since they did not respect the geometric ratios (Figure 65).

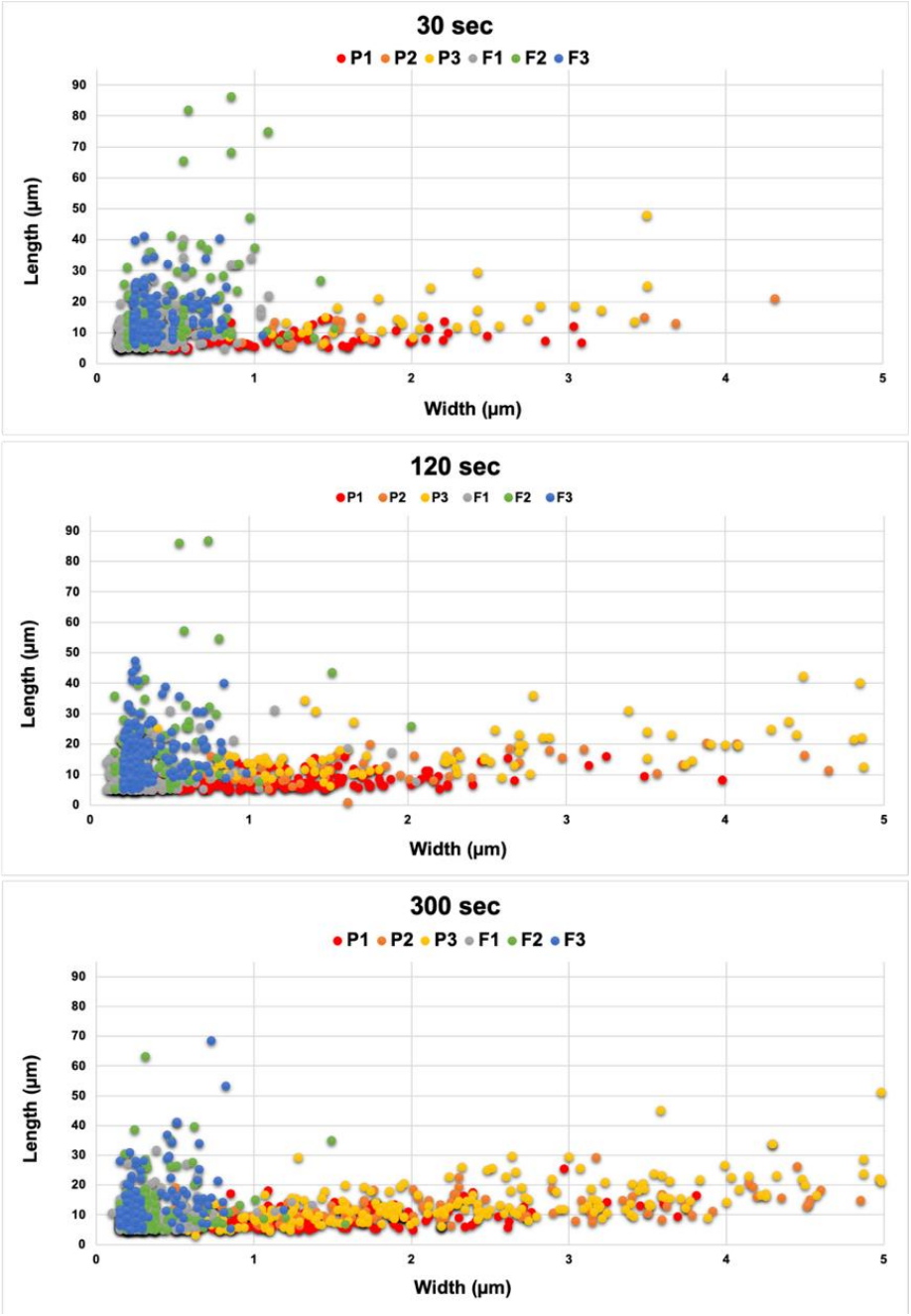

Figure 65. *Influence of milling time (30, 120, 300 seconds respectively) on length and width dimensions of particles.*

Finally, the aspect ratios *vs.* the diameters of the asbestiform amphiboles (samples F1, F2 and F3), were compared with those of non-asbestiform amphiboles (samples P1, P2 and P3), using a chart as in Van Orden et al., (2009). This graph unequivocally highlights that, even after the comminution, the two types of samples show distinct, differences in distribution. However, the distinction is not absolute because some asbestos amphiboles fall below the minimum aspect ratio, while some non-asbestiform particles exceed even greatly the 20:1 aspect ratio (Figure 66).

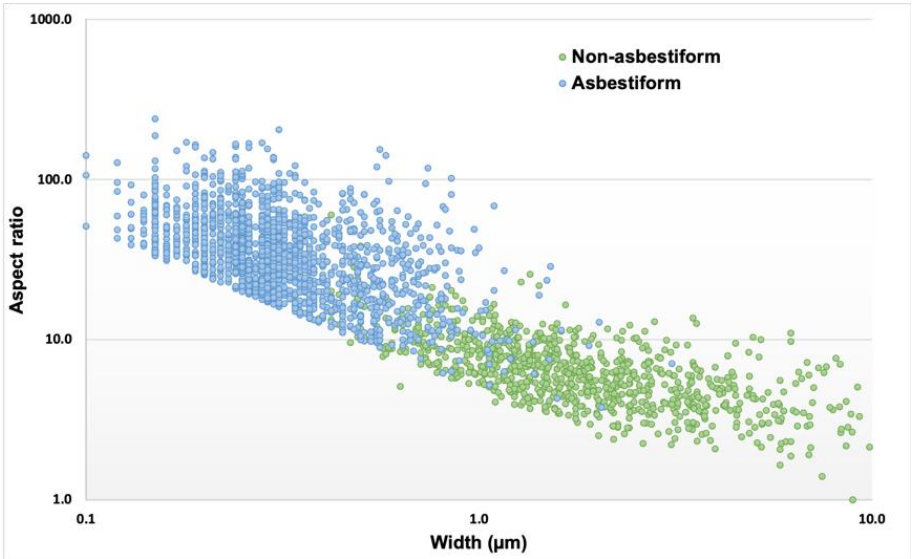

Figure 66. *Relationship between width and aspect ratio (logarithmic scale) for asbestiform and non-asbestiform amphiboles.*

9. THE CONCENTRATION OF ASBESTOS FIBRES: A COMPARATION OF DECREES

In this chapter the rationales and the limits of the regulations in force (M.D. 06/09/1994 and 161/2012) for the quantitative determination of asbestos in excavated earth and rocks have been analysed. The purpose of this part of the research project was to observe the distribution of fibres in the three particle size fractions, therefore also that which is discarded in the preparation phase (M.D. 161/2012) and understand how the choice of one of the two ministerial protocols used as guidelines for the preparation, analysis and calculation of the asbestos concentration can influence the result.

For each sample, the grain size fractions taken into consideration are respectively < 0.106 mm, 0.106 to 2 mm, and 2 to 20 mm.

The reliability and comparability of data are essential to avoid misunderstandings and to provide adequate control and prevention systems, above all, if that lead to social and environmental alerts about the disposal of excavated soils and rocks is of considerable importance.

9.1 Sample preparation

Each 500 g bulk sample was divided into four subsamples 125 g in weight, then was sieved according to the normative. Afterward, slightly different from the method of preparation described in paragraph 5.3, the passers-by the sieves, from 2 to 20 mm and 0.106 to 2 mm were mechanically milled to obtain powders with a grain size of < 0.106 mm. The third sieved fraction below 0.100 mm was instead not milled, in order to observe, without grinding, materials with grain size below 100 µm. After milling, all grain size classes were weighed and prepared for SEM analysis, according to protocol.

9.2 Data elaboration and statistical analysis

The analysis of calc-schist showed no asbestos fibres in any of the three grain size fractions, as expected from petrographic and chemical data. In the metabasalt, some actinolite–tremolite fibres were found in the three grain size fractions, especially in the non-milled fraction < 0.106 mm. However, the concentration in all fractions was much lower than 100 mg/kg. The meta-argillite, characterised by the occurrence of amphiboles of the actinolite–tremolite series, yielded values exceeding 100 mg/kg. However, as this sample presented only the fraction with grain size < 0.106 mm, it was not considered for further investigation because lacking comparative data with the other two size fractions. Therefore, 13 samples obtained from preparation of the six sampled rocks and meta-sediments were analysed by SEM–EDS. Only in the serpentinite, debris and soil, asbestos was

detected in the fractions of all grain size, therefore the attention was paid only to these; meta-argillites, metabasalts and calc-schists were discarded.

To provide the statistical significance of results, three replications were carried out for the three grain size fractions (< 0.106 mm, 0.106 to 2 mm, and 2 to 20 mm) of serpentinite, debris, and soil, yielding a dataset of 26 samples.

The pie charts in Figure 67 show the size fraction data for the sieved (but not yet milled) grain size fractions and therefore the sorting of the original sample.

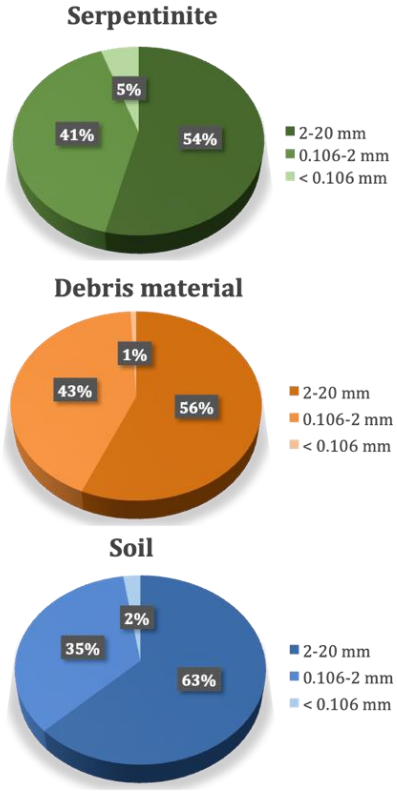

Figure 67. *Pie charts illustrating the percentages of grains in the three studied grain size fractions for serpentinite, debris material, and soil for sieved (but not yet milled) material (from Militello et al., 2019b).*

There were no substantial variations in the distribution of grain sizes across the granulometric fractions between the different samples, in spite of three very different lithotypes. Fraction 2 to 20 mm exceeded half of the material in all three samples (63% of the soil, 56% of the debris material, and 54% of the serpentinite). Fraction 0.106 mm to 2 mm constituted 35% of the soil, 43% of the debris material, and 41% of the serpentinite. The non-milled < 0.106 mm fraction made up < 5% of all materials.

Only particles belonging to asbestos by composition and a length of > 8 µm and a length: diameter ratio of ≥ 3:1 were counted. We considered fibres with these dimensions due to the presence

of a very high number of short fibres in the background of some filters, which would not provide useful information to assess asbestos abundance and therefore asbestos concentration. We did not attempt to measure morphological variation to avoid generating a further source of error in fibre counts. Furthermore, for fibres that did not lie completely in the read-fields, only those parts included within the fields were measured.

The calculation of the volume of each fibre or bundle of fibres was based on approximating them to cylinders with measured length and diameter and using the standard formula for cylinder volume. Although some fibres had an aspect ratio (i.e. length: width) that would make them countable, those with excessively large diameters unduly influence the measured asbestos volume and hence the final concentration. To understand how the presence and proportion of large fibres affect the concentration and to ensure that a representative population of asbestos fibres was captured, fibres presenting high individual volumes (in particular, those with large diameters) were defined as outliers. In the context of fibre counting, samples were also observed at lower magnification (500–1000×) modes in order to verify whether fibres identified as outliers were single or common cases. Therefore, we considered outliers those fibres whose number was around 6% on average of total counted fibres. Furthermore, such fibres were considered outliers because their individual volumes deviated excessively from the average volume of the fibres found in a given particle size fraction (Figure 68).

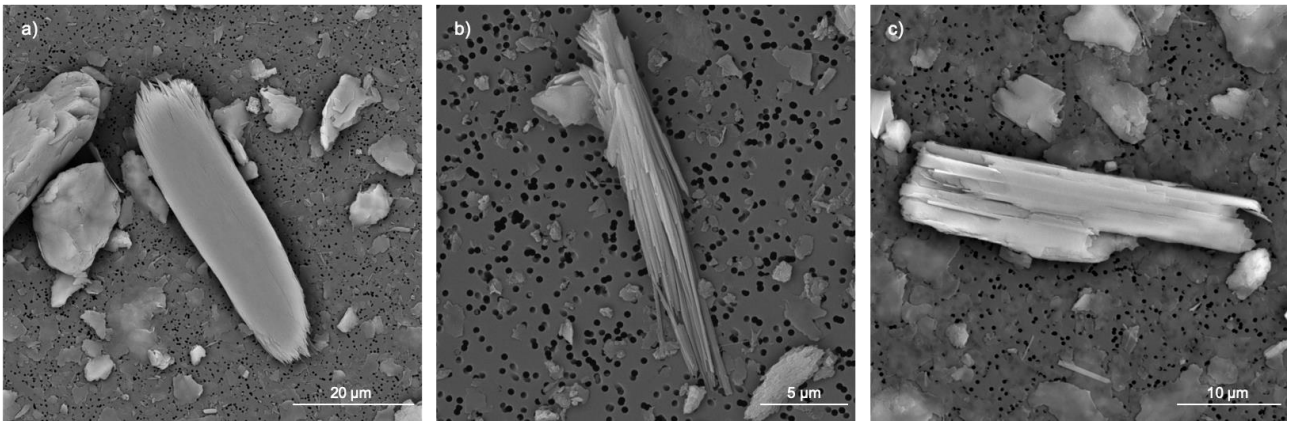

Figure 68. *SEM photomicrographs of outlier fibres. Examples from (a) serpentinite; (b) debris; and (c) soil (High Vacuum; 20 kV; magnification: 4000×, 1200×, 7000×; Detector: Back scattered electrons) (from Militello et al., 2019b).*

Specifically, a fibre was considered to be an outlier if its volume V:

$$V > Q3 + (3 \cdot IQR)$$

where V is the volume of an individual fibre, Q3 is the 3rd quartile, and IQR is the interquartile

range (from 1st to 3rd quartile) in the distribution of individual fibres volumes.

Investigation of descriptive statistics, such as frequency distribution (arithmetic mean) and an estimation of the population variability (standard deviation) of data, were calculated for asbestos concentration of each replica (R1, R2, R3) for all the samples (serpentinites, debris materials and soils). To evaluate the statistical reliability of the data, one-way analysis of variance (ANOVA) was performed. This permitted us to compare the internal variability in each group with the variability between the groups. Statistical significance was determined by a P value < 0.05. Where necessary, for the variation of significant differences Tukey's post-hoc test was done.

9.3 Results

In the serpentinite, only chrysotile was found in all three grain size fractions (Table 8).

Table 8. *Percentage values of asbestos varieties in the grain size fractions of each sample (from Militello et al., 2019b).*

Samples		Not milled <0.106 mm	Milled 0.106–2 mm	Milled 2–20 mm
Serpentinite	% chrysotile	100	100	100
	% actinolite–tremolite	0	0	0
Debris material	% chrysotile	55.38	51.28	6.77
	% actinolite–tremolite	44.62	48.72	93.23
Soil	% chrysotile	5.75	7.57	2.27
	% actinolite–tremolite	94.25	92.43	97.73

The highest number of fibres (206) was detected in the 2 to 20 mm size fraction, 161 fibres in the 0.106 to 2 mm fraction, and 84 fibres in the non-milled fraction. The corresponding average volume of asbestos fibres in each grain size fraction was lowest in the 2 to 20 mm size fraction and highest in the < 0.106 mm fraction (Table 9).

Table 9. *Average volumes of the three replicates (R1, R2, R3) for each particle size fraction. Average volume was calculated considering (first column) and not considering the outliers (second column). The total number of fibres and the total number of fibres excluding the outliers are also reported (from Militello et al., 2019b).*

Lithotype	Grain size intervals		Total fibres (n.)	Outlier fibres (n.)	Average volumes on 3 replicas (μm^3)	Standard Deviation (SD)	Average volumes (without outliers) on 3 replicas (μm^3)	Standard Deviation (SD)
Serpentinite	Not milled	< 0.106 mm	84	8	49.00	1.54	24.37	6.25
	Milled	0.106–2 mm	161	10	36.91	5.94	22.82	2.09
		2–20 mm	206	9	36.51	5.31	23.40	9.22
Debris material	Not milled	< 0.106 mm	20	1	4.54	1.31	3.34*	1.05
	Milled	0.106–2 mm	26	2	13.12	7.51	6.12*	1.18
		2–20 mm	44	1	7.26	5.05	4.18	2.63
Soil	Not milled	< 0.106 mm	25	2	13.03	4.02	9.30	1.11
	Milled	0.106–2 mm	22	2	13.56	4.99	10.56	2.31
		2–20 mm	15	0	13.97	0.00	13.97	0.00

This is consistent with the fact that the < 0.106 mm fraction was not milled, meaning that a large number of fibres was naturally produced by handling the sample. Excluding the outlier fibres from the average volume calculations from the three lithotypes, the values tended to be homogenised in the three granulometric fractions (Table 9). The asbestos concentration decreased monotonically at decreasing grain size class, both when outlier fibres were counted and not (Figure 69a). Asterisks in Figure 66 indicate significant differences between groups (* = $p < 0.05$).

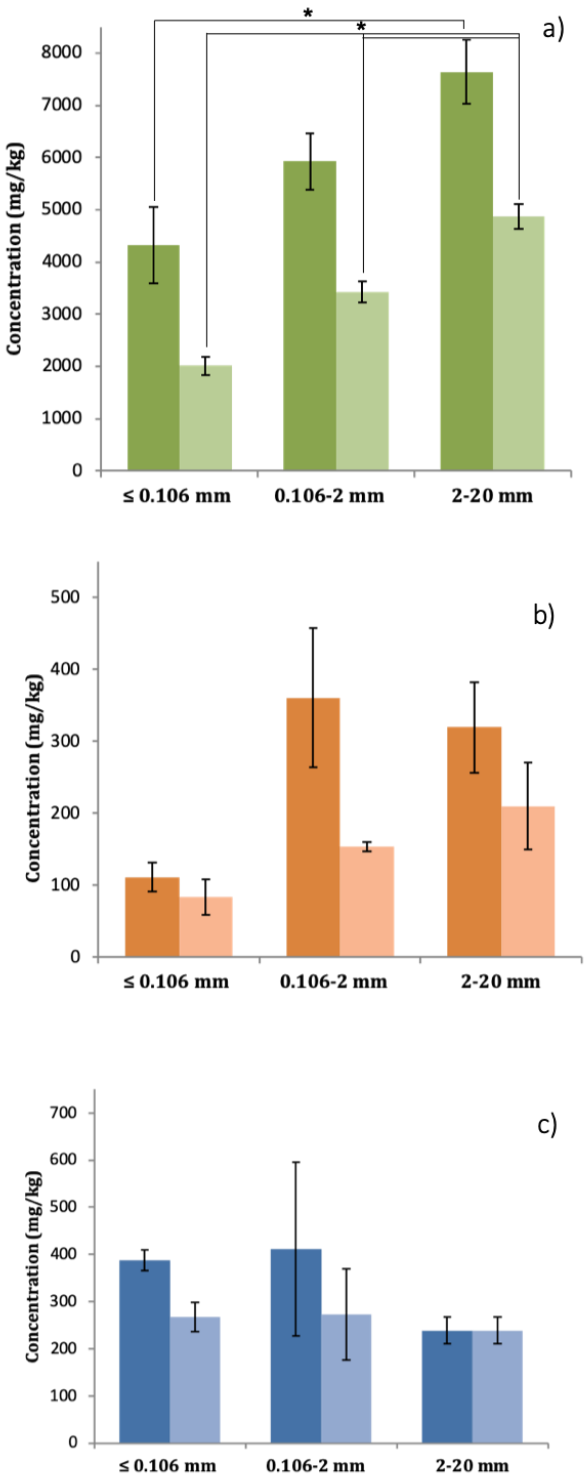

Figure 69. *Histograms representing the concentration of asbestos in each grain size class of each sample: (a) serpentinite; (b) debris; and (c) soil. The darker columns represent the mean of the concentrations of the three replications calculated for each grain size class. The lighter columns represent the mean of the concentrations of the three replications calculated for each grain size class excluding the outlier fibres from the calculation. The black bars represent the standard deviation. In a) asterisks indicate significant differences between groups (* = $p < 0.05$) (from Militello et al., 2019b).*

In the 2 to 20 mm fraction, the mean concentration of the three replications (R1, R2, and R3; Table 10) was 7640 mg/kg and was 4875 mg/kg excluding outliers from the calculation (R1, R2, and R3 without outliers; Table 10), representing a reduction of 36%. In the 0.106 to 2 mm fraction, the

mean concentration of the replications was 5924 mg/kg and was 3428 mg/kg excluding the outlier fibres, a reduction of 42%. In the < 0.106 mm fraction, the mean concentration of the replications was 4319 mg/kg and was 2013 mg/kg excluding the outlier fibres, a reduction of 53%.

The p-value corresponding to the F-statistic of one-way ANOVA was higher than 0.05 for soil and debris material, considering both the concentration values with and without outliers (Figures 69 b-c); therefore, asbestos concentration in these grain size classes was not significantly different. In the case of serpentinite, ANOVA p-value was < 0.05. Tukey test results showed significant differences of asbestos concentration between < 0.106 and 2–20 mm grain sizes ($p < 0.05$). Furthermore, in the case of asbestos concentration calculated without outlier fibres, the Tukey test result pointed out significant differences ($p < 0.05$) between the three grain size classes (Figure 69a).

Table 10. *Concentrations and intrinsic errors related to the method (for the three grain size fractions) of the three replicas (R1, R2, and R3), and concentrations calculated without outliers for each sample (from Militello et al., 2019b).*

Lithotype	Grain size intervals	R1 (mg/kg)	R1 without outliers (mg/kg)	R2 (mg/kg)	R2 without outliers (mg/kg)	R3 (mg/kg)	R3 without outliers (mg/kg)
Serpentinite	< 0.106 mm	5950 ± 1940	2388 ± 1117	3107 ± 1191	1699 ± 406	3899 ± 1180	1952 ± 457
	0.106–2 mm	7044 ± 1638	3457 ± 568	4923 ± 1290	2997 ± 544	5804 ± 1197	3829 ± 618
	2–20 mm	6210 ± 1132	4384 ± 652	8360 ± 1685	5328 ± 699	8350 ± 2140	4912 ± 767
Debris material	< 0.106 mm	140 ± 60	140 ± 60	66 ± 34	66 ± 34	128 ± 111	45 ± 22
	0.106–2 mm	528 ± 337	144 ± 74	407 ± 307	169 ± 70	147 ± 70	147 ± 70
	2–20 mm	348 ± 81	348 ± 81	427 ± 291	127 ± 54	182 ± 63	155 ± 48
Soil	< 0.106 mm	403 ± 167	235 ± 91	339 ± 110	339 ± 110	420 ± 230	227 ± 104
	0.106–2 mm	283 ± 142	205 ± 89	826 ± 291	492 ± 145	123 ± 63	123 ± 63
	2–20 mm	305 ± 117	305 ± 117	201 ± 90	201 ± 90	211 ± 100	211 ± 100

Serpentinite provided quantitative (according to M.D. 06/09/1994) results, as the asbestos concentration fell within the range of 1000–10,000 ppm. Indeed, the error calculated on the asbestos concentration values was quite low. The low error was principally due to the high number of fibres found in the serpentinite samples, obtaining an AC/C factor of R1 0.23–R2 0.28–R3 0.25. These values were much lower than the experimental factor 0.48 (1000 ppm)–0.35 (10,000 ppm), which was considered as a limit for obtaining quantitative results in the M.D. 06/09/1994 (attachment 1, Table 5) (Figure 70).

N	4	8	16	32	64	100	400
ΔN/N	0.5	0.35	0.25	0.18	0.13	0.10	0.05
Es/*f*				0.3	0.3	0.3	0.3
Δ*C*/C				0.48	0.46	0.40	0.35
C (ppm) (a)	120	250	500	1000	2000	3000	≈1%

Figure 70. *Table 5 of Annex 1 (Paragraph B) of Ministerial Decree No. 06/09/1994. Quantitative determination of asbestos in bulk samples. (a) The reported ppm concentration values were calculated using the same fibre number to weight conversion factor used in the previous point.*

Moreover, the high number of fibres allowed a significant estimate of the mean and standard deviation. The results were in a small range, so the standard deviation calculated from the mean asbestos concentration of the three replications for each particle size fraction was low (Figure 69a).

The debris material contained greater amounts of amphiboles of the tremolite–actinolite series (93.23%) compared with chrysotile (6.77%) only in the 2 to 20 mm fraction, and the percentages converged as the particle size fraction decreased (Table 8). The total number of fibres was highest in the 2 to 20 mm fraction (44 fibres) and lowest in the unmilled natural fraction (20 fibres). The highest mean volume (13.12 μm^3) was in the 0.106 to 2 mm fraction both with and without outlier fibres (Table 9) (for this sample, outlier fibres were those with a mean diameter of ≥ 1.67 μm). The smallest mean volume was in the unmilled fraction (4.54 μm^3).

In the grain size range from 2 to 20 mm, the mean concentration of the replications (R1, R2, and R3; Table 10) was 319 mg/kg and was 210 mg/kg excluding outliers from the calculation (R1, R2, R3 without outliers; Table 10), a reduction of 34%. In the 0.106 to 2 mm grain size fraction, the mean concentration of the replications was 361 mg/kg and was 153 mg/kg excluding the outlier fibres from the calculation, a reduction of 58%. Finally, in the < 0.106 mm fraction, the mean concentration of the replications was 111 mg/kg and was 84 mg/kg excluding the outlier fibres from the calculation, a reduction of 24% (Table 10).

Debris material provided semi-quantitative results (< 1000 ppm) according to the method used in Table 5 (Figure 70) of the decree, and the errors were reasonable with respect to the concentration values (Table 10). The standard deviation was slightly larger compared with the serpentinite results owing to the greater variability of the data (Figure 69b).

In the soil, about 95% of the asbestos fibres were amphiboles of the tremolite–actinolite series. Chrysotile had a maximum abundance (7.57%) in the 0.106 to 2 mm fraction (Table 8). The number of fibres increased with decreasing particle size fraction (Table 9). A total of 15 fibres were detected in the 2 to 20 mm fraction and 25 fibres in the unmilled < 0.106 mm fraction. However, the mean total asbestos fibre volume was similar between the three grain size fractions, whereas the mean volume excluding outlier fibres was highest in the 2 to 2 mm fraction and lower in the not milled fraction (Table 9). This is explained by the fact that in the coarser size fractions, the fibres were lower

in number but had larger volumes, and the volumetric effect outweighed the numeric effect.

In the 2 to 20 mm grain size fraction, the mean asbestos concentration of the replications was 239 mg/kg, and no outlier fibres were found. In the 0.106 to 2 mm fraction, the mean asbestos concentration was 411 mg/kg and that calculated without outlier fibres was 273 mg/kg, a reduction of 34%. The non-milled powder < 0.106 mm had a mean concentration of 388 mg/kg and of 267 mg/kg excluding the outlier fibres, a reduction of 31% (Table 10). For the soil sample, outlier fibres were those with a diameter of > 1.6 μm.

Soil provided semi-quantitative results (< 1000 ppm) according to the method used and described in Table 5 (Figure 70) as said above. The errors associated with the concentrations (Table 10) reflect the large dimensional variability of the fibres observed in the read-fields. Figure 69c shows a wide standard deviation as a result of the greater variability of the data population compared with debris material and mostly with serpentinite.

9.4 Discussion

After determining how the asbestos fibres were distributed across the three grain size fractions and after calculating the concentrations of asbestos in each fraction, we recalculated the concentrations according to both decrees: a) R.P.D. 120/2017 and b) M.D. 161/2012, respectively. The concentrations were obtained by recalculating the asbestos weight values of each particle size fraction. We also recalculated the asbestos concentrations of the 0.160–2 mm fraction that was unrelated to the lithic skeleton. In this case, the values shown are calculated without outlier fibres.

The results demonstrate that the recalculation according to M.D. 161/2012 involves a dilution effect, reducing the concentration of asbestos fibres compared with samples prepared according to R.P.D. 120/2017. In fact, asbestos concentration resulted reduced by 61%, 54%, and 50% for serpentinite, debris material and soil, respectively (Figure 71).

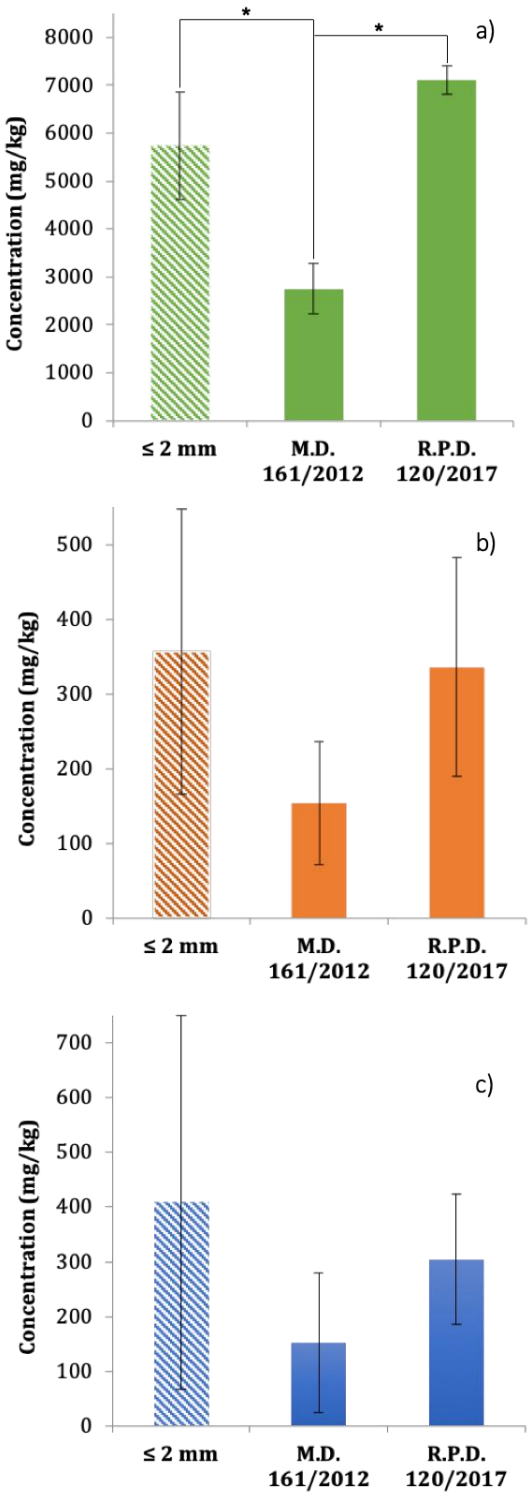

***Figure 71**. Histogram comparing the calculated average asbestos concentrations according to M.D. 161/2012 (middle column) and R.P.D. 120/2017 (right-hand column) for each sample: (a) serpentinite; (b) debris material, and (c) soil. The column to the left represents the concentration of asbestos in the grain size fraction ≤ 2 mm (0.160–2 mm) unrelated to the skeleton. The black bars represent the standard deviation (from Militello et al., 2019b).*

The p-value corresponding to the F-statistic of one-way ANOVA is higher than 0.05 for soil and debris material, suggesting that there are no significant differences between asbestos concentration calculated for grain size class ≤ 2 mm and according to M.D. 161/2012 and R.P.D.

120/2017. However, p-value for serpentinite is much lower than 0.05 (around 0.01). This suggested to proceed with the Tukey test, and it emerged that there are significant differences of asbestos concentration calculated according to M.D. 161/2012 with both concentrations in ≤ 2 mm grain size fraction and according R.P.D. 120/2017 (Figure 71a). This data could be explained observing asbestos concentration and SD values. In the case of asbestos concentration > 1000 ppm, as for serpentinite, results are quantitative, and errors associated with the method are low because the number of fibres is high (N > 30). Furthermore, the left-hand column of the histograms in Figure 71 a and b (for serpentinite and debris, respectively) show that the concentration for the ≤ 2 mm fraction (i.e., without the skeleton) is similar to the concentration calculated according to R.P.D. 120/2017, particularly for the debris sample. Conversely, for soil (Figure 71c) the asbestos concentration is reduced by 50% and the concentration calculated in the < 2 mm fraction is the highest.

Depending on the type of rock and especially on the asbestos mineral subjected to comminution, substantial differences can be seen for the three grain size classes (Figures 72 a-b).

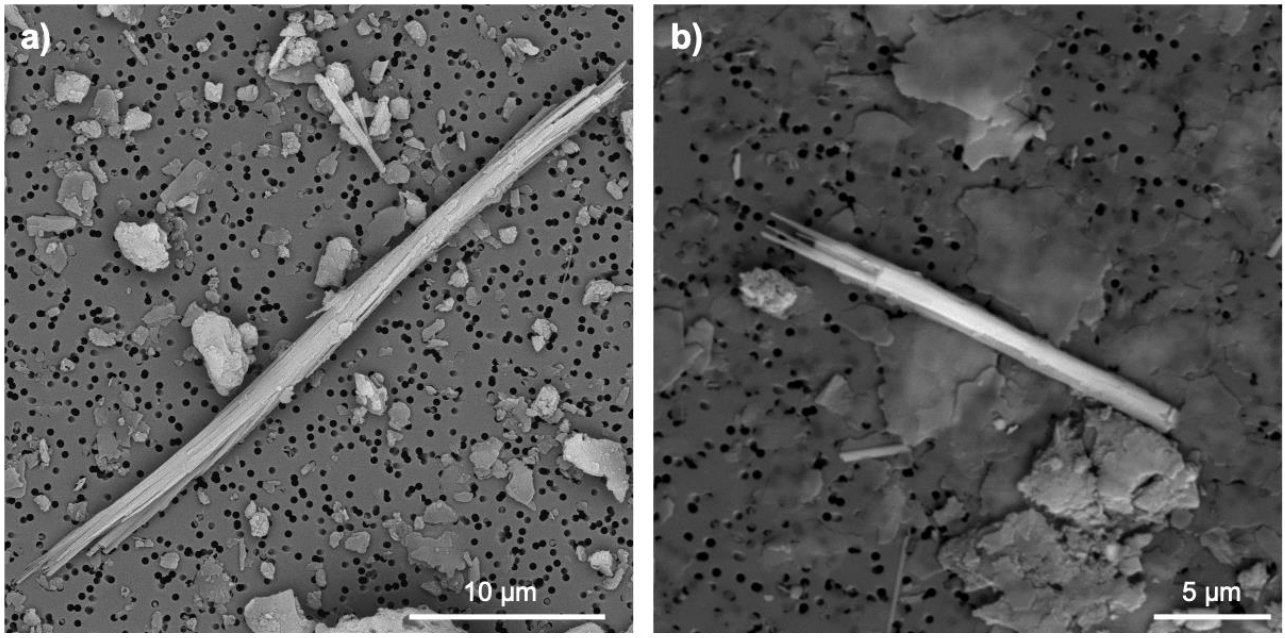

Figure 72. *SEM photomicrographs. Examples of fibres obtained from (a) chrysotile and (b) amphiboles (High Vacuum; 20 kV; Detector: Back scattered electrons).*

The asbestos fibres in serpentinite occur as large bundles in natural powders (< 0.106 mm) and subordinately in the 2 to 20 mm fraction. In the ≤ 2 mm fraction, the bundles tend to separate along the fibre length, causing a greater dispersion of the fibrils below the dimensions of fibres (width < 0.2 µm) liable to be counted (Figures 73 a–c). Although this explanation cannot be applied to either the debris or the soil, the asbestos amphibole reacts to the comminution differently from the chrysotile in those samples. In fact, amphiboles are mechanically more resistant and are homogeneously

distributed in the three fractions considered (Figures 73 d–i). Moreover, the lengths and diameters of the countable fibres are not significantly different between the natural and the milled powders for the debris and soil (Figures 73 d–i).

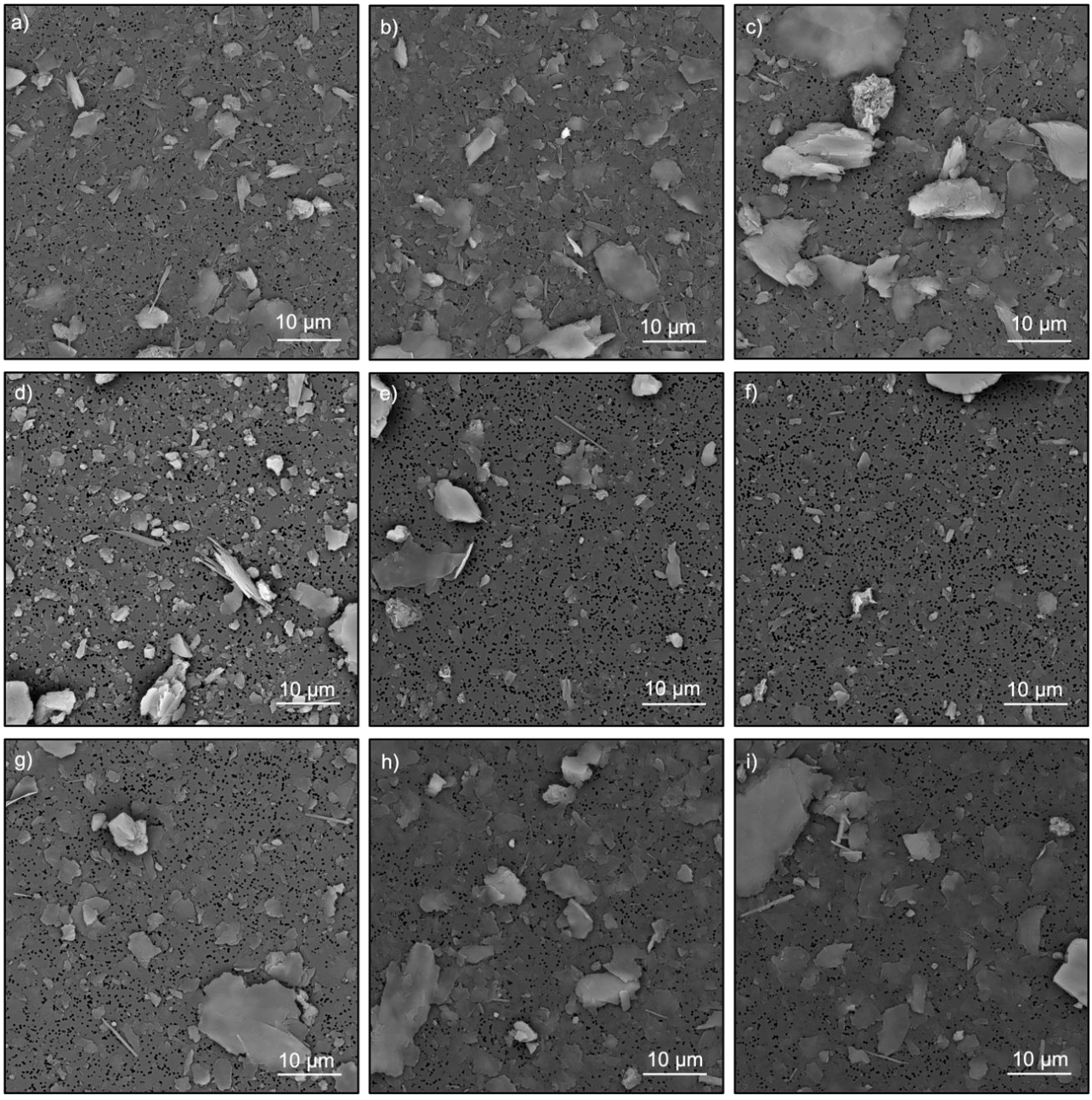

Figure 73. *SEM microphotographs of fibres from (a–c) serpentinite; (d–f) debris; and (g–i) soil representative of 2 to 20 mm, 0.106 to 2 mm, and non-milled fractions (High Vacuum; 20 kV; magnification: 5000×; Detector: Back scattered electrons).*

10.THE PATHOGENIC POTENTIAL OF ASBESTOS

The first asbestosis case was reported in 1906, when Dr Montague Murray documented pulmonary fibrosis in a Londoner worker. In 1927, Williams Cook coined the term “pulmonary asbestosis”. Only in 1955, Richard Doll carried out a case-controlled study on textiles, establishing the correlation between exposure to asbestos fibres and lung cancer. Consequently, an increasing number of studies were carried out on different populations, in particular professionally exposed to asbestos.

The International Agency for Research on Cancer (IARC) declared asbestos a proven carcinogen for humans, placing it in Group 1 (Carcinogenic to humans) (IARC 1977, 1987).

Moreover, the air quality guidelines from WHO (2000) have declared that to prevent carcinogenic risk is necessary not to exceed a level of asbestos fibres exposure equal to 1 ff/air litre over a lifelong daily exposition. However, it is worth noting that there are no threshold limits to date since any exposure can cause cancer. On the other hand, several studies indicate that morbid risk from asbestos is related to the duration of exposure and cumulative dose (IARC 1977; Luberto et al 2004; Szeszenia-Dąbrowska et al., 2016).

Although there are specific norms that suggest threshold values to ensure health protection and surveillance, it is noteworthy to highlight that these limits differ not only on a regulatory basis but also on measurement methods and acceptability levels. The acceptability value of asbestos differs according to the examined environment (living environment, working environment). For instance, in working environments, reference is made to the limit value of 100 fibres per litre (ff/l) per day, calculated as a normalised average concentration over 8 working hours (L.D. 81/2008). For living environments, reference is made to the limit value is 20 ff/l if the fibres are counted by optical phase contrast microscopy, while 2 ff/l if these are observed by scanning electron microscopy (M.D. 06/09/1994). This value agrees with the occupational exposure limit, ruled by Directive 2003/18/EC and Directive/2009/148/EC, for airborne asbestos in workplaces in EU countries (Gaggero et al., 2017).

According to WHO, the hazard of asbestos derives from its capability to release breathable fibres. The risk is linked to interconnected factors that control the degree of penetration into the respiratory tract. The different diseases, such as fibrosis, pulmonary, mesothelioma, and cancer, are triggered by asbestos due to its three main properties:

- shape factors: i.e., the length > 5 μm, the diameter < 3 μm and the length/diameter ratio greater than 3:1;
- chemical-mineralogical factors: the structure of the mineral, the chemical composition, the surface reactivity;
- biopersistence: the residence time of the fibre *in vivo*, before being dissolved or eliminated from the body.

Therefore, the inhalation and deposition in alveolar spaces directly correlate both with relative length/width ratio and shape. In case of higher length/width, the fibre is easily inhaled and deposited into the respiratory system. Moreover, the aspect ratio influences the phagocytosis process operated by macrophages. In particular, short asbestos fibres (< 5 μm) are enclosed in the phagosomes and cleared, without triggering chronic inflammation. In contrast, longer fibres (< 5 μm) cannot be fully engulfed by macrophages and can remain inside the lung for a longer time (Takenori et al 2019). The extreme flexibility shown by asbestos fibres favours the permanence in the lung environment. Conversely, cleavage fragments of amphiboles have weaker surfaces that favour breaking by breathing.

Finally, according to the WHO, both chemical composition and surface reactivity increase alveolar macrophage activation. Moreover, the fibre surface can trigger the imbalance of redox status, causing radical species formation and activating the inflammatory process (IARC, 2012c).

Asbestos has been linked to different pulmonary diseases, such as pleural fibrosis and plaques, asbestosis, benign asbestos pleural effusion, small cell lung carcinoma, non-small cell lung carcinoma and malignant mesothelioma. Different mechanisms induced by asbestos (chromosomal alterations, oncogenes activation, loss of tumour suppressor genes, generation of RNOS, and direct mechanical damage to cells from asbestos fibres) may be pathways involved in the development of the asbestos-related disease (La Maestra et al., 2020; Solbes et al., 2018).

Moreover, workers exposed to asbestos or other powders can be exposed to some other carcinogen such as diesel engine exhaust, crystalline silica dust, radon gas, nickel compounds, hexavalent chromium compounds, arsenic and inorganic arsenic, and compounds from cigarette smoke. These people have a significantly greater risk of developing lung cancer than people who have only been exposed to asbestos. For example, Irving et al. (1979) estimated that smokers and workers exposed to asbestos have roughly 90 times the risk of developing lung cancer than people who neither smoked nor worked with asbestos.

10.1 Non-asbestos related diseases studies

The effects of inhalation of non-asbestiform amphiboles are still poorly correlated with asbestos-related diseases. The NIOSH at the OSHA and Mine Safety and Health Administration meeting has confirmed that despite the similarity in size, shape, and equal composition between asbestos and non-asbestiform amphiboles, it is necessary to clarify the possible effects on the health of the latter. Thus, cautiously, NIOSH concluded that there is no evidence to exclude cleavage fragments from the current regulations. The Environmental Protection Agency (EPA) has stated that it would be prudent to assign equivalent relevance for cleavage fragments and fibres in cancer risk (Harper, 2008). However, the USA occupational regulations do not currently cover asbestiform amphiboles. Therefore, it is crucial to determine whether amphibole cleavage fragments differ sufficiently from asbestos fibres to pose different health risk levels, by examining fibres dimensions and shape that influence respirability, and fibre bio-persistence that influence carcinogenicity (Gamble & Gibbs, 2008). The few studies on cleavage fragment in literature denote a present insufficient knowledge.

10.1.1 Potential health effect of cleavage fragments

According to WHO, particles of amphiboles and serpentine groups can be defined as fibrous when having length > 5 µm, width < 3 µm and length/width > 3:1. Moreover, as for dimension, fibres are considered inhalable when having a diameter between 10 to 100 µm, while the thoracic fibres have a diameter between 4 to 10 µm (Figure 74). These typically are stopped in upper and lower airways. Conversely, the fraction with a diameter < 3µm (respirable fraction) is able to reach the alveolar space triggering inflammation and recruitment of inflammatory cells.

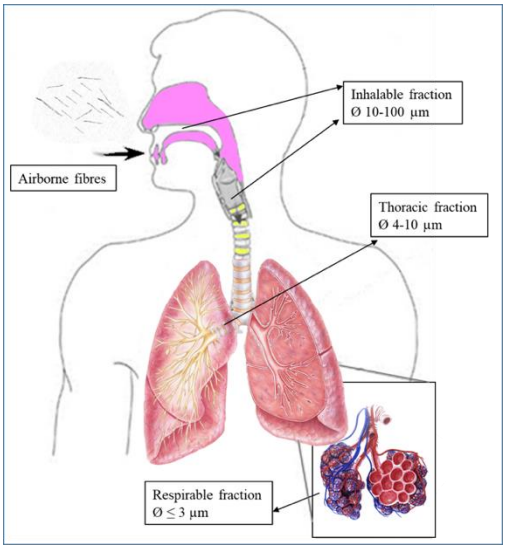

Figure 74. Size-selective inhalation of airborne fibres involves specific regions of the respiratory tract.

Different studies conducted *in vitro* and *in vivo* showed that particles not covered by the dimensions suggested by WHO could even trigger pathological effects when inhaled or ingested. In this respect, from the beginning of the 1970s several studies were conducted considering amphiboles with different geometrical ratio (Table 11). However, few *in vivo* and *in vitro* studies have been conducted on the fibrous varieties of antigorite and lizardite.

Table 11. *Synoptic table showing fibre dimensions that are the most liable to contribute to lung cancer risk. References: (1) Pott et al., 1989; (2) Hamra et al., 2014; (3) Wagner et al., 1974; (4) Suzuki et al., 2005; (5) Davis et al., 1991; (6) Adib et al., 2013; (7) Davis et al., 1986; (8) Donaldson et al., 1989; (9) Donaldson et al., 1991; (10) Goodglick, 1990; (11) Berman et al., 1995; (12) Stanton et al., 1981; (13) Donaldson et al., 1992; (14) Brown et al., 1986 (15) Hill et al., 1995; (16) Lippmann 1990; (17) Dement et al., 2008; (18) Berman et al., 2008.*

Minerals type	**Study types**	**Critical size of fibres**			**References**
		Length	**Width**	**Aspect ratio**	
Actinolite	*In vivo*	< 0.2 µm	-	3:1	(1)
Not specified	Mathematical model	> 1.5 µm	< 0.25 µm	3:1	(2)
Crocidolite	*In vivo*	> 3 µm	-	3:1	(3)
Not specified	Observational	≤ 5 µm	≤ 0.25 µm	3:1	(4)
Tremolite	*In vivo*	> 5 µm	≤ 0.5 µm	3:1	(5)
Not Specified	Observational	< 5 µm	< 3 µm	3:1	(6)
Tremolite and other	*In vivo*	> 5 µm	-	3:1	(7-11)
Amphiboles	*In vitro*	> 8 µm	< 0.25 µm	3:1	(12)
Tremolite and other	*In vitro*	> 10 µm	-	3:1	(8-9,13-15)
Tremolite	*In vivo*	> 10 µm	< 0.5 µm	3:1	(7)
Not specified	*In vivo*	> 20 µm	< 1 µm	3:1	(16)
EMP	Cohort studies	> 40 µm	< 3 µm	3:1	(17)
Asbestos group	Meta-analysis	-	< 0.4 µm	3:1	(18)

Different studies indicate that short respirable particles, that cannot be considered fibres, because they do not fall within the dimensions suggested by the WHO can trigger pathological injuries such as mesothelioma, lung cancer and asbestosis (Cunningham et al., 1977; Patel-Mandlik et al., 1983; Weinzweig et al., 1983).

Opinions diverge and are essentially divided into two positions. Some authors assert that non-asbestiform amphiboles fibres are not potentially carcinogenic. In contrast, other authors suggest a carcinogenic potential of these fibres. Davis et al. (1991) studied the Italian non-asbestiform tremolite effect from Ala di Stura in rats comparing to the asbestiform variety. Ala di Stura tremolite contains a subgroup of very long and fine asbestiform fibres and is described as

the correspondent non-asbestos variety of tremolite which would not be expected to cause tumours. However, the high tumour rate observed in the rats has suggested that non-asbestiform and asbestiform amphiboles indeed have similar carcinogenicity. In particular, 2/3 of the rats exposed to the Ala di Stura tremolite developed mesothelioma but very late in life (median survival time was 755 days). In contrast, the three asbestos samples induced much shorter median survival times, ranging from 301 days to 428 days.

Suzuki et al. (2005) analysed lung and mesothelial specimens from human patients and observed that amphibole particles shorter than 5 µm and thinner than 0.25 µm were strongly associated with neoplasms.

Adib et al. (2013) examined the lung of asbestos-exposed workers with asbestosis, lung cancer or mesothelioma founding about 50% of particles, including chrysotile, with length < 5µm and about 20% of fibres with length > 5µm, width < 3µm and aspect ratio > 3:1.

Donaldson et al. (1989, 1991) explored the effects induced in mice by intraperitoneal administration of single doses of amosite samples with fibres longer than 5 µm and amosite samples with particles shorter than 5 µm (with A/R > 3:1 for both categories). The different samples were injected in equal amount. Results showed that a single dose of particles shorter than 5 µm, injected in mice by intraperitoneal, did not trigger local inflammation, but repetitive exposures increased the inflammatory reactions.

Dement et al. (2008) showed that exposures to amphiboles with lengths ranging from < 1.5 µm to > 40 µm and widths ranging from < 0.25 µm to > 3.0 µm were highly associated with developing lung cancer and asbestosis. Moreover, further studies indicate that short particles can contribute to pathological injuries such as mesothelioma, lung cancer and asbestosis (Cunningham et al., 1977; Patel-Mandlik et al., 1983; Weinzweig et al., 1983). Dodson et al. (2003) suggested that particles shorter than 5 µm could trigger pathologic mechanisms such as cancer, and suggest including these particles as a possible risk factor for human health.

Wagner et al. (1974) showed that fibre persistence in the lung of rats exposed to long fibres (3–6 µm and > 6 µm) and short particles (3–5 µm) of crocidolite, increased over 365 days post-inhalation for both classes.

On the other hand, different studies reported no evidence when elongated mineral particles were tested on different models' study. According to the Stanton hypothesis (1981) fibres longer than 8 µm and thinner than 0.25 µm must be considered more dangerous for health. Nevertheless, even non-asbestiform fibres with "Stanton size" cannot be removed by phagocytic cells like macrophages, triggering the typical asbestos-induced pathobiological mechanisms such as

generation of free radicals, cell and DNA damage, chronic inflammatory reaction, delivery of chemical carcinogens (Di Giuseppe et al., 2019).

The cell culture studies conducted by Donaldson et al. (1989, 1991), Brown et al. (1986) and Hill et al. (1995) have generally confirmed that particles shorter than 5 μm have little pathologic effect, contrarily to what might be expected from a general respirable silicate mineral dust.

Timbrell et al. (1971) and Wylie et al. (1997) reported low cytotoxicity in culture cells exposed to non-asbestiform tremolite. The health effects due to asbestos short particles exposition were examined by Pott et al. (1989), which reported that 56% of rats had lung tumours and pleural mesotheliomas after intraperitoneal injection of asbestos actinolite. The size distribution showed that 90% of the asbestos particles have a length < 0.2 μm and 10% < 4.2 μm. In contrast, when a similar dose of non-asbestiform actinolite was used, no tumours were found (Pott et al., 1974; 1989 and Addison et al., 2008). Bermant et al. (1995) suggested that asbestos fibres longer than 5 μm contributed to lung tumour development, unlike those shorter than 5 μm. Wylie et al. (1993) exposed animals to asbestos and non-asbestos fibres. Asbestos fibre had diameters thinner than 1 μm, and nearly 90% were thinner than 0.5 μm. In contrast, about half of the non-asbestos amphibole particles were thinner than 1 μm, only 20% of which thinner than 0.5 μm. Results showed that tumours in the exposed animals are proportional to the log of the dose of fibres thinner than 1 μm.

A similar study (Hill et al., 1995), in which the authors used the same minerals, reported a significant release of superoxide anions by macrophages. These results support the view that fibre length is crucial in determining pathogenicity, since this factor is associated with the development of inflammation, pulmonary fibrosis and tumour formation. Goodglick & Kane (1990) evaluated the cytotoxicity on macrophages of mice by using crocidolite with long fibres (L > 5 μm) and short particles (L ≤ 5 μm). Although a comparison based on the number of fibres showed lower toxicity for the short fibres, cytotoxicity was demonstrated for both types of samples. However, the authors considered that these differences in effect were substantially dependent on iron content in the samples, as a pre-treatment by a chelating agent inhibited the toxicity. Riganti et al. (2003), compared the effects of long asbestos fibre (L > 5 μm (70%) and < 2 μm (25%)) and short amosite particles (L < 5 μm (98%) and < 2 μm (75%)) on human epithelial cells. A higher effect was evidenced from the long asbestos fibre sample, generating free radicals and inhibiting glucose metabolism on A549 cells.

Davis et al. (1986) exposed for six months rats to the injection of samples with elongated mineral particles and long fibres of amosite. The first group of samples contained about 0.1% of fibres longer than 10 μm and about 2% longer than 5 μm, while the second group contained more than 11% of fibres longer than 10 μm and 3% longer than 25 μm. The diameter distributions were very similar, about 50% less than 0.5 μm in width. The experiments produced mesothelioma in 88% and 95% of rats treated, respectively, with 10 and 25 mg powder of long asbestos fibres. Simultaneously, the short fibres of asbestos produced 0% and 4% tumours with the same respective doses. Moreover, experiments conducted with other minerals suggest that fibres exceeding 20 μm and thinner than 1 μm are necessary to cause cancer. According to the authors, this probably happens because the long fibres cannot be phagocytised by macrophages or removed from the lungs (Lippmann, 1990).

In 1982, Wagner et al. (1982) tested three samples of asbestos tremolite in different cell lines showed that longer fibres induced enzymatic release of LDH and BGL when treated peritoneal macrophages mice, and caused the formation of giant cells in A549 cell. Berman et al. (2003) showed that tumours generation is related to the concentration of fibres longer than 40 μm but acknowledged that an aspect ratio of 20:1 or greater should eliminate most of the asbestos and non-asbestos particles. This information was incorporated into a new risk model protocol that considers only the concentration of fibres longer than 10 μm and thinner than 0.4 μm, not differentiating between asbestiform and non-asbestiform fibres. Long-term inhalation studies were performed in hamsters using the “nose only” method of exposure to amosite samples with lengths > 5 μm and > 20 μm. The numbers of amosite fibres did not decrease at low (0.8 mg/m^3), and medium doses and no difference in the retention rate between the two groups of fibres with different lengths were detected at the highest dose (McConnell et al., 1999).

Although many studies have considered the fibre length as a determinant of pathogenicity, expressing differing opinions, other authors reported the necessity of further studies to elucidate the importance of the geometric ratio of fibre (Vallero et al., 2009).

Gamble & Gibbs (2008), in agreement with Addison et al. (2008), have summarized the health effects of non-asbestos amphiboles. The health studies indicate the necessity of correctly identifying asbestos fibres. The authors argue that relying solely on the aspect ratio of the particles, to classify them as asbestos, will lead to significant errors. They addressed amphibole particles with aspect ratios of at least 3:1, as defined in many analytical procedures. This classification involves an overestimation, including the non-asbestos amphibole and byssolite samples as asbestos, leading to a considerable risk overvaluation. Mossman (2008), commenting

about the size distribution data from Wylie et al. (1990), suggested that cleavage fragments are less bio-reactive and cytotoxic than asbestiform fibres. Later, Mossman et al. (2011) recognized that a possible role of fibres < 5 μm cannot be ruled out.

Berman and Crump (2008) extended the Stanton hypothesis to create a risk model based on long fibres thinner than 0.4 μm, showing a relationship between disease and long-thin concentration asbestos fibres. Chatfield (2008) proposed a protocol that defined as asbestiform only those fibres whose widths range from 0.04 μm to 1.5 μm and aspect ratio from 20 to 1000. Accordingly, elongated particles out of these ranges are considered non-asbestiform.

Belardi et al. (2018) reported no epidemiological evidence in cancer development from cleavage fragments exposure. In contrast, epidemiological studies (Hamra et al., 2014; Stayner et al., 2008; Loomis et al., 2009; 2010; 2012) showed that higher lung cancer rates are attributable to long fibres exposure. Perhaps, the authors did not provide any definitive conclusions for the other size classes. In fact, they observed that short-thin fibres represented the majority of fibres counted by Transmission Electron Microscopy. However, they did not determine whether the association of short fibres with lung cancer is a spurious effect or it evidences that short fibres play a specific role in carcinogenesis.

10.1.2 Critical considerations

This literature review did not reveal strong evidence indicating that cleavage fragments have the same or greater carcinogenic potential than asbestos. Most of the data collected by the different authors suggest that the toxic effect of asbestos fibres increases with length, despite some notable exceptions. However, the extent to which mineral with an asbestiform habit affects cell behaviour relative to that of a cleavage fragment of the same mineral still remains open to investigations. Moreover, the chemical composition of a particle can influence the pathogenic response of the tissue it comes into contact with. For instance, iron content may exacerbate reactive species and inflammation response production.

Different experimental studies show that short asbestos fibres are less active than long asbestos fibres. However, if short asbestos fibres are used in high doses, they can cause inflammation, interstitial pulmonary fibrosis and pleural reactions. Certainly, the different methodologies used for sample preparation, analytical techniques, duration of exposure and post-exposure monitoring are discriminating factors (Boulanger et al., 2014).

For health safety purposes, the assessment of asbestos air contamination is carried out considering only the particles with a specific length-diameter ratio (3:1) and a length greater than 5 µm. The value 5 µm as the limit of length was arbitrarily chosen in the 1960s due to the resolution of transmitted optical microscopy in quantitative analysis and because it was fairly consistent with literature data highlighting the role of fibre size in asbestos toxicity.

Indeed, it is true that most risk assessment models have shown that adverse health effects are associated with fibres longer than 5 µm or even longer than 10 µm. Only a few risk assessment models believe that even fibres shorter than 5 µm should be considered dangerous, suggesting that they may play a role, albeit much less significant than the effect of longer fibres. No agreement has currently been reached on this distinction. According to Hwang et al. (2014), a lack of consensus on the appropriate exposure metric can partially explain the different exposure response relationships obtained in an epidemiological study. Finally, the potential genotoxicity of non-asbestiform fibres with equal critical size to asbestos have been poorly tested.

International health and safety organizations agree on the absence of a "safe" level of asbestos exposure and agree that it should be minimized (IARC, 2012c; WHO, 2014). However, reference values are necessary to ensure the protection and surveillance of workers health. Despite the known carcinogenic nature of asbestos, this topic still remains a controversial issue globally in the science of disease prevention as debates on health impact, identification criteria and regulatory limits are still ongoing (Finkelstein, 2013; Bernstein et al., 2013; Baur et al., 2016; Jargin, 2015).

There is currently insufficient and contradictory evidence to explain the pathogenic role of cleavage fragments for both amphibole and serpentine.

Differently, humans can inhale fibres in diameter ≤ 3 µmµm depositing in the thoracic and gas exchange regions of the lung. This physiological difference makes the animal study less specific (Hesterberg, 2009), as e.g., rodents breathe only nasally, inhaling fibres with a diameter ≤ 1 µm.

Some authors state that the lack of carcinogenic effects of the fibres of the cleavage fragment of amphiboles is due to the failure in reaching the critical dimensions indicated by the WHO for the asbestiform fibre. On the other hand, many studies showed that the size of asbestiform and non-asbestiform elongated particles is often comparable (Militello et al., 2020). Therefore, the pathogenicity of the short fibres cannot be completely ruled out, especially in high exposure situations. Further studies are needed to clarify the role of cleavage fragments, especially in case of professional exposure.

11. EVALUATION OF THE CYTOTOXIC AND TRANSFORMING EFFECTS INDUCED BY CLEAVAGE FRAGMENTS

The term "carcinogen" denotes a chemical substance or a mixture of chemical substances that induces cancer or increases its incidence. Substances which have induced benign and malignant tumours in well performed experimental studies on animals are considered also to be presumed or suspected human carcinogens unless there is strong evidence that the mechanism of tumour formation is not relevant for humans.

The knowledge of the possible effects on human health by occupational exposure to potential carcinogen (i.e., asbestos fibres) derives from different studies, such as *in vivo* and *in vitro* as well as epidemiological studies. A complete study aimed at defining the effects of acute, subchronic and chronic toxicity (carcinogenicity) has a duration of 3 years and a very substantial cost, requires appropriate facilities and highly qualified staff. Long-term tests on animals represent a traditionally point of sure reference for the categorization of carcinogens, in the case of absence of epidemiological data or to reinforce them. On the other hand, *in vivo* studies have shown limits such as to induce more than one uncertainty.

Usually, the available data from chronic inhalation tests are obtained from studies that use rodents, which have very different susceptibility to tumour induction by fibrous materials when compared to the human. In particular, pulmonary mesotheliomas are rare in this mammals order, and their appearance is always biologically significant.

The administration of a probable carcinogen in an animal model does not often reflect the real routes of human exposure and forced administration like the tracheal installation or implantation in the abdominal pleural cavities will never be superimposable in human exposure because it led to overcoming some of the mechanisms of defence and clearance that act on inhaled fibres. Normally the rodents breathe through the nose, this physiological characteristic could be the reason which the fibres with a diameter greater than 1 μm do not reach the alveolar space. Humans can inhale fibres up to 3.5 μm of diameter that can deposited in the thoracic region and in the environment alveolar where gas exchange occurs. These physiological differences prevent the evaluation of the inhalation effect of fibres with a diameter between 1 and 3.5 μm, which would have relevance for humans health. These hypotheses are supported by animal inhalation studies conducted with asbestos, the sensitivity of rats to induction of lung tumours is clearly lower than that of humans (NIOSH, 2006).

In vitro genotoxicity and cytotoxicity studies can be used as preliminary screening tests for new materials and can help to elucidate the molecular mechanisms underlying the biological effects of the exposition to suspected substance or materials as well as fibres, thus constituting an important complement to animal studies. These also offer the possibility to evaluate dose-response relationships and correlations between fibre size and their toxicity with faster and more efficient methods than *in vivo* studies.

The carcinogenic potential of fibrous materials like asbestos was evaluated *in vitro* by mutagenesis and transformation assays in mammalian cells and bacterial models. Materials like asbestos, induce the appearance of free radicals, micronuclei, polynuclear, chromosomal breaks and hyperdiploid (La Maestra et al., 2020). Asbestos fibres exert direct effects on cell proliferation and viability, involving damage to DNA and the mitotic spindle and indirect effects. The latter involves the interaction of asbestos fibres with cells of the immune system, such as macrophages, which can be activated to produce inflammatory mediators (cytokines, ROS, prostaglandins and leukotrienes), which, once released, can directly affect target cells or attract locally other cells which in turn act on target cells. Both direct and indirect effects of fibres can result in genotoxic effects on target cells.

Genetic disorder triggered by asbestos inhalation is underlain the formation of the tumours in various site. Asbestos acts on two different contingents: the mechanical breakdown of the genetic material contained in the nucleus and the oxidative stress caused by the presence of specific ions, such as iron, in the fibrous mineral. This triggers redox reactions which lead to the breakdown of biological macromolecules like DNA. These processes can help each other. Asbestos fibre breaks the DNA structure, causing the loss of chromosome (aneuploidy) or part of it (clastogenicity). On the other hand, the ROS, triggered mainly by Fenton reaction, resulting in genotoxic damage underlying the mutagenic events.

Asbestos is a carcinogen complete with both initiating and promoting action. In fact, asbestos creates inflammation as well as causing DNA break. On the basis of a large amount of experimental data, five hypotheses on the mechanisms of carcinogenicity from fibres can be proposed.

1) Fibres catalyse the formation of ROS which can cause genotoxic damage interacting with DNA;
2) fibres interfere with the mitotic spindle by altering the migration of chromosomes in the two daughter cells during cellular division. This can lead to the appearance of polynuclear cells, and to alterations in the number of chromosomes;

3) fibres stimulate cell proliferation such as response to a toxic action, through the stimulation of intracellular signals that promote mitosis, through the expression of proto-oncogenes and growth factors;
4) fibres cause a chronic inflammatory reaction that leads to the release of free radicals, cytokines and lung growth factors. The persistence of the fibres in the lung interstitium or in the tissue subpleural connective can lead to a reaction of chronic inflammatory accompanied by fibrosis;
5) fibres play a co-carcinogenetic role as a vehicle for chemical carcinogens (this is linked in particular to the mechanisms of interaction between asbestos and smoke cigarette in the onset of lung cancer). The mechanisms proposed for the carcinogenicity of fibres with respect to the induction of mesothelioma comply, therefore, both in the initial phases (initiation) and in the phases finals (promotion). In this context, fibres can either directly or indirectly damage mesothelial cells, even with genotoxic mechanisms, and/or stimulate their proliferation. The stimulation of the chronic proliferation of mesothelial cells can lead to an accumulation of spontaneous mutations, which confer proliferative advantages to populations pre-neoplastic cell phones. Persistent fibres in the submesothelial connective may trigger the chronic release of cytokines and growth factors by activated macrophages, resulting in a continuous stimulus to cell growth.

Although the fibres could act in all stages of multiphase carcinogenesis, *in vitro* genotoxicity tests can only highlight the genotoxic effects involved in the early stages of tumour initiation. Commonly used assays do not detect effects related to biopersistence (frustrated phagocytosis) and secondary genotoxic activities produced by ROS and cytokines. Therefore, negative results indicate the absence of genotoxic starting effects but do not exclude effects on the later carcinogenesis stages (WHO, 2006). Therefore, deepening the studies on cleavage fragments given the limited literature, and tests aimed at verifying the later stages of carcinogenesis are needed.

In *in vivo* exposure, the fibres are physically and chemically modified by the lung microenvironment, whose conditions are difficult to mimic in short-term tests. *In vitro* tests, therefore, do not evaluate the influence of the dissolution of the fibres and their variation in composition over time and, due to their rapidity of development, they do not even consider the durability of the fibre, i.e., the time required to fragment it mechanically or to dissolve it in biological fluids.

11.1 The BALB/c 3T3 model for the study of cytotoxic and transforming activity

The BALB/c 3T3 cell transformation test represents a flexible tool to study the carcinogenic potential of chemical compounds, single or in complex mixtures, and define their role in the multiphase process of carcinogenesis (Colacci et al, 1990, 1995 and 1996). BALB/c 3T3 cells are mouse embryonic fibroblasts adapted to growth *in vitro* (immortalised). T immortalization is an early event in the cellular transformation process. BALB/c 3T3 cells retain some properties of normal cells and grow adherent to the substrate, forming a continuous and regular monolayer and do not exhibit the characteristics of transformed cells, such as tumorigenicity or the ability to form colonies in soft agar. Treatment with a carcinogen causes the onset of transformed cell clones (foci), whose phenotype is frankly malignant. The frequency of transformation is generally a function of the treatment dose and follows a pattern typical of a rare event (Poisson distribution), in line with the possibility of tumour development *in vivo*.

11.2 Methods and materials

Experiments that compare the cytotoxic and transforming effects of sample F3, representing the pure asbestos (as a positive control), fibrous but not asbestiform amphiboles of the tremolite-actinolite series (P1, P2, P3/A5, A1, A2, A4) and a sample of fibrous lizardite (S1/A3) were carried out.

11.2.1 Preparation of the powders

In order to evaluate the most suitable sample preparation method for carrying out the study, several tests were performed. The most suitable protocol for preparing the powders to be subjected to *in vitro* tests was the following. Using a bistoury, the amphibole or lizardite veins were isolated and separated from the host rock. Each sample was preliminarily ground by hand using an agate mortar. The powder obtained was sieved with a 63 μm mesh sieve to obtain omeogranular powders before moving on to mechanical grinding. The sieved powder was placed inside the Mc Chrone micronizer. The grinding (20 minutes, speed 4) was wet by inserting 5 ml of distilled water at the concentration of 0.5 mg/ml. Subsequently, the powders were dehydrated by freeze-dried, weighed, resuspended in deionised water at a known concentration and sonicated for 5 min.

11.2.2 Cell culture and cytotoxic test

BALB/c 3T3 were obtained from the Biological Bank, IRCCS San Martino Hospital, Genoa. Working cultures were expanded from the original cryopreserved stock and kept at 37°C in a 5% CO_2 atmosphere in Dulbecco's Modified Eagle's Medium (D-MEM, GIBCO BRL, USA) added with 10% Newborn Calf Serum (NCS, GIBCO BRL, USA). For the experiments, cells cultured maintained in a sub-confluence state (70%) were used. BALB/c 3T3 cells, exponentially growing, were seeded at a density of 250 cells/plate in 60 mm diameter plates (5 replicates per treatment) and incubated in standard culture conditions (37°C, atmosphere at 5 % of CO_2). 48 hours after sowing, the cells were exposed to the suspension containing the fibres under examination for a duration of 48 hours, untreated cells were used as negative controls. At the end of the exposure period, the cells were washed with PBS and kept in a complete medium (D-MEM + 10% FBS), which was replaced twice a week for the test duration. After 10-12 days, the plates were washed with PBS, fixed with methanol and stained with 10% Giemsa. Subsequently, after washing with distilled water, the plates were examined under the optical microscope (400x). Only colonies with more than 50 cells were considered, and the results were expressed as clonal efficiency relative to the control (Ctr) expressed as a percentage between the mean of the colonies in the treatment group and Ctr group. The treatment concentration that reduces clonal efficiency by 50% (inhibitory concentration 50%, IC50) was obtained by linear regression analysis from the interpolation line equation.

The graphs below show the viability in the different concentrations of each powders tested (Figure 75). By interpolating the data, it was possible to calculate the dose with no observable effects (Noel).

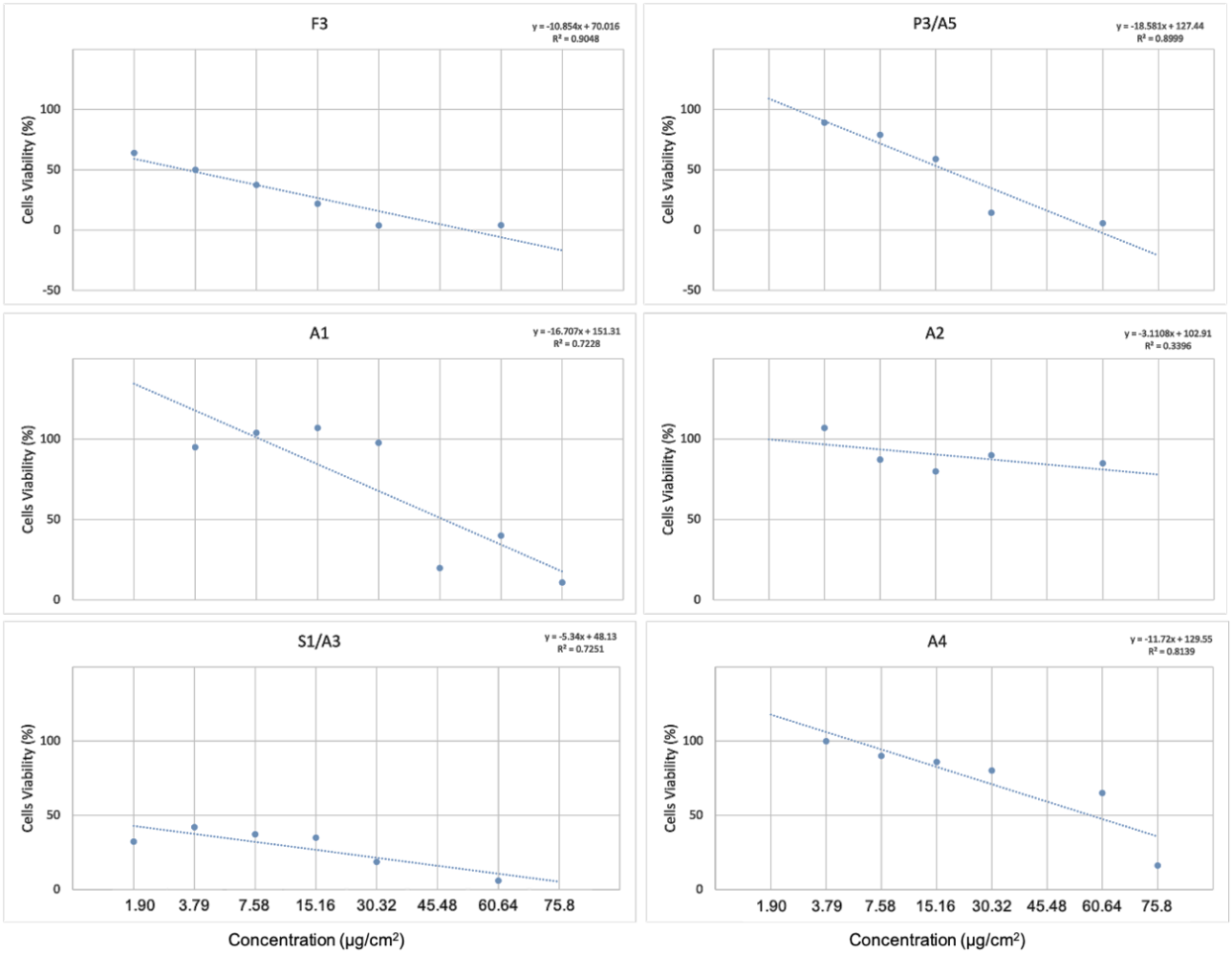

Figure 75. *The graphs show the different cell viability of BALB/C3 expressed as % of viability as compared with untreated controls of the corresponding cell lines. BALB/C3 cells were exposed to different concentrations either to asbestos or cleavage fragment.*

The NOEL is characteristically defined as the concentration or dose of a substance that causes no detectable alterations in an organism in the context of a given (safety) experiment. Furthermore, the mean lethal dose (IC50) and IC90 were determined (Figure 76). The toxicological data will be used later to perform the transformation tests.

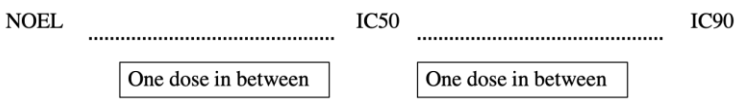

Figure 76. *Doses required in the preliminary dose range finding tests for selecting the dose to be used (Sasaki et al, 2012).*

Afterwards, to established interaction between cleavage fragments and BALB/c 3T3 cells was done by using the SEM. Exponentially growing BALB/c 3T3 cells were seeded for culture in 12-well

plates (4 × 104 cells/well) and incubated in a complete medium. After 24 h, the medium was replaced with fresh medium contend 7.81 µg/cm^2 of different tested samples, were used 2 wells per each dose. The cut section was then placed on a specific aluminum sample holder (stub), to proceed with the graphitation. The SEM observation were carried out at different magnifications, up to 2000x by measuring the diameter and length of the fibres inside the cells.

11.3 Observation of the cell/powder interaction

Images a and b (Figure 77) represent the unexposed cells, while images c and d (Figure 77) represent the interaction of BALB/c 3T3 cells with the fibres of sample F3 (Asbestos). Photomicrographs c-d shows longer asbestos fibres in the whole cellular environment.

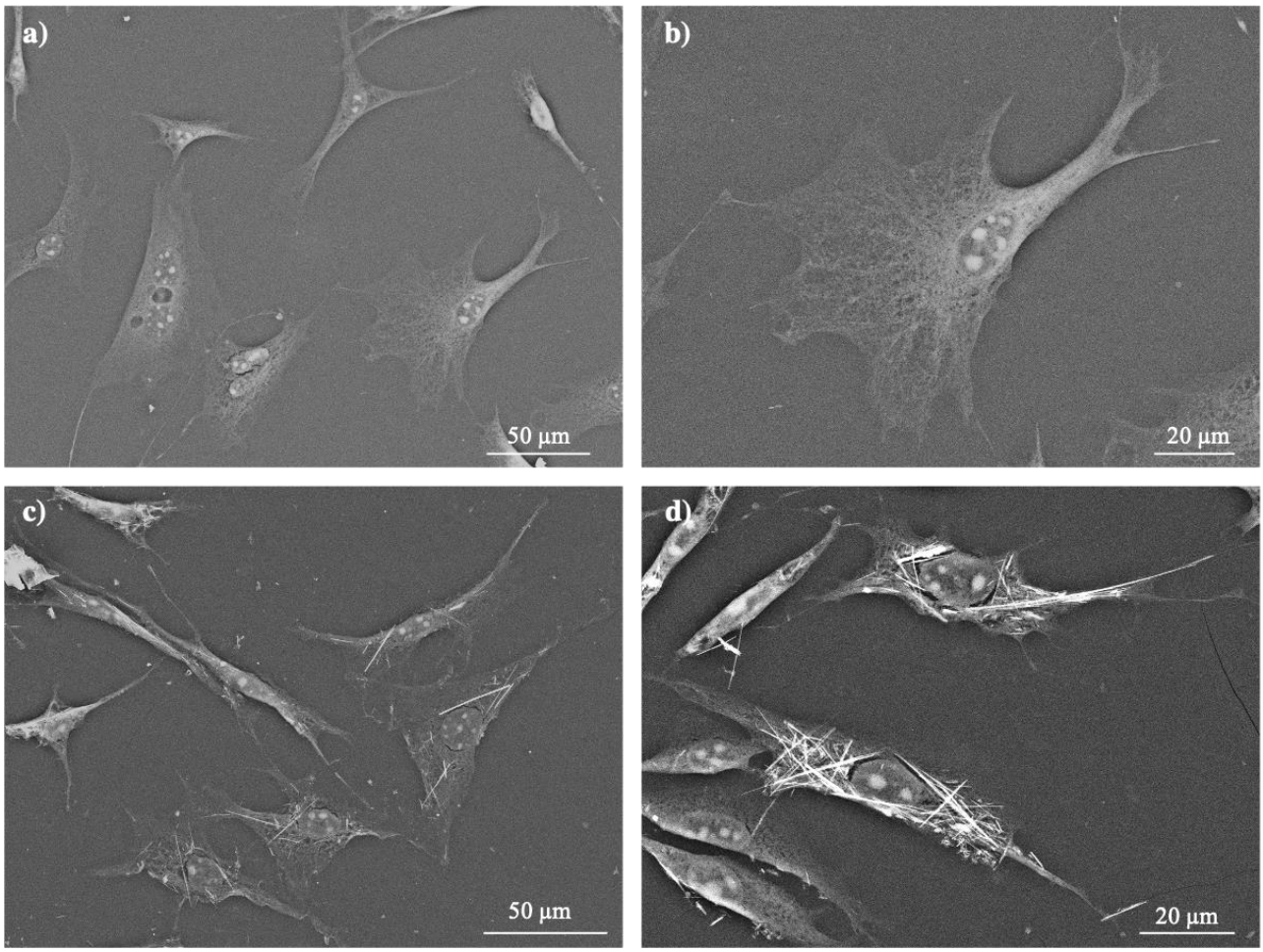

Figure 77. *Images of cells not exposed to powders K* ***(a-b)*** *and cells exposed to asbestos F3(****c-d****) (High Vacuum: 20 kV; Detector: Back scattered electrons).*

As regards sample A1 (Figures 78 a-b), fibres of different sizes are evident inside the cells. The longest ones reach an average of 7 µm in length and 1 µm thickness. Lower ratio fibres with lengths

of 6 µm and diameter of 3 µm are also observed. Chlorite grains sometimes represent finer and coarser powders.

In sample S1/A3 (Figures 78 c-d) the cells are entirely covered with serpentine powders, the length and width dimensions reach very low values (L: 2 µm, D: 0.35 µm).

Inside the cells of sample A4 (Figures 78 e-f) there are fibres with dimensions with maximum lengths of 11.40 µm and an average diameter of 0.85 µm. The stockier fragments have average lengths of 1.87 µm and a diameter 0.67 µm. In this case, as for sample F3, the longest fibres rarely enter the core, except for Figure f where the fibre also pierces the core.

Finally, in sample A5 we observe the more prismatic varieties of fibres. The main dimensions vary from 6 µm to 4.30 µm in maximum lengths and from 1.60 µm to 1.45 µm in maximum diameters. (Figures 78 g-h)

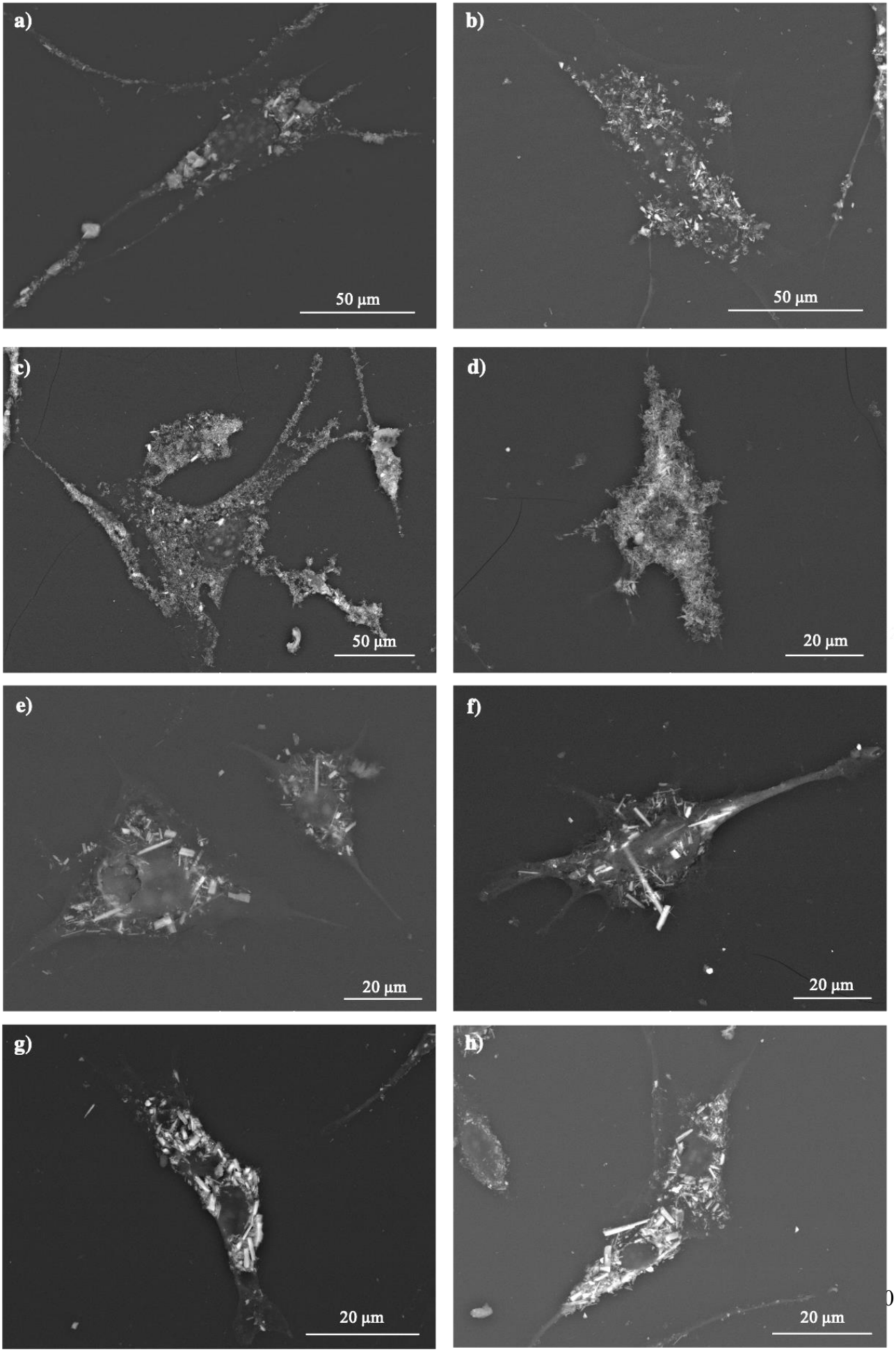
a)
50 µm
b)
50 µm
c)
50 µm
d)
20 µm
e)
20 µm
f)
20 µm
g)
20 µm
h)
20 µm

Figure 78. *Interaction between sample powders A1 (a-b), S1/A3 (c-d), A4 (e-f), A5 (g-h) and the cells (High Vacuum; 20 kV; Detector: Back scattered electrons).*

11.4 *In vitro* cell transformation test

In vitro cell transformation, assayed with BALB/c 3T3, has been recognised as being directly relevant to carcinogenesis (Kakunaga, 1973; Reznikoff et al., 1973) and is regarded as a useful method for screening potential carcinogens (Heidelberger et al., 1983; Dunkel et al., 1981; Meyer, 1983). In 1985, an IARC/NCI/ EPA Working Group proposed a recommended standard protocol for the BALB/c 3T3 and C3H10T1/2 cell transformation assays. However, the recommended protocol has not been widely used, as the method it outlines is time-consuming, expensive, and laborious compared to routine genotoxicity tests. Meanwhile, the *in vitro* two-stage model of the cell transformation assay has been useful in defining the carcinogenic events of initiation and promotion (Mondal et al., 1976; Sakai et al., 2002). A further technical modification to improve the efficacy of the original procedure has been previously proposed, namely, the use of DF2F medium, which comprises enriched basal medium DMEM/F12, containing 2% (v/v) fetal bovine serum (FBS) and supplemented with 2 mg/ml of insulin, instead of M10F medium (MEM Recently, the cell transformation assay has been put forward as a promising alternative method to animal carcinogenicity tests and thus needs standardisation (OECD, 2007). The protocol, in order to increase the practicability of the assay, we used the following changes: a) the use of larger (100 mm diameter) dishes, instead of 60 mm-diameter dishes; b) the replacement of insulin alone, as an additive to the 2% serum medium; and c) the extension of the culture period from 24–25 days to 31–32 days, with less frequent medium changes applied (i.e., once a week) during the last 2 weeks. The procedure outlined in the Technical Report by the Japanese Standards Association was modified, and the procedure finally adopted was as follows (Figure 79): A cell suspension of BALB/c 3T3 cells was prepared in M10F medium at 2x 10^3 cells/ml and distributed into 100mm-diameter dishes in 10ml aliquots (i.e., 2 x 10^4 cells/dish, Day 0). Four dishes were prepared for each test concentration. On the following day, the cells were treated with fresh M10F medium, containing a chemical with tumour initiating activity (the initiation stage). This was replaced with fresh M10F medium alone (i.e., with no chemical) on Day 4, and this in turn replaced with fresh DF2F2I medium containing a chemical with tumour promoting activity on Day 7, Day 10/11, and on Day 14 (the promotion stage was added 5µg/ml of insulin). This was subsequently replaced with fresh DF2F2I medium alone on Day 17/18, and on Day 24/25. The cells were fixed with methanol on Day 31/32 and stained with a 5% (w/v) Giemsa solution. The following morphological criteria characterised transformed foci: deep

basophilic staining; dense multi-layering of cells; random orientation of cells at the edge of the focus; and the presence of more than 50 cells within a focus (Hayashi et al., 2008).

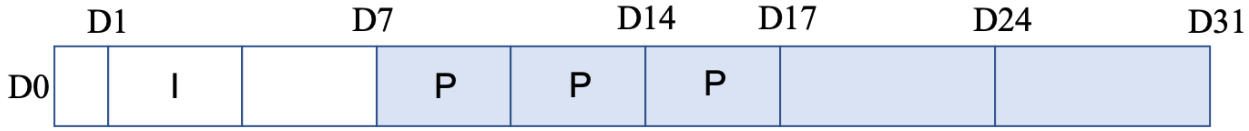

Figure 79. *Timelines for the protocols of the BALB/c 3T3 cell transformation assay. I = initiator treatment; P = promoter treatment 5µg/ml insulin; D = day. White Boxes: MEM + 10% FBS (M10F), Light blue boxes: DMEM/F12 + 2% FBS + 2 mg/ml insulin (DF2F21) (Modified from Hayashi et al., 2008).*

From the cytotoxicity tests, samples A1, S1/A3, A4, P3/A5 and clearly F3 were selected, then samples P1, P2 and A2 were excluded as they did not register any toxic effect.

12. CONCLUSIONS

In these three years, the work carried out provided advances in the knowledge of fibrous minerals and cleavage fragments thanks to the multidisciplinary approach of the project, which integrated geological and mineralogical data with bioassays data. The new results achieved have provided useful indications for future research also in other areas than those investigated. The petrographic study of samples made it possible to recognize metamorphic veins associated with amphibole and serpentine enrichments. A complete characterization was carried out, through microscopic and spectroscopy techniques, of the phases that may occur with asbestiform and non-asbestiform fibrous habit: minerals of the serpentine group (antigorite, chrysotile and lizardite) and minerals of the amphibole group (actinolite and tremolite). Finally, it has been demonstrated that the identification of the serpentine requires the combined use of several analytical techniques.

The observations under OM allowed to investigate the textures and the spatial relations between the mineralogical phases. Under SEM the aspect ratios and the textural relations between the various phases were characterised, but the discrimination among the serpentine polymorphs was impossible specially when embedded in the host rock. TEM analysis permitted the high-resolution discrimination for EMP and an effective distinction between asbestos minerals. However, observing the macroscale habit does not always correspond to that observed at the microscale (i.e., not repeated with fractal geometries). For example, when the elongated particles are very thin, even with TEM, it may not be possible to differentiate asbestiform fibres from prismatic crystals or cleavage fragments adequately.

12.1 Synchrotron Radiation X-ray microtomography

An unconventional methodology, based on image analysis, was tested to have original morphological information. Preliminary results showed that SR-μCT offers the possibility to observe and image the 3D morphology and the spatial relationship between the mineral phases that constituted the investigated samples in a complementary way to the conventional analytical techniques. Furthermore, it is a semi-destructive technique which allows the analysis of samples under high magnification and without loss of their morphology; it provides qualitative and volumetric but not quantitative information of the mineralogical phases. Therefore, it proved a useful technique to implement the research, but not an effective activity for quantitative data restitution in environmental monitoring.

It is noteworthy that none of the mentioned instruments is individually suitable for the unique and time-efficient identification of asbestos and non-asbestiform but still fibrous phases, particularly

if these phases occur within massive rocks and are therefore not isolated. If a unique and comprehensive knowledge of asbestos-bearing rock is needed, it is important to plan and carry out a multi-analytical approach that takes into consideration the several aspects related to NOA occurrences within the various lithotypes.

12.2 In what percentages are asbestiform and non-asbestiform minerals present when ground?

Preliminary results showed that the different behaviour of asbestiform and non-asbestiform amphiboles is confirmed in a distinct distribution length: width ratio of fibres, as effect of the comminution.

i. In both cases, small distinctions are observed between the samples ground for 30 seconds compared with the others. By extending the time of grinding between 120 seconds and 300 seconds prismatic and asbestos amphiboles do not show significant differences. However, the one-way analysis of variance (ANOVA) highlighted statistically significant differences also in this regard.

ii. In the case of non-asbestiform amphiboles, the number of fibres increases after longer milling time because they separate, producing cleavage fragments. These shorten considerably in length but also in the diameter, however, they do not reach widths below 0.6 μm. Conversely, for asbestiform amphiboles, as the grinding time increases, the bundles disaggregate and the number of counted fibres decreased because many turned below the detectable dimensions at 2000x, so fibrils reached a diameter even lower than 0.1 μm; length does not seem affected by the milling.

Overall, these results highlight how comminution is a critical phase in the preparation of the samples. The shape of produced particles could depend on lithology, type of the instrument (in particular, the specific breakage mechanism in a grinding device), the time of milling applied in the sample and the relative application of the stress. In order to obtain comparable quantitative results, our data strongly support the need to select the same equipment in each laboratory and standardize the method of sample preparation.

Moreover, the geometric overlap of particle sizes could cause an incorrect classification because it can lead to over- or underestimation of the concentrations and, therefore, the risk. More data on the shape and the size of particles are the benchmarks to new perspectives into the study of morphological features and mutagenic mechanisms of a presently misunderstood material.

12.3 Quantitative analysis: methods compared

The quantitative analysis of asbestos in rock samples has been tackled regarding the regulations in force. The whole of analyses demonstrated that asbestos concentration results are strongly dependent on the type of rock, the grain size prepared for analysis, and the criteria used to count fibres. The distribution of fibres, as the number and volumetric ratios in massive rocks it is not the same as that found in soils and debris materials.

i. In comparison with chrysotile, amphiboles (more resistant to comminution) are more evenly distributed in the three granulometric fractions, notwithstanding the same percentage in abundance for each sample.

ii. Asbestos fibres that lie outside the geometric ratio of fibres suggested in the decrees and by the World Health Organization are excluded from the definitions of "fibre" because too large. However, these large fibres might become broken or milled and, in such cases, would contribute to the fibre count. Such a process might influence the measured asbestos concentration, as outliers.

iii. In the case of occurring naturally asbestos in rocks the use of R.P.D. 120/2017 is considered more suitable for determinations and technical-scientific investigations. In such cases, the definition of a particle as part of the skeleton (the 2 to 20 mm fraction) is pointless if it is generated artificially according to the mode of rock disintegration. Therefore, it is considered more appropriate to express the concentration of the substance in terms of total content, without referring to the skeleton. This is the most precautionary result because it provides a determination of the total fibres released by a rock.

12.4 Cytotoxicity and transformation tests

The literature review did not reveal strong evidence indicating that cleavage fragments have the same or greater carcinogenic potential than asbestos. Different published data suggest that the asbestos fibres toxic effect increases with length, despite some notable exceptions. However, the extent to which a mineral with asbestiform habit affects its toxicologic or carcinogenic mechanisms relative to that of a cleavage fragment of the same mineral remains a matter of debate.

The data presented in this study highlighted that cleavage fragments of amphiboles and lizardite *in vitro* could induce cytotoxic effects and transformation process as carcinogenic potential.

The demonstration of the cytotoxic and transforming activity of fibres in the 3T3 model could constitute a starting point for further studies that may lead to the extrapolation of the risk related to exposure and categorization of fibres by the relevant regulatory institutions.

13. CONCLUDING REMARKS

Characterizing non-asbestiform fibres and understanding their hazard is important above all because are more common than asbestos in many geologic environments, and disturbance can result in the release of prismatic or acicular single crystals or cleavage fragments resembling asbestos fibres.

To date, workers may not be exposed to asbestos, but they can be for non-asbestiform amphiboles. Considering only the geometry, both prismatic and asbestiform amphiboles and serpentine may show inhalable elements with width < 3 μm, length > 5 μm and width length ratio > 1:3. Furthermore, although studies confirm that amphiboles are not carcinogenic if not in size greater than 1:20, because they are not easily engulfed by macrophages, more in-depth studies are necessary, especially because carcinogenicity of the cleavage fragments is not completely excluded.

Although asbestos minerals have been banned, their non-asbestiform analogues are not yet univocally regulated as asbestos, despite their geometric ratios fit within the concept of fibres. We demonstrated that, under the same chemical composition, the morphological characterization of the phases could not be disregarded to evaluate carcinogenicity.

REFERENCES

Abbate E., Bortolotti V., Principi G. (1980). Apennine ophiolites: a peculiar oceanic crust. Ofioliti, Special Issue on Tethyan ophiolites. (Rocci G. Ed), Western area; 5: 59-96.

Abelmann, A., Glynn, M.E., Pierce, J.S., Scott, P.K., Serrano, S., Paustenbach, D.J. Historical ambient airborne asbestos concentrations in the United States - an analysis of published and unpublished literature (1960s-2000s). Inhal Toxicol. 2015. 27(14), 754-766.

Addison, L., and McConnel, E.E. 2008, A review of carcinogenicity studies of asbestos and non-asbestos tremolite and other amphiboles. Regulatory Toxicology and Pharmacology, 52/1, S187-S 199. DOI: 10.1016/j.yrtph.2007.10.001.

Adib, G., Labreche, F., De GL, Dion C, Dufresne A: Short, fine and WHO asbestos fibres in the lungs of Quebec workers with an asbestos-related disease. Am J Ind Med 2013, 56:1001–1014.

AHERA (Asbestos Hazardous Emergency Response Act), 1987, Interim transmission electron microscopy analytical methods - mandatory and non-mandatory - and mandatory section to determine completion of response. Federal Register, 52, 41857-41897, October 30.

American Society for Testing and Materials International (ASTM): Standard Practice for Sampling and Counting Airborne Fibres, Including Asbestos Fibres, in Mines and Quarries, by Phase Contrast Microscopy and Transmission Electron Microscopy (D7200-06). [Standard] West Conshohocken, Pa.: ASTM International, 2006.

Agence nationale de sécurité sanitaire (ANSES) Opinion of the French Agency for Food, Environmental and Occupational Health & Safety. Health Effects and the identification of cleavage fragments of amphiboles from quarried minerals. Request No. 2014_SA_0196.

ASTM D6281: Standard test method for airborne asbestos concentration in ambient and indoor atmospheres as determined by transmission electron microscopy direct transfer (TEM): Annual Book of ASTM Standard, 1998; 11.03.

ASTM, I. (2016). Standard Test Method for Determination of Asbestos in Soil1. Designation: D7521 − 16. Available online: https://www.astm.org. (Accessed on 1 May 2016).

Baietto, O., Diano M., Zanetti G., and Marini P., 2019, Grinding Test on Tremolite with Fibrous and Prismatic Habit. Fibres, 7, 52-67. DOI: 10.3390/fib7060052.

Ballirano, P.; Bloise, A.; Gualtieri, A.F.; Lezzerini, M.; Pacella, A.; Perchiazzi, N.; Dogan, M.; Dogan, A.U. The Crystal Structure of Mineral Fibres. In Mineral Fibres: Crystal Chemistry, Chemical-Physical Properties, Biological Interaction and Toxicity; Gualtieri, A.F., Ed.; European Mineralogical Union: London, UK, 2017; Volume 18, pp. 17–53.

Ballirano, P.; Pacella, A.; Bloise, A.; Giordani, M.; Mattioli, M. Thermal Stability of Woolly Erionite-K and Considerations about the Heat-Induced Behaviour of the Erionite Group. Minerals 2018, 8, 28.

Baumann, F.; Ambrosi, J.-P.; Carbone, M. Asbestos is not just asbestos: An unrecognised health hazard. Lancet Oncol.

2013, 14, 576–578.

Baur, X., Soskolne C.L., Lemen, R.A., Schneider J., Woitowitz H.J., Budnik L.T. How conflicted authors undermine the World Health Organization (WHO) campaign to stop all use of asbestos: spotlight on studies showing that chrysotile is carcinogenic and facilitates other non-cancer asbestos-related diseases. Int J Occup Environ Health. 2015. 21(2), 176-179.

Baur X., Frank A.L., Budnik L.T., Woitowitz H.J., Oliver L.C., Welch L.S., Landrigan P., Lemen R., 2016. Collegium Ramazzini: comments on the 2014 helsinki consensus report on asbestos. Am. J. Ind. Med. 59 (7), 591-594.

Belardi, G., Vignaroli, G., Trapasso, F., Pacella, A., and Passeri, D., 2018, Detecting asbestos fibres and cleavage fragments produced after mechanical tests on ophiolite rocks: clues for the asbestos hazard evaluation. Journal of Mediterranean Earth Sciences 10, 63-78. DOI: 10.3304/JMES.2018.016.

Belluso, E.; Compagnoni, R.; Ferraris, G. Occurrence of Asbestiform Minerals in the Serpentinites of the Piemonte Zone,Western Alps. 1995. Available online: https://iris.unito.it/handle/2318/23533#.XMxmpGixXIU (accessed on 1 April 2019).

Belluso, E.; Cavallo, A.; Halterman, D. Crystal habit of mineral fibres. In Mineral Fibres: Crystal Chemistry, Chemical-Physical Properties, Biological Interaction and Toxicity; Gualtieri, A.F., Ed.; Mineralogical Society of Great Britain and Ireland, 2017; Volume 18, pp. 65–109. Available online: https://www.minersoc.org/emu-notes-18.html (accessed on 1 April 2019).

Bellomo D., Gargano C., Guercio A., Punturo R., Rimoldi B. *(2018). Workers' risks in asbestos contaminated natural sites*. *Journal of Mediterranean Earth Sciences 10 (2018), 97-106. doi: 10.3304/JMES.2018.019*

Berman, W., K. Crump, E. Chatfield, J. Davis, and A. Jones: The sizes, shapes, and mineralogy of asbestos structures that induce lung tumors or mesothelioma in AF/HAN rats following inhalation. Risk Anal. 15(2):181–195 (1995).

Berman D.W., Crump K.S., 2003. Final draft: Technical support document for a protocol to assess asbestos-related risk. Prepared for Office of Solid Waste and Emergency Response, U.S. Environmental Protection Agency, Washington, DC.20460, USEPA #9345.4-06 October 2003.

Berman, DW, Crump, KS: A meta-analysis of asbestos-related cancer risk that addresses fibre size and mineral type: Crit Rev Toxicol 2008; 38(S1):49–73.

Bernstein D., Dunnigan J., Hesterberg T., Brown R., Legaspi Velasco J.A., Barrerao R., Hoskins J., Gibbs A., 2013. Response to Murray M. Finkelstein, letter to the editor re Bernstein et al: health risk of chrysotile revisited. Crit. Rev. Toxicol. 43 (2), 154e183. Crit. Rev. Toxicol. 43(8), 709-710.

Bloise, A.; Critelli, T.; Catalano, M.; Apollaro, C.; Miriello, D.; Croce, A.; Barrese, E.; Liberi, F.; Piluso, E.; Rinaudo, C.; et al. Asbestos and other fibrous minerals contained in the serpentinites of the Gimigliano-Mount Reventino unit (Calabria, S-Italy). Environ. Earth. Sci. 2014, 71, 3773–3786.

Bloise, A.; Punturo, R.; Catalano, M.; Miriello, D.; Cirrincione, R. Naturally occurring asbestos (NOA) in rock and soil and relation with human activities: the monitoring example of selected sites in Calabria (southern Italy). Ital. J. Geosci. 2016, 135, 268–279.

Bloise, A.; Kusiorowski, R.; Lassinantti Gualtieri, M.; Gualtieri, A.F. Thermal behavior of mineral fibres. In Mineral Fibres: Crystal Chemistry, Chemical-Physical Properties, Biological Interaction and Toxicity; Gualtieri, A.F., Ed.; European Mineralogical Union: London, UK, 2017; Volume 18, pp. 215–252.

Bloise, A.; Catalano, M.; Critelli, T.; Apollaro, C.; Miriello, D. Naturally occurring asbestos: Potential for human exposure, San Severino Lucano (Basilicata, Southern Italy). Environ. Earth Sci. 2017, 76, 648.

Bloise, A., Catalano, M., and Gualtieri, A.F., 2018 Effect of Grinding on Chrysotile, Amosite and Crocidolite and Implications for Thermal Treatment. Minerals, 8, 135-152. DOI: 10.3390/min8040135.

Bloise A., Ricchiuti C., Punturo R., Pereira D. (2020). Potentially toxic elements (PTEs) associated with asbestos chrysotile, tremolite and actinolite in the Calabria region (Italy). Chemical Geology 558 (2020) 119896. https://doi.org/10.1016/j.chemgeo.2020.119896.

Bortolotti. V, Principi G. (2005). Tethyan ophiolites and Pangea break-up. The Island Arc; 14: 442-470.

Boulanger, G, Andujar, P, Pairon J-C et al (2014). Quantification of short and long asbestos fibres to assess asbestos exposure: a review of fibre size toxicity. Environ Health 13:59. https://doi.org/10.1186/1476-069X-13-59.

Burragato F., Comba P., Baiocchi V., Palladino D.M., Simei S., Gianfanga A., Paoletti L., Pasetto R., 2005. Geo-volcanological, mineralogical and environmental aspects of quarry materials related to pleural neoplasm in the area of Biancavilla, Mount Etna (Eastern Sicily, Italy). Environmental Geology 47; 855-868.

Brown, GM, Cowie, H, Davis, JMG, Donaldson, K: In vitro assays for detecting carcinogenic mineral fibres: a comparison of two assays and the role of fibre size. Carcinogenesis 1986, 7:1971–1974.

Brun, F.; Massimi, L.; Fratini, M.; Dreossi, D.; Billé, F.; Accardo, A.; Pugliese, R.; Cedola, A. SYRMEP Tomo Project: a graphical user interface for customizing CT reconstruction workflows. Adv. Struct. Chem. Imaging 2017, 3.

Brun, F.; Accardo, A.; Kourousias, G.; Dreossi, D.; Pugliese, R. Effective implementation of ring artifacts removal filters for synchrotron radiation microtomographic images. In Proceedings of the 8th International Symposium on Image and Signal Processing and Analysis (ISPA), Trieste, Italy, 4–6 September 2013; Ramponi, G., Lonˇcari´c, S., Carini, A., Egiazarian, K., Eds.; Available online: https://ieeexplore.ieee.org/document/6703823 (accessed on 1 April 2019).

Cardile, V.; Lombardo, L.; Belluso, E.; Panico, A.; Capella, S.; Balazy, M. Toxicity and carcinogenicity mechanisms of fibrous antigorite. Int. J. Environ. Res. Public Health 2007, 4, 1–9.

Cavariani, F., Marconi, A., Sala, O., 2010. Asbestos: sampling, analytical techniques and limit values. 549 Ital. J. Occup. Environ. Hyg. 1(1), 18–28.

Chatfield E.J., 2008. A procedure for quantitative description of fibrosity in amphibole minerals. In 2008 Johnson Conference: Critical Issues in Monitoring Asbestos, ASTM International, Burlington, Vermont, July 14–July 18, 2008. Available at: www.astm.org.

Chatfield, E.J., 2018, Measurement of elongate mineral particles: What we should

measure and how do we do it? Toxicology and Applied Pharmacology 361, 36–46. DOI: 10.1016/j.taap.2018.08.010.

Cloetens, P.; Pateyron-Salome, M.; Bu_˙ ere, J.Y.; Peix, G.; Baruchel, J.; Peyrin, F.; Schlenker, M. Observation of microstructure and damage in materials by phase sensitive radiography and tomography. J. App. Phys. 1997, 81.

Commission Directive 1999/77/EC adapting to technical progress for the sixth time Annex I to Council Directive 76/769/EEC on the approximation of the laws, regulations, and administrative provisions of the member states relating to restrictions on the marketing and use of certain dangerous substances and preparations (asbestos). Official Journal L 207, 06/08/1999 P. 0018 – 0020.

Compagnoni, R.; Groppo, C. Gli amianti in Val di Susa e le rocce che li contengono. Rend. Soc. Geol. It. 2006, 3. Nuova Serie, 21-28, 11 ff., 3 tabb. Available online: https://www.socgeol.it/files/download/workshop/05% 20VS%20 (21-28).pdf (accessed on 1 April 2019).

Cook, W. E., 1927. Pulmonary asbestosis. British Medical Journal, pp. 1024-1025.

Coraglia, B., Forlati, F., Fusetti, E., Giacomelli, L., Morelli, M., Piazzano, P, Wojtowicz, M. (2006). Naturally Occurring Asbestos Mapping Project: the experience of Regione Piemonte. European Conference on Asbestos Risk and Management. Roma.

Cossio, R., Albonico, C., Zanella, A. Fraterrigo-Garofalo, S., Avataneo, C., Compagnoni, R., and Turci, F. 2018, Innovative unattended SEM-EDS analysis for asbestos fibre quantification. Talanta 190, 158–166. DOI: 10.1016/j.talanta.2018.07.083.

Cunningham, H. M., Moodie, C. A., Lawrence, G. A., and Ponterfract, R. D. _1977_. "Chronic effects of ingested asbestos in rats." Arch. Environ. Contam. Toxicol., 6, 507–513.

Davis, J. M. G. et al., 1985. Inhalation studies on the effects of tremolite and brucite dust in rats. Carcinogenesis, Volume 5, pp. 667-674.

Davis, JMG, Addison, J, Bolton, RE: The pathogenicity of long versus short fibre samples of amosite asbestos administered to rats by inhalation and intraperitoneal injection. Br J Exp Pathol 1986, 67:415–430.

Davis, J.M.G., Bolton, R.E., Douglas, A.N., Jones, A.D., Smith, T. Effects of electrostatic charge on the pathogenicity of chrysotile asbestos. British Journal of industrial medicine (1988); 45:292-299 http://dx.doi.org/10.1136/oem.45.5.292.

Davis, JMG, Addison, J, McIntosh, C, Miller, BG, Niven, K: Variations in the carcinogenicity of tremolite dust samples of differing morphology: Ann NY Acad Sci 1991;643: 473–490.

Decandia F. A., Elter P. (1972). La zona ofiolitifera del Bracco nel settore compreso tra Levanto e la Val Graveglia (Appennino Ligure). Mem. Soc. Geol. It; 11: 503-530.

Decree of the President of the Republic No. 120/2017. Regolamento recante la disciplina semplificata della gestione delle terre e rocce da scavo, ai sensi dell'articolo 8 del decreto-legge 12 settembre 2014, n. 133, convertito, con modificazioni, dalla legge 11 novembre 2014. n. 164. Available online: http://www.bosettiegatti.eu/info/norme/statali/2017_0120.htm (Accessed on 7 August 2017).

Decreto Ministeriale 06 settembre 1994: Normative e metodologie tecniche di

applicazione dell'art. 6, comma 3, e dell'art. 12, comma 2, della legge 27 marzo 1992, n. 257, relativa alla cessazione dell'impiego dell'amianto.

Decreto del Ministero dell'ambiente e della tutela del territorio e del mare 10 agosto 2012, n. 161 Regolamento recante la disciplina dell'utilizzazione delle terre e rocce da scavo.

Dement, J. M., E. D. Kuempel, R. D. Zumwalde, R. J. Smith, L. T. Stayner, and D. Loomis: Development of a fibre size-specific job-exposure matrix for airborne asbestos fibres. Occup. Environ. Med. 65(9):605–612 (2008).

Di Giuseppe, D., Zoboli, A., Vigliaturo, R., Gieré, R., Bonasoni, MP, Sala, O., Gualtieri, A.F. Mineral Fibres and Asbestos Bodies in Human Lung Tissue: A Case Study. Minerals 2019, 9, 618; doi:10.3390/min9100618

Directive 2003/18/EC of the European Parliament and of the Council of 27 March 2003 amending Council Directive 83/477/EEC on the protection of workers from the risks related to exposure to asbestos at work. Done at Brussels, 27 March 2003.

Directive 2009/148/EC of the European Parliament and of the Council of 30 November 2009 on the protection of workers against the risks associated with exposure to asbestos. Done at Brussels, 30 November 2009.

Dodson, R., Atkinson, M.AL., Levin, JL. Asbestos fibre length as related to potential pathogenicity: a critical review. Am J Ind Med. 2003 Sep;44(3):291-7. doi: 10.1002/ajim.10263.

Dogan, M.; Emri, S. Environmental health problems related to mineral dusts in Ankara and Eskisehir, Turkey. Yerbilimleri 2000, 22, 149–161.

Doll, R., 1955. Mortality for lung cancer in asbestos workers. British Journal of Industrial Medicine, Issue 12, pp. 81-86.

Donaldson, K, Brown, GM, Brown, DM, Bolton, RE, Davis, JMG: Inflammation generating potential of long and short fibre amosite asbestos samples. Br J Ind Med 1989, 46:271–276.

Donaldson, K, Szymaniec, S, Li XY: Inflammation and immunomodulation caused by short and long amosite asbestos samples. In Mechanisms in Fibre Carcinogenesis. Edited by Brown RC, Hoskins J. New-York: Plenum Press; 1991:121–130.

Donaldson, K., Li, X.Y., Dogra, S., Miller, B.G., Brown, G.M., 1992. Asbestos-stimulated tumour-necrosis-factor release from alveolar macrophages depends on fibre length and opsonization. J. Pathol. 168, 243–248.

Dunkel, V.C., Pienta, R.J., Sivak, A. & Traul, K.A. (1981). Comparative neoplastic transformation responses of BALB/3T3 cells, Syrian hamster embryo cells, and Rauscher murine leukaemia virus-infected Fischer 344 rat embryo cells to chemical carcinogens. Journal of the National Cancer Institute 67, 1303–1315.

Elter P., Pertusati P. C., (1973). Considerazioni sul limite Alpi-Appennino e sulle relazioni con l'arco delle Alpi Occidentali. Mem. Soc. Geol. It.; 12: 359-375.

Elter, F.M.; Elter, P.; Eva, C.; Eva, E.; Kraus, R.K.; Padovano, M.; Solarino, S. An alternative model for the recent evolution of the Northern–Central Apennines (Italy). J. Geodyn. 2012, 54, 55–63.

Elter P. (1975a). Introduction à la gèologie de l'Appennin Septentrional. Bull. Soc. Geol. France; 17: 956-962.

Elter P. (1975b). L'ensemble ligure. Bull Soc Geol France; 17: 984-997.

European Commission, Directive 2003/18/EC and Directive/2009/148/EC, Protection of workers from the risks related to exposure to asbestos at work.

European Parliament 2012/2065(INI), Motion for a European Parliament Resolution on asbestos related occupational health threats and prospects for abolishing all existing asbestos.

EPA (Environmental Protection Agency): Method for Determination of Asbestos in Bulk Building: Materials Perkins RL, Harvey BW: Method for the determination of asbestos in bulk building materials: 1993, U.S. Environmental Protection Agency EPA/600/ R-93/116, Office of Research and Development, Washington, D.C.

Finkelstein M.M., 2013. Letter to the Editor re Bernstein et al: health risk of chrysotile revisited. Crit. Rev. Toxicol. 43 (2), 154e183. Crit. Rev. Toxicol. 43(8), 707-708.

Gaggero L., Crispini L., Marescotti P., Malatesta C., Solimano 4-6 December, 2006. Structural and microstructural control on chrysotile distribution in serpentinites from eastern Ligurian ophiolites. In: European Conference on Asbestos Risks and Management, 134-139, Rome.

Gaggero, L.; Crispini, L.; Isola, E.; Marescotti, P. Asbestos in natural and anthropic ophiolitic environments: A case study of geohazards related to the northern Apennine ophiolites (Eastern Liguria, Italy). Ofioliti 2013, 31, 29–40.

Gaggero L., Sanguineti E., Yus Gonzales A., Militello G.M., Scuderi A., Parisi G. (2017). Airborne asbestos fibres monitoring in tunnel excavation. Journal of Environmental Management 196C (2017) pp. 583-593.

Gaggero, L.; Ferretti, M. The Self-sustained High temperature Synthesis (SHS) technology as novel approach in the management of asbestos waste. J. Environ. Manag. 2018, 216, 246–256.

Gamble, J.F., and Gibbs, G.W., 2008, An evaluation of the risks of lung cancer and mesothelioma from exposure to amphibole cleavage fragments. Regulatory Toxicology and Pharmacology 52, S154-S186. DOI: 10.1016/j.yrtph.2007.09.020.

Gamble, J. F. & Gibbs, G. W., 2008. An evaluation of the risks of lung cancer and mesothelioma from exposure to amphibole cleavage fragments. Regulatory Toxicology and Pharmacology, Volume 52, pp. S154-S186.

Giacomini, F., Boerio, V., Polattini, S., Tiepolo, M., Tribuzio, R., Zanetti. A., 2010 Evaluating asbestos fibre concentration in metaophiolites: a case study from the Voltri Massif and Sestri– Voltaggio Zone (Liguria, NW Italy). Environ. Earth. Sci. 61, 1621–1639.

Goodglick, LA, Kane AB: Cytotoxicity of long and short crocidolite asbestos fibres in vitro and *in vivo*. Cancer Res 1990, 50:5153–5163.

Groppo, C.; Rinaudo, C.; Cairo, S.; Gastaldi, D.; Compagnoni, R. Micro-Raman spectroscopy for a quick and reliable identification of serpentine minerals from ultramafics. Eur. J. Miner. 2006, 18, 319–329.

Gualtieri, A.F., 2017, Mineral fibres: Crystal chemistry, chemical-physical properties, biological interaction and

toxicity. Volume 18 EMU Notes, 536 pp., ISBN: 9780903056656.

Gualtieri, A.F.; Gandolfi, N.B.; Pollastri, S.; Rinaldi, R.; Sala, O.; Martinelli, G.; Bacci, T.; Paoli, F.; Viani, A.; Vigliaturo, R. Assessment of the potential hazard represented by natural raw materials containing mineral fibres—The case of the feldspar from Orani, Sardinia (Italy). J. Hazard. Mater. 2018, 350, 76–87.

Ham, S., Hwang, S., and Yoon, C., 2019, Comparison of Methods for Pre-treatment and Quantification of Bulk Asbestos Samples for Polarized Light Microscopy Analysis to Evaluate Asbestos-Containing Waste. Sustainability, 11, 6440-6453. DOI:10.3390/su11226440.

Hamra, GB, Loomis D, Dement, J: Examining the association of lung cancer and highly correlated fibre size-specific asbestos exposures with a hierarchical Bayesian model. Occup Environ Med 2014.

Harris, K.E., Bunker, K.L., Strohmeier, B.R., Hoch, R., and Lee, R.J., 2007, Discovering the True Morphology of Amphibole Minerals: Complementary TEM and FESEM Characterization of Particles in Mixed Mineral Dust. RJ Lee Group, Inc., 350 Hochberg Road, Monroeville, PA, 15146, USA Modern Research and Educational Topics in Microscopy. A. Méndez-Vilas and J. Díaz (Eds.).

Harper, M., Lee, E.G., Doorn, S.S., and Hammond, O., 2008, Differentiating non-asbestiform amphibole and amphibole asbestos by size characteristics. Journal of Occupational and Environmental Hygiene 5, 761-770. DOI: 10.1080/15459620802462290.

Harper, M. 10th Anniversary Critical Review: Naturally occurring asbestos. J. Environ. Monit. 2008, 10, 1394.

Harper, M., Lee, E.G., Slaven, J., and Bartley, D., 2012, An inter-laboratory study to determine the effectiveness of procedures for discriminating amphibole asbestos fibres from amphibole cleavage fragments in fibre counting by phase-contrast microscopy. Annals of Occupational Hygiene 56, 645-659. DOI: 10.1093/annhyg/mer123.

Harper, M. 10th Anniversary Critical Review: Naturally occurring asbestos. J Environ Monit. 2008. 10, 1394–1408.

Hashim, D., Boffetta, P. Occupational and Environmental Exposures and Cancers in Developing Countries. Ann Glob Health. 2014. 80, 393-411.

Hawthorne, F.C. & Oberti R.. Amphiboles: Crystal Chemistry. Reviews in Mineralogy & Vol. 67, pp. 1-54, 2007. DOI: 10.2138/rmg.2007.67.1

Hawthorne F.C., Oberti R., Harlow G.E., Maresch W.V., Martin R.F., Schumacher J.C. and Welch M.D. Nomenclature of the amphibole supergroup. American Mineralogist, Volume 97, pages 2031–2048, 2012.

Hayashi Kumiko, Kiyoshi Sasaki, Shin Asada,1 Toshiyuki Tsuchiya,2 Makoto Hayashi, Isao Yoshimura,4 Noriho Tanaka1 and Makoto Umeda. Technical Modification of the BALB/c 3T3 Cell Transformation Assay: The Use of Serum-reduced Medium to Optimise the Practicability of the Protocol. ATLA 36, 653–665, 2008.

Heidelberger, C., Freeman, A.E., Pienta, R.J., Sivak, A., Bertram, J.S., Casto, B.C., Dunkel, V.C., Francis, M.W., Kakunaga, T., Little, J.B. & Schechtman, L.M. (1983). Cell transformation by chemical agents — a review and analysis of the literature. Mutation Research 114, 283–385.

Herman, G.T. Image Reconstruction from Projections: The Fundamentals of Computerized Tomography, 1st ed.; Academic Press: New York, NY, USA, 1980; Available online: https://www.springer.com/us/book/9781825233 6172 (accessed on 1 April 2019).

Hesterberg, T. W. 2009. Comments on NIOSH asbestos roadmap—Animal bioassays. Workshop on the NIOSH Research Roadmap on Asbestos Fibres and Other Elongated Mineral Particles, Washington, DC: National Institute of Occupational Safety and Health.

Hill., IM., Beswick, PH. Differential release of superoxide anions by macrophages treated with long and short fibre amosite asbestos is a consequence of differential affinity for opsonin. Occup Environ Med. 1995 Feb;52(2):92-6. doi: 10.1136/oem.52.2.92.

Hwang, J., Ramachandran, G., Raynor, P.C., Alexander, B.H., and Mandel, J.H., 2014, The Relationship Between Various Exposure Metrics for Elongate Mineral Particles (EMP) in the Taconite Mining and Processing Industry. Journal of Occupational and Environmental Hygiene, 11/9, 613-624. DOI.org/10.1080/15459624.2014.890287.

IARC, 1977. Monographs on the evaluation of the risk to human. IARC Scientific Publication International Agency for Research on Cancer, Volume 14.

IARC, 1987. Monograph on the evaluation of the risk to human- Asbestos – Supplement 7. IARC Scientific Publication International Agency for Research on Cancer.

IARC, 2012. Working Group on the Evaluation of Carcinogenic Risk to Humans. IARC Monographs on the Evaluation of Carcinogenic Risks to Humans, no. 100C. International Agency for Research on Cancer, Lyon, France.

IARC, (2012c). Biological agents. IARC Monogr Eval Carcinog Risk Hum, 100B: PMID:18335640.

Ilgren, E. B. & Penna, B. M., 2004. The Biology of Cleavage Fragments: A Brief Synthesis and Analysis of Current Knowledge. Indoor and Built Environment, 19 Giugno, p. 14.

ISO (International Organization for Standardization), 1999. ISO 13794. Ambient air - Determination of asbestos fibres - Indirect-transfer transmission electron microscopy method.

International Standardization Organization (ISO), ISO/DIS 22262-2, Bulk materials, Part 2: Quantitative determination of asbestos by gravimetric and microscopical methods. 10.08.2009b. Available online: https://www.iso.org/standard/56773.html. (Accessed on September 2014).

International Standardization Organization (ISO). ISO/DIS 22262-2, Bulk Materials, Part 2: Quantitative determination of Asbestos by Gravimetric and Microscopical Methods. 10.08.2009b. Available online: https://www.iso.org/standard/56773.html (accessed on 1 April 2019).

Irving, J., Selikoff, I.J., Hammond, E.C. Asbestos and Smoking. JAMA. 1979;242(5):458–459. doi:10.1001/jama.1979.03300050048029

Italian Ministerial Decree No. 06/09/1994. All. 1B- Quantitative determination of asbestos in bulk samples.

Italian Ministerial Decree No. 06/09/1994. All. 2B. Determinazione Quantitativa Delle Concentrazioni di Fibre di Amianto Aerodisperse in Ambienti Indoor Mediante Microscopia Elettronica a Scansione. Available online:

http://www.earaonline.eu/wp-content/uploads/Decreto-Ministeriale-06-09-94.pdf (accessed on 1 April 2019).

Italian Legislative Decree No. 152/2006. Norme in materia ambientale. Part IV, norme in materia di gestione dei rifiuti di bonifica dei siti inquinati. All. 5, concentrazione soglia di contaminazione nel suolo, nel sottosuolo e nelle acque sotterranee in relazione alla specifica destinazione d'uso dei siti. Available online: https://www.camera.it/parlam/leggi/deleghe/06152dl3.htm. (Accessed on 3 April 2006).

Jargin S.V., 2015. Asbestos-related research: first objectivity then conclusions. J. Environ. Stud. 1 (1), 6.

Kakunaga, T. (1973). A quantitative system for assay of malignant transformation by chemical carcinogens using a clone derived from BALB/3T3. International Journal of Cancer 12, 463–473.

Keane, M.J., Stephens, J.W., Zhong, B.Z., Miller, W.E., and Wallace, W.E., 1999, A study of the effect of chrysotile fibre surface composition on genotoxicity *in vitro*. Journal of Toxicology and Environmental Health, Part A, 57/8, 529-541. DOI: 10.1080/009841099157494.

Labagnara, D., Patrucco, M., Rossetti, P., Pellegrino, V., 2013. Predictive assessment of the asbestos content in the Western Italian Alps: an essential tool for an effective approach to risk analysis and management in tunnelling operations and muck reuse. Environ. Earth Sci. 70, 857–868.

La Maestra, S., Micale, R.T., Ferretti, M., Izzotti, A., Gaggero, L. Attenuation of oxidative stress and chromosomal aberrations in cultured macrophages and pulmonary cells following self-sustained high temperature synthesis of asbestos. Sci Rep. 2020 May 22;10(1):8581. doi: 10.1038/s41598-020-65620-x. PMID: 32444646; PMCID: PMC7244567.

Langer, A. M., Nolan, R. P. & Addison, J., 1991. Distinguishing between amphibole asbestos fibres and elongate cleavage fragment of their non-asbestos analogues. In: Mechanism in Fibre Carcinogenesis. New York: Plenum Press, pp. 253-267.

Leake, B.E., Woolley, A.R., Arps, C.E.S., Birch, W.D., Gilbert, M.C., Grice, J.D., Hawthorne, F.C., Kato, A., Kisch, H.J., Krivovichev, V.G., Linthout, K., Laird, J., Mandarino, J.A., Maresch, W.V., Nickel, E.H., Rock, N.M.S., Schumacher, J.C., Smith, D.C., Stephenson, N.C.N., Ungaretti, L., Whittaker, E.J.W., Guo, Y., 1997. Nomenclature of amphiboles: report of the subcommittee on amphiboles of the International Mineralogical Association, Commission on New Minerals and Mineral Names. Canadian Mineralogist 35, 219–246.

Lee, R.J., Strohmeier, B.R., Bunker, K.L., Van Orden, D.R. Naturally occurring asbestos - A recurring public policy challenge. J Hazard Mater. 2008. 153, 1–21.

LEGGE N° 257 del 27/03/1992, Norme relative alla cessazione dell'impiego dell'amianto, Gazz. Uff. Suppl. Ordin. n° 87 del 13 Aprile 1992.

Lippmann, M. 1990. Effects of fibre characteristics on lung deposition, retention, and disease. Environ. Health Perspect. 88: 311–317.

Loomis, D, Dement, JM, Wolf, SH, Richardson, DB: Lung cancer mortality and fibre exposures among North Carolina asbestos textile workers. Occup Environ Med 2009, 66:535–542.

Loomis, D, Dement, J, Richardson, D, Wolf S: Asbestos fibre dimensions and lung cancer mortality among workers exposed to chrysotile. Occup Environ Med 2010, 67:580–584.

Loomis, D, Dement, JM, Elliott, L, Richardson, D, Kuempel, ED, Stayner, L: Increased lung cancer mortality among chrysotile asbestos textile workers is more strongly associated with exposure to long thin fibres. Occup Environ Med 2012, 69:564–568.

Luberto, F., Amendola, P., Belli, S., Bruno, C., Candela, S., Grignoli, M., & Comba, P. (2004). Mortality study of asbestos cement workers in Emilia-Romagna. Epidemiologia e prevenzione, 28(4-5), 239-246.

Maino, M.; Casini, L.; Ceriani, A.; Decarlis, A.; Di Giulio, A.; Seno, S.; Setti, M.; Stuart, F.M. Dating shallow thrusts with zircon (U-Th)/He thermochronometry—The shear heating connection. Geology 2015, 43(6), 495–498, doi:10.1130/G36492.1.

Maire, E.;Withers, P.J. Quantitative X-ray tomography. Int. Mat. Rev. 2014, 59, 1–43.

Marroni M., Pandolfi L. (2007). The architecture of the Jurassic Ligure-Piemontese oceanic basin: tentative reconstruction along the Northern Apennine - Alpine Corsica transect. International Journal of Earth Science; DOI: 10.1007/s00531-006-0163-x.

Marsili D., Terracini B., Santana V.S., Ramos-Bonilla J.P., Pasetto R., Mazzeo A., Loomis D., Comba P., Algranti E. Prevention of Asbestos-Related Disease in Countries Currently Using Asbestos. Int J Environ Res Public Health. 2016. 13, 494-513.

McConnell, EE, Axten, C, Hesterberg, TW, Chevalier, J, Miiller, WC, Everitt J, Oberdorster, G, Chase, GR, Thevenaz, P, Kotin, P: Studies on the inhalation toxicology of two fibreglasses and amosite asbestos in the Syrian golden hamster. Part II. Results of chronic exposure. Inhal Toxicol 1999, 11:785–835.

McCrone W.C., 1987. Asbestos Identification. McCrone Research Institute, Chicago, IL ISBN 0-904962-11-3.

Meyer, A.L. (1983). In vitro transformation assays for chemical carcinogens. Mutation Research 115, 323–338.

Militello G.M, Yus Gonzàlez A., Sanguineti E., Gaggero L. (2017). Comparison among Italian normative methods for asbestos quantification in massive lithotypes by SEM-EDS. Plinius.

Militello, G.M., Bloise, A., Gaggero, L., Lanzafame, G., Punturo, R., 2019a, Multi-Analytical Approach for Asbestos Minerals and Their Non-Asbestiform Analogues: Inferences from Host Rock Textural Constraints. Fibres, 7, 42. https://doi.org/10.3390/fib7050042.

Militello, G.M. Sanguineti, E., Yus González, A., Mantovani, F., and Gaggero, L. 2019b, The Concentration of Asbestos Fibres in Bulk Samples and Its Variation with Grain Size. Minerals 2019, 9, 539-558. https://doi.org/10.3390/min9090539.

Militello, G.M., Sanguineti, E., Yus González, A. and Gaggero, L. 2020. Asbestos amphiboles: effects of comminution on tremolite and actinolite regulated and unregulated fibres. https://doi.org/10.18814/epiiugs/2020/

Ministerial Decree No. 06/09/1994. (All.1–paragrafo B). Determinazione quantitativa dell'amianto in campioni in massa. Available online: Gazz. Uff. Suppl. Ordin. n° 220 del 20/09/1994.

Ministerial Decree No. 06/09/1994. (All.1–paragrafo B). Determinazione Quantitativa Dell'amianto in Campioni in Massa. Available online: https://www.gazzettau_ciale.it/atto/serie_ generale/ caricaArticolo?art.progressivo=0&art.idArticolo=1&art.versione=1&art.codiceRedazionale= 094A5917&art.dataPubblicazioneGazzetta=1994-09 20&art.idGruppo=0&art.idSottoArticolo1=10& art.idSottoArticolo=1&art.flagTipoArticolo=2 (accessed on 1 May 2016).

Mossman, B: Assessment of the pathogenic potential of asbestiform vs. non asbestiform particulates (cleavage fragments) in in vitro (cell or organ culture) models and bioassays: Reg Tox Pharmacol 2008; 52:S200–S203.

Mondal, S., Brankow, D.W. & Heidelberger, C. (1976). Two-stage chemical oncogenesis in cultures of C3H10T1/2 cells. Cancer Research 36, 2254– 2260.

Mossman BT, Lippmann M, Hesterberg TW, Kelsey KT, Barchowsky A, Bonner JC: Pulmonary endpoints (lung carcinomas and asbestosis) following inhalation exposure to asbestos. J Toxicol Environ Health Part B Critical Rev 2011, 14:76–121.

National Institute for Occupational Safety and Health (NIOSH): Method 7400, Asbestos and other fibres by PCM. Issue 2 (8/15/94). In NIOSH Manual of Analytical Methods (4th ed.). DHSS (NIOSH) Pub. No. 2003-154. Cincinnati, Ohio: NIOSH, 2003.

National Institute for Occupational Safety and Health (NIOSH): Method 7402: Asbestos by TEM, Issue 2, August 15, 1994. In NIOSH Manual of Analytical Methods (NMAM) (4th ed.). DHSS (NIOSH) Pub. No. 2003-154. Cincinnati, Ohio: NIOSH, 2003.

NIOSH (National Institute for Occupational Safety and Health), 2011. Asbestos fibres and other elongate mineral particles: state of the science and roadmap for research. DHHS Publication No. 2011-159. Curr. Intell. Bull. 2011, 62. Available online: https://www.cdc.gov/niosh/docs/2011-159/pdfs/2011-159.pdf (accessed on 1 April 2019).

National Research Council (US), 1984. Asbestiform Fibres Nonoccupational Health Risks. Washington (DC): National Academies Press (US).

OECD (2007). Detailed Review Paper on Cell Transformation Assays for Detection of Chemical Carcinogens. OECD Series on Testing and Assessment, No. 31, 164pp. Paris, France: Organisation for Economic Co-operation and Development.

Oehlert, GW: Testimony at the OSHA hearings on the exposure to asbestos, tremolite, anthophyllite, and actinolite, May, 1990.

OSHA (Occupational Safety and Health Administration), 1994a. Rules and Regulations, Department of Labor: 29 CFR Parts 1910, 1915 and 1926, 59 FR 40964, RIN: 1218-AB25; Occupational Exposure to Asbestos; August 1994-Final Rule; Appendix B of 1910.1001; 1. Introduction.

OSHA (Occupational Safety and Health Administration), 1994b. Rules and Regulations, Department of Labor: 29 CFR Parts 1910, 1915 and 1926, 59 FR 40964, RIN: 1218-AB25; Occupational Exposure to Asbestos; August 1994-Final Rule; Appendix K of 1915.1001; Polarized Light Microscopy of Asbestos. 3.5 Analytical Procedure. 4.

Paganin, D.; Mayo, S.C.; Gureyev, T.E.; Miller, P.R.; Wilkins, S.W. Simultaneous phase and amplitude extraction from a single defocused image of a homogeneous object. J. Microsc. 2002, 206, 33–40.

Patel-Mandlik, K. J., and Millette, J. R. _1983_. "Chrysotile asbestos in kidney cortex of chronically gavaged rats." Arch. Environ. Contam. Toxicol., 12, 247–255.

Petriglieri, J.R.; Laporte-Magoni, C.; Salvioli-Mariani, E.; Gunkel-Grillon, P.; Tribaudino, M.; Bersani, D.; Lottici, P.P.; Mantovani, L.; Bursi Gandolfi, N. Fibrous minerals in New Caledonia: A comparison of different analytical strategies for environmental monitoring. Conference Paper: Congresso Congiunto SIMP-AIV-SoGeI-SGI. Geosciences: A Tool in a Changing World, Pisa, Italy, 3–6 September 2017; Available online: https://www.socgeol.it/files/download/pubblicazioni/Abstract%20Book/abstract_book_pisa_2017_ doi.pdf (accessed on 1 April 2019).

Petriglieri, J.R.; Salvioli-Mariani, E.; Mantovani, L.; Tribaudino, M.; Lottici, P.P.; Laporte-Magoni, C.; Bersani, D. Micro-Raman mapping of the polymorphs of serpentine. J. Raman Spettrosc. 2015, 46, 953–958.

Pisu, R., Cinus, S., Demuru, S., Di Gregorio, A., Manca, P., Marras, M., Perezzani, S.(2008). Direttive Generali per la redazione del piano regionale di protezione, decontaminazione, smaltimento e bonifica dell'ambiente ai fini della difesa dai pericoli derivanti dall'amianto. Regione Autonoma della Sardegna: Assessorato della difesa dell'Ambiente.

Pollastri S., Perchiazzi N., Lezzerini M., Plaisier J.R., Cavallo A., Dalconi M., Bursi Gandolfi N., Gualtieri A. F. The crystal structure of mineral fibres. 1. Chrysotile. Periodico di Mineralogia (2016) 85, 249-259. DOI: 10.2451/2016PM655.

Pott, F., Roller, M., Ziem, U., Reiffer, F.J., Bellmann, B., Rosenbruch, M., Huth, F., 1989. Carcinogenicity studies on natural and man-made fibres with the intraperitoneal test in rats. In: Bignon, J., Peto, J., Saracci, R. (Eds.), Non-occupational Exposure to Mineral Fibres. IARC Scientific Publications No. 90 International Agency for Research on Cancer, pp. 173–179.

Pott, F., Huth, F., Friedrichs, K.H., 1974. Tumorigenic effects of fibrous dusts in experimental animals. Environ. Health Perspect. 9, 313–315.

Pott, F., Roller, M., Ziem, U., Reiffer, F.J., Bellmann, B., Rosenbruch, M., Huth, F., 1989. Carcinogenicity studies on natural and man-made fibres with the intraperitoneal test in rats. In: Bignon, J., Peto, J., Saracci, R. (Eds.), Non-occupational Exposure to Mineral Fibres. IARC Scientific Publications No. 90 International Agency for Research on Cancer, pp. 173–179.

Punturo R., Bloise A., Critelli T., Catalano M., Fazio E. & Apollaro C. (2015) - Environmental implications related to natural asbestos occurrences in the ophiolites of the Gimigliano-Mount Reventino Unit (Calabria, Southern Italy). International Journal of Environmental Research, 9 (2), 405-418.

Punturo, R., Ricchiuti, C., Mengel, K., Apollaro, C., De Rosa, R., Bloise, A., 2018. Serpentinite-derived soils in southern Italy: potential for hazardous exposure. J. Mediterr. Earth Sci 10, 51–61.

Reznikoff, C.A., Bertram, J.S., Brankow, D.S. & Heidelberger, C. (1973). Quantitative and qualitative studies of chemical transformation of cloned C3H mouse embryo cells sensitive to post-confluence inhibition of cell division. Cancer Research 33, 3239–3249.

Riganti, C, Aldieri, E, Bergandi, L, Tomatis, M, Fenoglio, I, Costamagna, C, Fubini, B, Bosia, A, Ghigo, D: Long and short fibre amosite asbestos alters at a different extent the redox metabolism in human lung epithelial cells. Toxicol Appl Pharmacol 2003, 193:106–115.

Righi, A., Ricci, P., Baccaglini, A., Campana, M., Ferri, C., Guarnieri, E, Melli, R. (2003, Novembre 21). amianto e bonifica. Mantova.

Ross, M., 1981. The geologic occurrences and health hazards of amphibole and serpentine asbestos. Rev. Mineral. Geochem. 9A(1), 279-323.

Ross, M., & Nolan, R. P. (2003). History of asbestos discovery and use and asbestos-related disease in context with the occurrence of asbestos within ophiolite complexes. Geological Society of America Special Paper No. 373, 447-470.

Sakai, A., Iwase, Y., Nakamura, Y., Sasaki, K., Tanaka, N. & Umeda, M. (2002). Use of a cell transformation assay with established cell lines, and a metabolic cooperation assay with V79 cells for the detection of tumour promoters: a review. ATLA 30, 33–59.

Salamatipour, A., Mohanty, S.K., Pietrofesa, R.A., Vann, D.R., Christofidou-Solomidou M., and Willenbring, J.K., 2016, Asbestos Fibre Preparation Methods Affect Fibre Toxicity. Environmental Science and Technology Letters, 3, 270−274.
DOI:10.1021/acs.estlett.6b00174.

Sasaki, K., Bohnenberger, S., Hayashi K., Kunkelmann, T., Muramatsu D., Phrakonkham, P., Poth, A., Sakai, A., Salovaara, S., Tanaka, T., Claire Thomas, B., Umeda, M. Recommended protocol for the BALB/c 3T3 cell transformation assay. Mutation Research 744 (2012) 30–35. doi:10.1016/j.mrgentox.2011.12.014.

Schreirer H., 1989. Asbestos in the natural environment. Studies in Environmental Science 37, Elsevier, Amsterdam.

Shelley, D: Manual of Optical Mineralogy. Elsevier Scientific Publishing Company, New York 1975;158–170.

Solbes, E., Harper, R.W. Biological responses to asbestos inhalation and pathogenesis of asbestos-related benign and malignant disease. J Investig Med. 2018 Apr;66(4):721-727. doi: 10.1136/jim-2017-000628. Epub 2018 Jan 6. PMID: 29306869.

Stanton, M.F., Layard, M., Tegeris, A., Miller, E., May, M., Morgan, E., Smith, A., 1981, Relation of particle dimension to carcinogenicity in amphibole asbestos and other fibrous minerals. Journal of the National Cancer Institute 67, 965- 976.

Stayner, L, Kuempel, E, Gilbert, S, Hein, M, Dement, J: An epidemiological study of the role of chrysotile asbestos fibre dimensions in determining respiratory disease risk in exposed workers. Occup Environ Med 2008, 65:613–619.

Surace, I. R., Torri, R., Murgese, D., & Dematteis, A. (2011, agosto). Gestione dei materiali di scavo: valutazione della presenza di amianto in rocca e suoli tramite microscopia ottica a luce polarizzata. Geoingegneria Ambientale e Mineraria, p. 27-46.

Suzuki, Y., Yuen, and R. Ashley: Short, thin asbestos fibres contribute to the development of human malignant mesothelioma: Pathological evidence. Intern. J. Hyg. Environ. Health 208(3):201–210 (2005).

Szeszenia-Dąbrowska, N., Wilczyńska, U. Medical monitoring of asbestos-exposed workers: experience from Poland Beata Świątkowska. Bull World Health Organ. 2016. 94(8), 599–604.

Takenori Ishida, Nobutoshi Fujihara, Tomoki Nishimura, Hisakage Funabashi, Ryuichi Hirota, Takeshi Ikeda, Akio Kuroda. Live-cell imaging of macrophage phagocytosis of asbestos fibres under fluorescence microscopy. Genes Environ. 2019 Jun 5;41:14. doi: 10.1186/s41021-019-0129-4. eCollection 2019.

Timbrell, V., Griffiths, D. & Pooley, F., 1971. Possible importance of fibre diameters of South African Amphiboles. Nature, Volume 232, p. 55–56.

Turci F. et al. (2015) Geological and Analytical Procedures for the Evaluation of Asbestos-Related Risk in Underground and Surface Rock Excavation. In: Lollino G., Manconi A., Guzzetti F., Culshaw M., Bobrowsky P., Luino F. (eds) Engineering Geology for Society and Territory - Volume 5. Springer, Cham.

Valberg, P. & Blanchard, J., 1991. Pulmonary macrophage physiology: origin, motility, and endocytosis. In: Comparative Biology of the Normal Lung. Florida: CRC Press, Boca Rotan, pp. 618-715.

Vallero, D. A. & Beard, M.E. Selecting Appropriate Analytical Methods to Characterize Asbestos in Various Media. Pract. Period. Hazard. Toxic Radioact. Waste Manage., 2009, 13(4): 249-260.

Van Orden, D.R., Allison, K.A., and Lee R.J., 2008, Differentiating amphibole asbestos from non-asbestos in a complex mineral environment. Indoor and Built Environment, 17, 58-68. https://doi.org/10.1177/1420326X07087006.

Van Orden, D.R., Lee, R.J., Allison, K.A., and Addison J., 2009, Width distributions of asbestos and non-asbestos amphibole minerals. Indoor and Built Environment 18, 531-540. https://doi.org/10.1177/1420326X09341503.

Wagner, J. C., Slegs, C. & Marchands, P., 1960. Diffuse pleural mesothelioma and asbestos exposure in the north Western Cape Province. British Journal of Industrial Medicine, Issue 17, pp. 260-271.

Wagner, J. C., Berry, G., Skidmore, J. W., and Timbrell, V. 1974. The effects of the inhalation of asbestos in rats. Br. J. Cancer 29:252–269.

Wagner, J. C. et al., 1982. Biological effects of tremolite. British Journal of Cancer, 45(952), pp. 352-360.

Wagner, J., 2015. Analysis of serpentine polymorphs in investigations of natural occurrences of asbestos. Environ. Sci. Process. Impacts 17, 985e996.

Weinzweig, M., and Richards, R. J. _1983_. "Quantitative assessment of chrysotile fibrils in the bloodstream of rats which have ingested the mineral under dietary conditions." Environ. Res., 31, 245–255.

Williams, C., Dell, L., Adams, R., Rose, T., and Van Orden, D., 2013, State-of-the-science assessment of non-asbestos amphibole exposure: is there a cancer risk? Environmental Geochemistry and Health 35:357–377. DOI: 10.1007/s10653-012-9500-0.

Whitney, D.L.; Evans, B.W. Abbreviations for Names of Rock-Forming Minerals. *American Mineralogist* **2010**, 95, 185-187.

WHO (World Health Organization), 1997. The world health report 1997 - conquering suffering, enriching humanity.

World Health Organisation, 2000. WHO Air Quality Guidelines, second ed. Asbestos. Regional Office for Europe, Copenhagen, Denmark.

World Health Organisation, 2014. Chrysotile Asbestos. World Health Organization. Geneva, Switzerland. http://www.who.int/ipcs/assessment/public_health/chrysotile_asbestos_summary.pdf

Wylie, A. & Mossman, B., 1997. Mineralogical features associated with cytotoxic and proliferative effects of fibrous talc and asbestos on tracheal epithelial and pleural mesothelial cells. Journal of Toxic and Applied Pharmacology, Volume 147, p. 153–160.

Wylie, A.G., Virta, R.L., and Russek, E., 1985, Characterizing and discriminating airborne amphibole cleavage fragments and amosite fibres: implications for the NIOSH method. American Industrial Hygiene Association Journal 46, 197- 201. https://doi.org/10.1080/15298668591394653.

Wylie, A.G., Bailey, K.F., Kelse, J.W., and Lee, R.J., 1993, The importance of width in asbestos fibre carcinogenicity and its implications for public policy. American Industrial Hygiene Association Journal; Akron Vol. 54, Fasc. 5, (May 1993): 239. DOI: 10.1080/15298669391354621.

Wylie A.G., Candela P.A. (2015). Methodologies for determining the sources, characteristics, distribution, and abundance of asbestiform and nonasbestiform amphibole and serpentine in ambient air and water. J. Toxicol. Environ. Health. B Crit. Rev. 18 (1), 1 - 42.

Wruke, C.T. (1986) – Serpentine and carbonate hosted asbestos deposits. In "Mineral Deposit Models" Cox D.P. & Singer D.A. Ed.s, U.S Geol. Survey Bull., 1693, pp. 39-46.

Yada, K.; Lishi, K. Growth and Microstructure of Synthetic Chrysotile. Am. Miner. 1977, 62, 958–965.

SITOGRAPHY

http://www.ibasecretariat.org/alpha_ban_list.php

www.isprambiente.gov.it

Sintesi delle conoscenze relative all'esposizione e al profilo tossicologico Amianto. Available online: http://www.salute.gov.it/portale/temi/documenti/acquepotabili/parametri/Val_Amianto_documento_completo.pdf.

LIST OF FIGURES

LIST OF TABLES

LIST OF MINERAL ABBREVIATIONS

Symbol	Mineral name
Ab	albite
Act	actinolite
Ap	apatite
Atg	antigorite
Cal	calcite
Cpx	clinopyroxene
Chl	chlorite
Ctl	chrysotile
Clc	clinochlore
Di	diopside
Do	dolomite
Ed	Edenite
Lz	lizardite
Mag	Magnetite
Phl	phlogopite
Srp	Serpentine
Spl	Spinel
Tlc	talc
Ttn	titanite
Tr	tremolite

(Whitney & Bernard, 2010)